UNIVERSITÀ DEGLI STUDI DI PALERMO

Dottorato Di Ricerca in Biologia Cellulare e Scienze e Tecnologie Del Farmaco

Indirizzo Biologia Cellulare

Dipartimento Scienze e Tecnologie Biologiche Chimiche e Farmaceutiche

BIO/06

CELLULAR AND MOLECULAR MECHANISMS ACTIVATED IN SEA URCHIN EMBRYOS EXPOSED TO GADOLINIUM, EMERGING ENVIRONMENTAL CONTAMINANT

LA DOTTORESSA	IL COORDINATORE
CHIARA MARTINO	**MARIA CARMELA ROCCHERI**

IL TUTOR	CO-TUTOR
MARIA CARMELA ROCCHERI	**VALERIA MATRANGA**

CICLO XXVI
ANNO CONSEGUIMENTO TITOLO: 2017

In memory of my great mentor and scientist,

Dr. Valeria Matranga

Ringraziamenti

Sono infinitamente grata per ogni singolo evento e persona che hanno contribuito a rendere questo percorso di dottorato possibile fino alla fine. Ringrazio l'Università di Palermo per avermi sostenuta economicamente in questi tre anni; ringrazio tutto il collegio dei Docenti del dottorato per avermi insegnato che le domande non vanno temute, ma apprezzate come fonte di dialogo costruttivo e nuova sintesi; in particolare ringrazio i miei due referees, la prof.ssa Albanese ed il prof. Di Liegro, per i loro sempre utili commenti, il prof. Cavalieri per le interessanti conversazioni, la prof.ssa Puglia per la sua carica energetica contagiosa.

Ringrazio la prof.ssa Roccheri per essere stata un tutor eccezionale, disponibile, aperta al dialogo, dotata delle capacità e dell'autorevolezza necessarie per incoraggiarmi e stimolarmi. Ringrazio tutti i collaboratori del gruppo Roccheri, in particolare Liana per avermi spiegato la differenza fra amici e colleghi ma essere stata anche un'amica e Roberto per avermi accolta nel laboratorio ed avermi passato i suoi preziosi insegnamenti con la pazienza di un ottimo professore. Ringrazio anche i miei amici "dall'altra parte del bancone" del Lab 3, Sara e Walter, per aver reso allegro e pieno di risate ogni giorno passato con le pipette in mano.

Ringrazio il mio co-tutor, la dott.ssa Matranga, per essere stata al contempo il mio più grande critico e la mia più grande sostenitrice, e per avermi insegnato la perseveranza e la scrupolosità scientifica. Ringrazio tutti i collaboratori del gruppo Matranga, in particolare Erina per la sua instancabile pazienza e caparbietà nell'indagine genetica e Roberta per aver sempre saputo avere una parola di conforto nei momenti peggiori.

Ringrazio la prof.ssa Maria Byrne per avermi dato la fantastica opportunità di lavorare nel suo laboratorio presso la University of Sydney, per la sua incredibile forza d'animo e per la sua straordinaria capacità di istillare entusiasmo. Ringrazio tutti i collaboratori del suo gruppo che mi hanno aiutata durante il soggiorno a Sydney, un ringraziamento particolare va a Demian Koop per avermi introdotta nel laboratorio e per la sensazione di benessere che ha saputo costantemente creare lavorando insieme.

Ringrazio tutti i miei familiari: i miei cugini e i miei zii per aver rappresentato il senso vero di *famiglia*, mia sorella per essere sempre stata il mio modello da seguire, mio padre per avermi portata a capire che la vita non va mai data per scontata, ma che è un dono da coltivare ogni giorno, ed in particolar modo mia madre per essermi sempre stata accanto e per aver rappresentato l'elemento saldo della mia vita: senza di lei mi sarei persa più volte.

Ringrazio tutti i miei amici, quelli che mi sono sempre stati vicini, quelli che l'hanno fatto a tratti, quelli che sono scomparsi per poi ricomparire, ma soprattutto quelli che mi hanno insegnato cosa significa avere una *famiglia per scelta*, che ne hanno fatto parte e che continuano a farlo: grazie a loro la vita è sempre sembrata affrontabile ed ha avuto quel gusto piacevole e leggero.

Dodici anni fa, appena diplomata, mio padre mi portò a visitare il laboratorio della dott.ssa Matranga al CNR e casualmente mentre guardavamo le uova di riccio passò un paramecio, di cui a quel tempo sapevo poco e niente. Quel paramecio, ignaro e inaspettato, ha fatto scattare in me la scintilla, l'amore per quella vita invisibile eppure così perfetta, e mi ha portata a iscrivermi in Scienze Biologiche. Senza quella visita oggi non starei concludendo il dottorato in Biologia Cellulare, e per questo devo ringraziare le due persone che quel giorno permisero a quella ragazzina di innamorarsi di un paramecio, e che oggi non ci sono più. Quindi sono riconoscente a mio padre e alla dott.ssa Matranga: senza di loro, questa tesi non sarebbe mai esistita.

Table of Contents

1. INTRODUCTION

"The sea, the great unifier, is man's only hope. Now, as never before, the old phrase has a literal meaning: we are all in the same boat."

Jacques Yves Cousteau, XX century

1.1 Marine chemical pollution

The marine environment is the sink for a range of anthropogenic contaminants, the diversity of which is increasing rapidly as new chemicals are produced and new applications developed (Fig. 1). Although the history of aquatic environmental pollution goes back to the very beginning of the history of human civilization, aquatic pollution did not receive much attention until a threshold level was reached with adverse consequences on ecosystems and organisms. Aquatic pollution has become a global concern, but even so, most developing nations are still producing huge pollution loads and the trends are expected to increase. Knowledge of the pollution sources and impacts on ecosystems is important not only for a better understanding on the ecosystem responses to pollutants but also to formulate prevention measures (Islam and Tanaka, 2004). Monitoring chemical pollution in the marine ecosystems and understanding their toxic effects is critical for environmental management (European Marine Board, 2013), particularly in light of the EU Marine Strategy Framework Directive (Directive 2008/56/EC). Understanding the impact of human activities and human-derived waste on the marine environment is a major issue for the world scientific community, with major aim to translate this understanding to a global awareness and to inform politics to protect our valuable marine resources. As the Rome Declaration states, "it is imperative to achieve human wellbeing by combining economic benefit with environmental protection" (Larkin et al., 2014).

Pharmaceuticals are a class of emerging environmental contaminants that are extensively and increasingly being used in human and veterinary medicine (Fent et al., 2006). During drug treatment, the active components of pharmaceutical products are largely excreted from the patient's body and introduced into the sewage disposal system and consequently into wastewater.
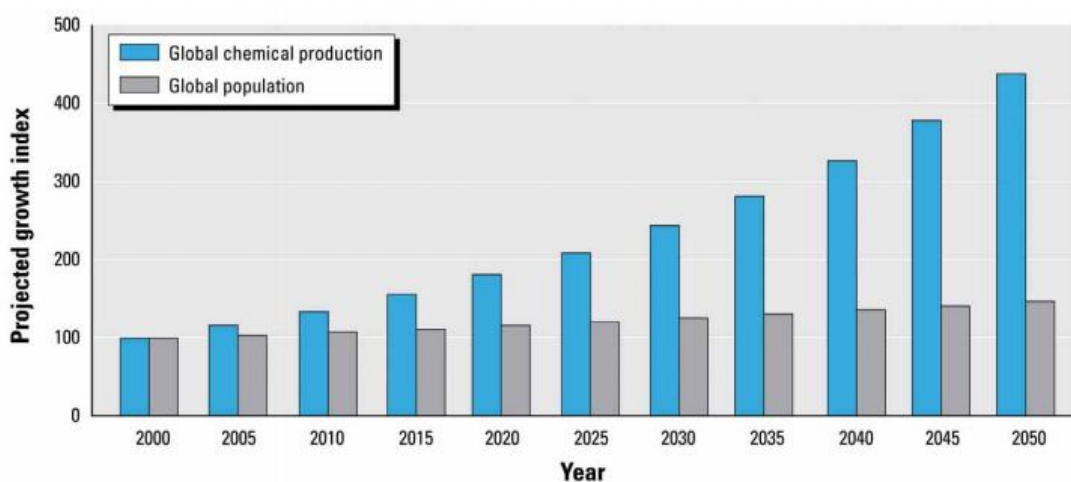
Fig. 1 Global chemical production is projected to grow at a rate of 3% per year, rapidly outpacing the global population growth. On this trajectory, chemical production will double by 2024, indexed to 2000 (Adapted from Wilson and Schwarzman, 2009).

Wastewater treatment plants are currently not designed to remove pharmaceutical compounds and both solid and liquid outputs from wastewater treatment plants contain a mixture of pharmaceutical residues. Over 200 pharmaceutical agents have been detected in aquatic and terrestrial environments around the world, including areas as remote as the Antarctic (Fig. 2). Pharmaceuticals have been found in aquatic systems globally, due to a combination of worldwide usage and low removal efficiency of these agents in sewage treatment plants or the absence of water treatment (Brodin et al., 2014; Lindberg et al., 2014). Pharmaceuticals are highly active compounds that target specific biological systems and can have adverse impacts on the physiology and behaviour of a variety of organisms even at low concentrations (Murdoch, 2015). Many pharmaceuticals including therapeutic and prognostic drugs pollute the marine environment. Recently the International Conference

on Chemicals Management (ICCM) highlighted the need for global cooperation to build awareness and push for action to address drug pollution in aquatic marine environments (Time To Get Clean, 2015).
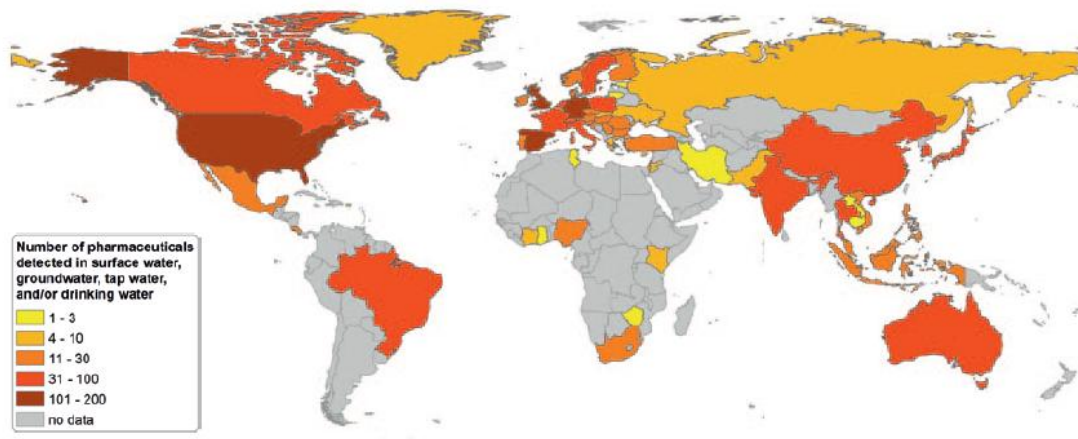
Fig. 2 Global occurrence of pharmaceuticals. Number of pharmaceuticals detected in surface water, groundwater, tap water, and/or drinking water (adapted from IWW 2014).

The ecosystem impact of chemical pollution can only be determined by coupling investigations of exposure (i.e. chemical concentrations) and the effects of these agents in ecotoxicological tests. This allows the determination of the risks due to the contamination (Lyons et al., 2010; Chapman, 2007). Although some studies exist, there is still a scientifically challenging lack of understanding of the interactions between various environmental stressors and their biological effects and ecological consequences. A major challenge in impact and risk assessment as part of environmental management is to link harmful effects of pollution (including toxic chemicals) in individual sentinel animals to their ecological consequences (Moore et al., 2004). Part of the solution may lie with the use of diagnostic, clinical-type, laboratory-based ecotoxicological tests or biomarkers (e.g. Rapid Assessment of Marine

Pollution, RAMP; Depledge, 2000), utilizing sentinel animals. To determine toxicity effects.

1.2 Gadolinium
1.2.1 Chemical and application aspects

Gadolinium (gadolinite, a mineral named for Gadolin, a Finnish chemist; Gd; atomic weight 157.25; atomic number 64; melting point 1313°C; boiling point 3273°C; valence 3) is a metal of the lanthanide series of the elements (fig. 3). With a relative abundance in the Earth crust of about 5.9 ppm, gadolinium belongs to the rarest elements on Earth. It is found in nature in several minerals, including monazite and bastnasite, which are of commercial importance (Lide et al., 2010).

Gadolinium was isolated only in recent years. It is a silvery white, malleable and ductile element. The metal is relatively stable in dry air, but in moist air it tarnishes with the formation of a loosely adhering oxide film which splits off and exposes more surface to oxidation. The metal reacts slowly with water and is soluble in dilute acid (Lide et al., 2010).

The most common oxidation state for the lanthanide elements is +3 and this is the only important ionic form found in aqueous complexes. Gd^{3+} has an ionic radius of 0.99A˚, very nearly equal to that of divalent Ca^{2+} (Sherry et al., 2009). This is one of the reasons why Gd^{3+} is so toxic in biological systems: it can compete with Ca^{2+} in all biological systems that require Ca^{2+} for proper function and, in doing so, the trivalent ion binds with much higher affinity (Sherry et al., 2009).

There are 31 isotopes of gadolinium, seven of which are stable and occur naturally in nature as a mixture. Gadolinium has no large-scale applications but has a variety of specialized uses: it is used to target tumors in neutron therapy; it has microwave applications and is used in fabrication of various

optical components and for computer bubble memory; ^{153}Gd is used as a gamma ray source in X-ray absorption measurements; gadolinium compounds are used in making phosphors for color TV tubes and as intravenous contrast agent to enhance images in medical magnetic resonance imaging (Lide et al., 2010).
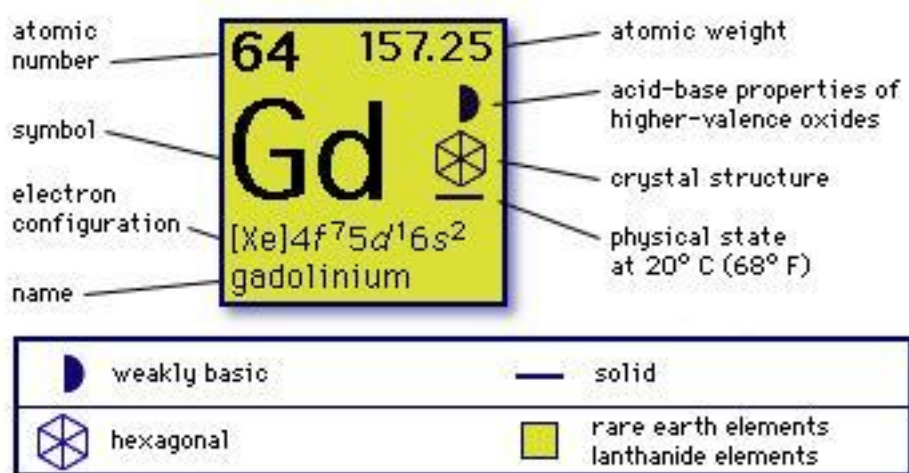
Fig. 3 Chemical properties of Gadolinium, a chemical element with symbol Gd and atomic number 64. It is strongly paramagnetic above 20°C
(from Encyclopaedia Britannica, Inc. 2006).

Gadolinium chelates are employed as contrast agents for magnetic resonance imaging (MRI) since the 1980s (Runge VM, 1988). The first and most often employed MRI contrast agents are based on gadolinium(III) ions. Due to the high toxicity of free Gd(III) ions, they are commonly complexed with polyaminocarboxylic acid chelating agents without loss of magnetic properties (Spencer et al., 1997; Gries, 2002). In general they were considered as safe and well-tolerated, when in 2006, the disease nephrogenic systemic fibrosis (NSF) was connected to the administration of MRI contrast agents based on Gd (Cowper and Boyer, 2006).

1.2.2 Gadolinium toxicity

Gd^{3+} is highly toxic, a very potent calcium antagonist, and can block voltage-gated calcium channels or inhibit calcium-activated enzymes (Hirano and Suzuki, 1996).

Mitsunaga et al. (1986) and Hwang and Lennarz (1993) showed that several organic Ca^{2+} channel blockers inhibit spicule formation in cultures of micromeres isolated from 16-cell stage sea urchin embryos. David et al. (1988) suggested that gadolinium ions (Gd^{3+} above 200 μM) are able to block Ca^{2+} channels in the membranes of unfertilized sea urchin eggs. In more recent years, Gd^{3+} has been shown to inhibit some Ca^{2+} channels. Luo et al. (2011) found that 10 μM Gd^3 inhibits Ca^{2+} channels in human embryonic kidney cells (HEK293), while an arachidonic acid-activated Ca^{2+} channel in rat smooth muscle cells (A7r5) is inhibited by 100 μM Gd^{3+} (Broad et al., 1999). Using mouse cells, it was shown that dihydropyridine-sensitive Ca^{2+} channels in muscle cells (C2) are inhibited by ~50 μM Gd^{3+} (Lansman, 1990), and half maximal inhibition of similar stretch-sensitive channels is attained at ~6 μM Gd^{3+} (Franco and Lansman, 1990). Using *Xenopus* oocytes, Yang and Sachs (1989) found that Ca^{2+} ion channels are blocked by 5–10 μM Gd^{3+}. Accordingly, Spencer et al. found deposits into liver of rats after Gd chloride administration (1997).

Gadolinium causes short term toxicity to aquatic algae and bacteria, as the microbial density decreased with the increase of the Gd concentration (Wilde et al., 2002).

GdCl is suggested to alter the susceptibility of liver hepatocytes to toxicity caused by certain chemicals (i.e. cadmium chloride and beryllium sulfate) (Badger et al., 1997). Furthermore, it induces apoptosis in rat alveolar macrophage in both time- and dose-dependent fashions, probably reflecting stable binding and internalization since Gd was observed within endosomes (Mizgerd et al., 1996).
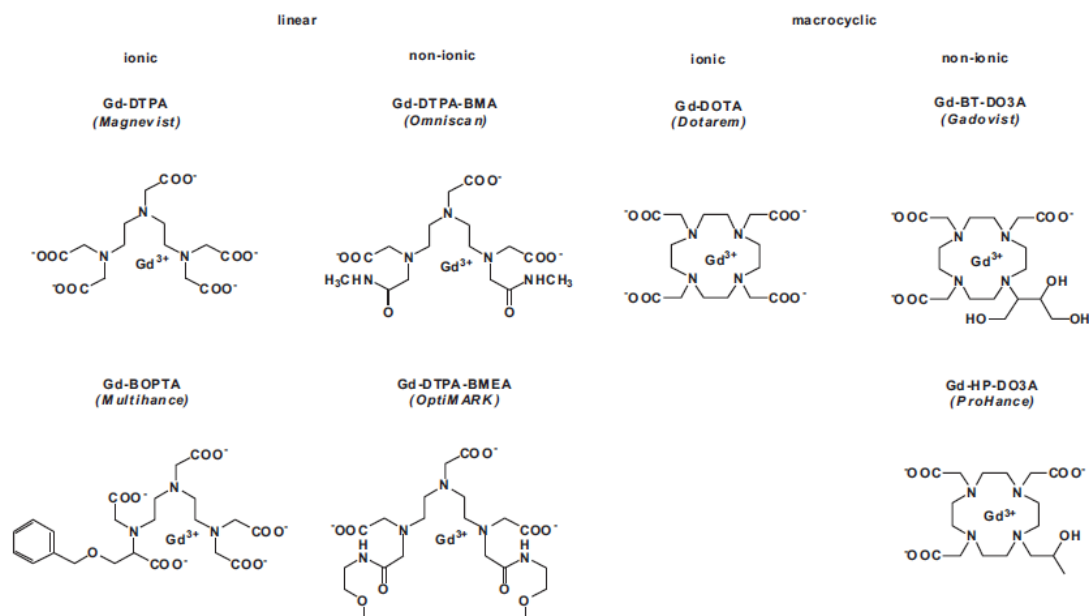
Fig. 4 Structures of several Gd-based MRI contrast agents and the respective trademarks. The complexes can be separated in ionic and macrocyclic complexes and in complexes with linear or macrocyclic ligands (adapted from Telgmann et al., 2013).

Neurotoxicity was reported for MRI contrast agents in rats with disrupted blood-brain barrier (Spencer et al., 1997).

The exposure to Gd containing MRI contrast agents in humans (fig. 4, 5) is associated with the development of Nephrogenic systemic fibrosis (NSF), first described in literature in 2000 (Cowper et al., 2000). NSF is a dermatological fibrosis disease with potential systemic manifestations that can lead to severe symptoms, and is lethal in a subset of cases. Almost all the patients with NSF have had severe renal insufficiency and have received administrations of gadolinium-based contrast agents. High concentrations of Gd associated with calcium and phosphorus in the skin was shown to persiste even 3 years after the last exposure to Gd. Residual Gd chelates, after initial and rapid renal clearance, can dissociate into toxic Gd^{3+} that form insoluble precipitates. Bone serves as a site for Gd storage: long-term persistence and slow release of Gd^{3+} from bone stores can be a cause for concern of Gd-associated toxicity with

long latency (Thakral et al., 2007). Generally, the toxic effects differ depending on dose, organism and type of Gd-containing chelate.
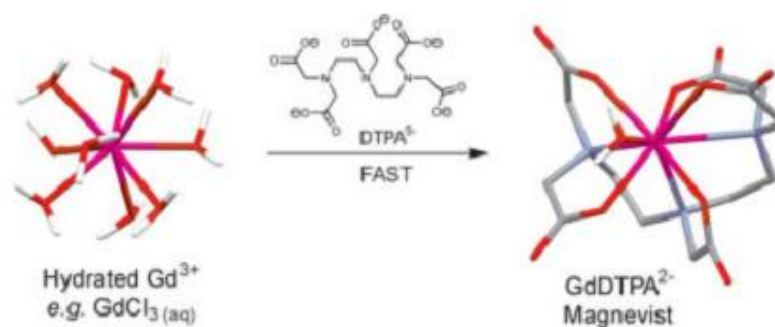
Fig. 5 Chemical reaction to synthesize Magnevist, the first intravenous contrast agent to become available for clinical use.

1.2.3 Gadolinium in the environment

Gd-based MRI contrast agents are stable complexes and so they are not metabolized leaving the human body within a few hours after application (Kümmerer and Helmers, 2000). After excretion, these agents enter the public sewer and subsequently the wastewater treatment plant. These treatment plants are not specifically designed to remove toxic matter, contaminants and pharmaceuticals. Because of their polar or anionic nature, the Gd complexes are most likely neither adsorbed onto surfaces nor by particulate organic matter (Knappe et al., 2005).

Studies over the last 15 years indicate that Gd chelates are relatively unaffected by the sewage treatment process. Gd has been determined with ICP-OES (Inductively Coupled Plasma Optical Emission Spectrometry) or ICP-MS (Inductively Coupled Plasma Mass Spectrometry) in diverse water samples. Elevated Gd concentrations were observed in surface waters near

populated areas all over the world, indicating that the source of anthropogenic Gd is the increasing application of Gd-based MRI contrast agents (Zhu et al., 2014; Hatjie et al., 2016). High concentrations of Gd were detected in hospital effluents and later, in the effluent of wastewater treatment plants. These findings indicate that the Gd complexes applied during MRI examinations pass the sewage treatment mainly unhindered. Consequences of Gd accumulation in surface waters, oceans and even drinking water have not been evaluated yet due to limited knowledge about ecotoxicity of the respective compounds nature (Telgmann et al., 2013).

To evaluate the impact of the Gd output of wastewater treatment plants on the aqueous environment, it is important to know in which form Gd is present. The comparison of speciation analysis of the Gd complexes and total Gd quantification in the effluent of the plant and in surface waters indicated that not all Gd remains complexed. This is an important aspect for future investigations, as the metal species in the excess Gd have to be identified nature (Telgmann et al., 2013).

Gd pollution is measured as "the Gd anomaly", calculated as the ratio of the measured Gd concentration in a sample with respect to the background levels of Gd due to geological processes. The Gd anomaly is determined using the total Gd concentration, with no information about the speciation of the Gd present in the sample (Bau and Dulski, 1996). The analysis of wastewater effluent revealed an anomaly ratio of 1680; this significant output of Gd emphasizes its anthropogenic nature (Telgmann et al., 2013). Positive Gd anomalies are reported for several rivers, lakes and seawater from different locations. Nozaki et al. (2000) determine the Rare Earth Elements concentrations in rivers draining highly populated areas in Japan and the Tokyo Bay. ICP-MS measurements showed highly elevated Gd concentrations compared to the geogenic background. In 2002, Elbaz-Poulichet et al. published a report that confirmed anthropogenic Gd findings in a small river and a French Mediterranean lagoon (Elbaz-Poulichet et al., 2002). The ICP-

MS measurements also indicated Gd excess in the effluents of the local sewage treatment plant. Calculations showed that the amount of anthropogenic Gd was compatible with the medical use of Gd-based MRI contrast agents. Similarly, high values of Gd concentrations were found with positive Gd anomalies in the studies of Bau and Dulski (1996). Zhu et al. analyzed samples from coastal seawater and river waters near Nagoya in Japan (Zhu et al., 2004). Significant Gd anomalies were found, especially in river water from urban areas as well as near sewage treatment plants. Anthropogenic Gd was also reported in river waters in Pennsylvania and in Lake Erie in the United States (Bau et al., 2006). High Gd concentrations were found in creeks in the Czech Republic (Morteani et al., 2006). Positive Gd anomalies were determined in Southern France (Rabiet et al., 2009). A detailed study on anthropogenic Gd showed large positive Gd anomalies were found in tap water samples in the area of Berlin, Germany (Kulaksiz and Bau, 2011).

Strikingly, the Gd anomalies in seawater around the urban areas with large human populations have increased greatly over time, all over the world, demonstrating that Gd anomalies are caused by the emission release from anthropogenic sources (Zhu et al., 2004). Recent measurements revealed a temporal increase in the Gd anomaly in San Francisco Bay from the early 1990s to the present (fig. 6). The highest Gd anomalies were observed in the southern reach of San Francisco Bay, which is surrounded by several hospitals and research centers that use Gd-based contrast agents for MRI (Hatje et al., 2016).

The presence of Gd in the marine environment poses a potential hazard to the marine biota. Although it is recognized that Gd has negative consequences on human health, the effects of Gd exposure on aquatic organisms are poorly understood. A single study carried out by Saitoh and colleagues (2010) using sea urchin embryos described the impairment of skeleton deposition in embryos raised in seawater containing submicromolar to a few micromolar Gd^{3+}.
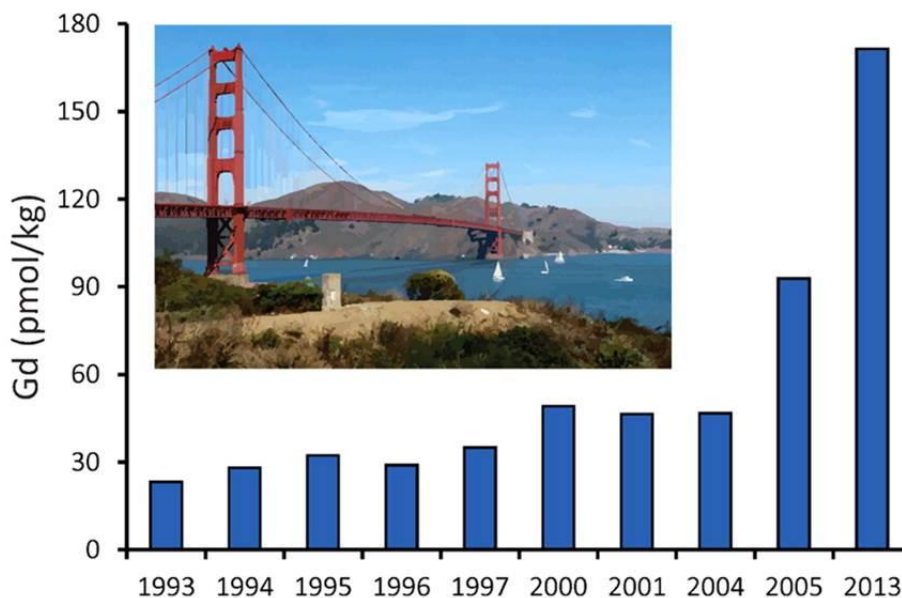
Fig. 6 anthropogenic Gd concentrations increased substantially over a 20 year period (adapted from Hatje et al., 2016)

1.3 Choice of the model system: the sea urchin embryo

Marine organisms are highly sensitive to several kind of stressors, and able to activate different defense strategies. The sea urchin embryo has long been an important model organism in developmental biology and eco-toxicology to assess the hazard posed by contaminants entering the marine environment (Radenac et al., 2001; Russo et al., 2003), as it continuously faces environmental, chemical, physical and biological stressors (Roccheri et al., 2004; Hereu et al., 2005; Bonaventura et al., 2005; Matranga et al., 2010; Byrne et al., 2013). The high number of gametes, its external fertilization, the high developmental synchrony and embryo transparency make the sea urchin embryo a suitable model organism for cellular and developmental biology studies. A wealth of research with sea urchin embryos and larvae have shown that chemical pollutants impair development and that the larval skeleton is a particularly vulnerable response variable for ecotoxicological tests

(Bonaventura et al., 2015; Byrne et al., 2013). For instance, exposure to toxic elements (e.g. cadmium and manganese), UVB and X rays inhibits skeletogenesis (Filosto et al., 2008; Pinsino et al., 2011; Bonaventura et al., 2005; Matranga et al., 2010).

The sea urchin has been recently introduced in the list of alternative methods proposed by the European Union Reference Laboratory for alternatives to animal testing (EURL EVCAM), for the validation of methods which reduce, refine or replace (the 3Rs rule, 86/609/CEE) the use of animals for safety testing and efficacy/potency testing of chemicals, biologicals and vaccines.

In this study I investigated the effects of a range of concentrations of Gd on the development of sea urchin embryos and larvae from four species (fig. 7), two from Europe (*Paracentrotus lividus*, Parechinidae, *Arbacia lixula*, Arbaciidae), and two from eastern Australia (*Heliocidaris tuberculata*, Echinometridae, *Centrostephanus rodgersii,* Diadematidae). These species were chosen on the basis of their comparable developmental timeline. This allowed to compare the responses to Gd and sensitivity across phylogenetically and geographically distant species.

P. lividus is distributed throughout the Mediterranean Sea and in the north eastern Atlantic and is typically a subtidal species, living from the mean low-water mark down to depths of 10 to 20 m and in intertidial rock pools (Boudouresque and Verlaque, 2013). The black *A. lixula* is a common inhabitant of shallow water hard grounds throughout the Mediterranean, the Atlantic coast of Spain, Portugal and Noth-western Africa, as well as off the coast of Brazil; it is well adapted to the turbulent waters of the first few meters of the upper infralitoral (Gianguzza and Bonaviri, 2013). *H. tuberculata* is endemic to Australia and it is distributed on rocky reefs from the intertidial zone down to a depth of about 35 m (Keesing, 2013). *C. rodgersii* is a large sea urchin found on subtidal rocky reefs in southeastern Australia and in the northern New Zealand between depths of 2 and 20 m (Byrne and Andrew, 2013).

As all four species are ecologically important members of rocky reef communities and develop through a feeding echinopluteus larva, information of their sensitivity to Gd will aid in the understanding of the hazard posed and of the conserved morphological response across species to provide insights into potential mechanisms of Gd toxicity.
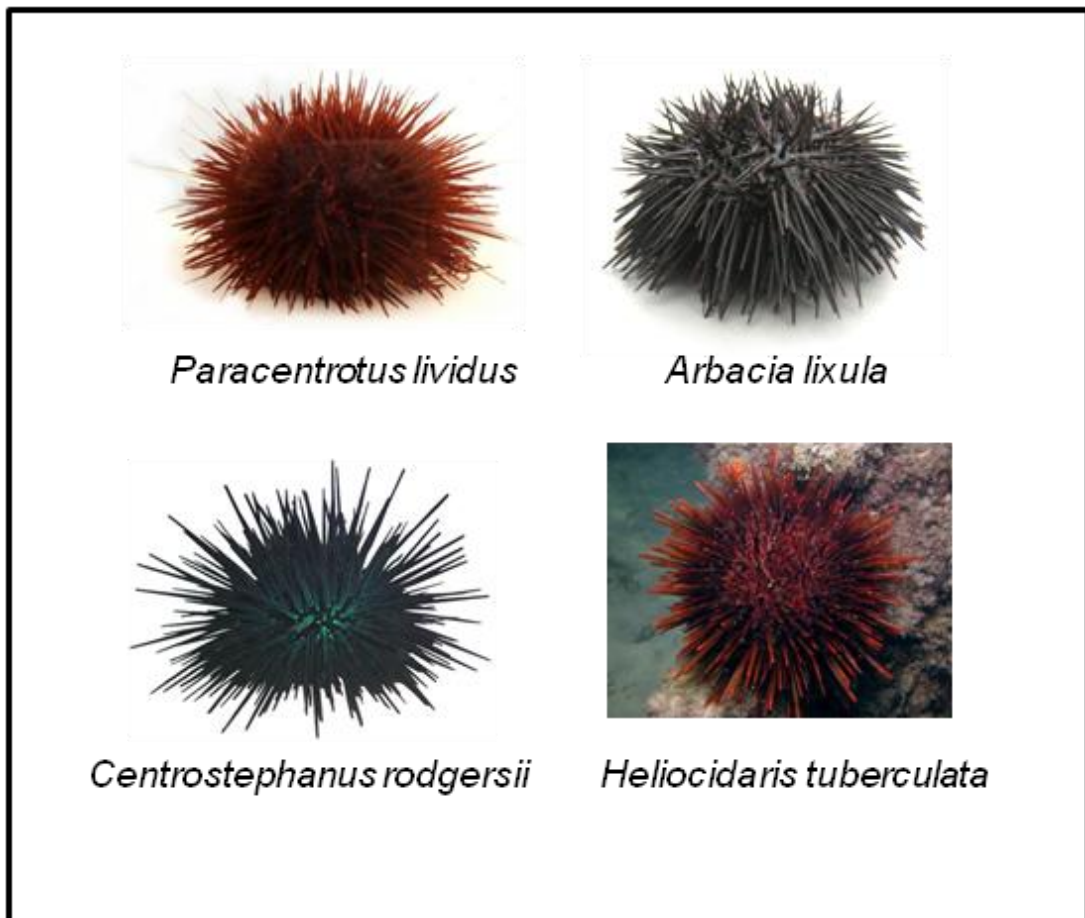
Fig. 7 Pictures of the adults of the four sea urchin species used during the project.

1.4 Sea urchin embryo development

Two poles can be distinguished in the unfertilized egg (Fig. 8A): the animal pole and the opposite vegetal pole. After fertilization (Fig. 8B), the sea urchin embryo exhibits radial holoblastic cleavage. While unequal cell division is highly unusual for normal mitotic cells, it is common in the early cleavages of embryos. After the fourth cleavage, the embryo is easily seen to be composed of three layers of cells: the top tier of medium-sized cells (mesomeres) produced by symmetrical cell division, a middle tier of large cells (macromeres) and a bottom tier of small cells (micromeres) that derive from the unequal cleavages.

At the seventh cleavage, the embryo is now a hollow ball of 128 cells: this is the blastula stage (Fig. 8E). The blastula rotates within the fertilization envelope and then produces a hatching enzyme that dissolves the fertilization envelope (Lepage et al., 1992) allowing the blastula to freely swim in the seawater using the cilia: that's the swimming blastula (Fig. 8F). Later on, the large micromere descendants undergo the epithelial-mesenchymal transition, becoming motile mesenchymal cells, and then pass through the basement membrane, entering the blastocoel. At that point, at the vegetal pole the blastocoelic wall becomes thicker and flat to form the so called vegetal plate. This then starts to invaginate forming the archenteron (Fig. 8G), the primitive gut (Fink and Mc Clay, 1985). The large micromere descendants, the Primary Mesenchyme Cells (PMCs), will then form a typical array in the vegetal portion of the blastocoel, where they will begin to build the embryonic endoskeleton.
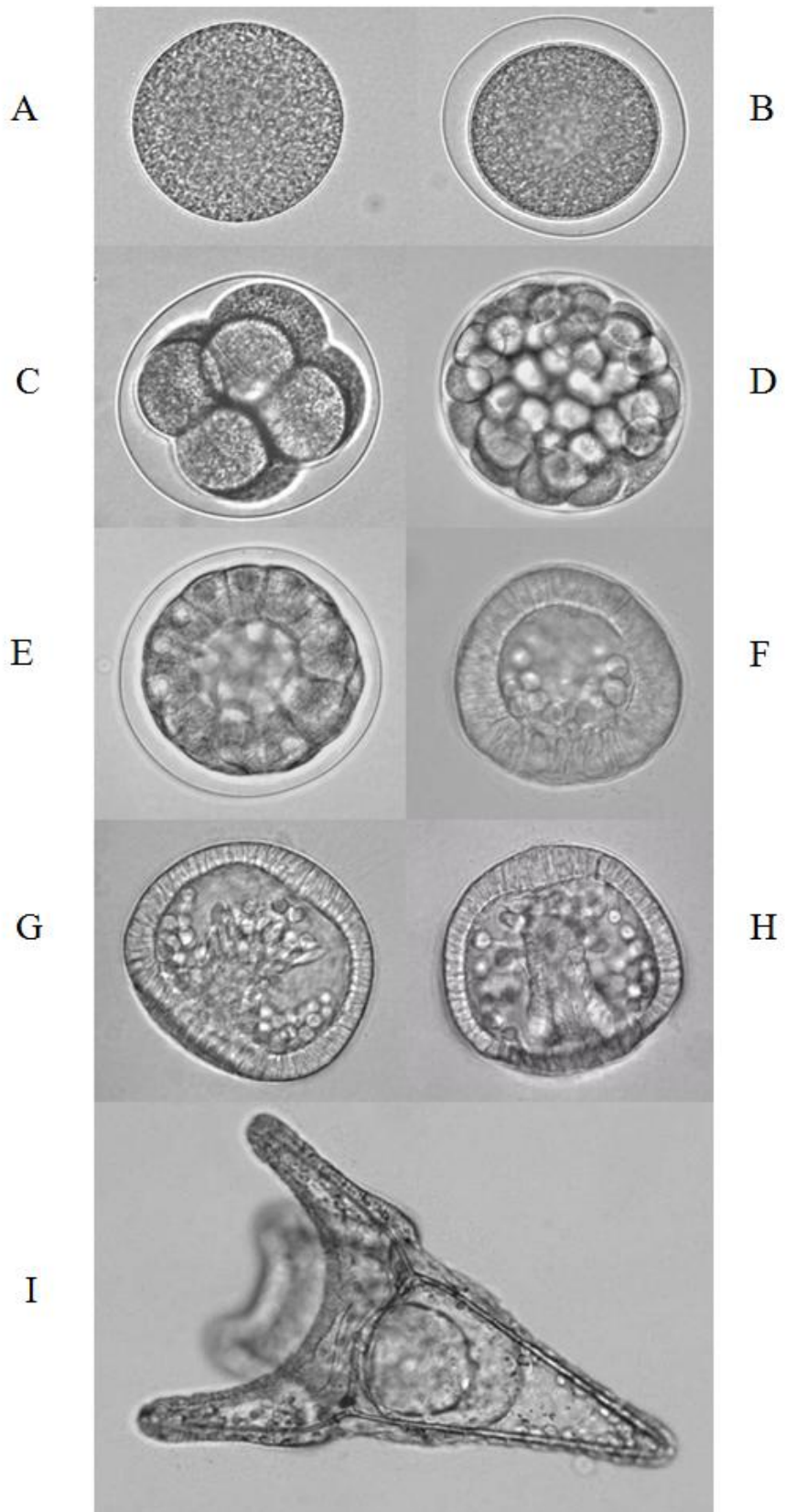
Fig. 8 *P. lividus* embryo development: A) unfertilized egg; B) fertilized egg; C) 8 blastomeres; D) morula; E) early blastula; F) mesenchyme blastula; G) early gastrula; H) mid gastrula; I) pluteus (adapted from Matranga and Bonaventura, 2002).

Eventually, the archenteron elongates toward the opposite side of the gastrula (Fig. 8H), bends, and contacts the animal pole, where the cell-cell interactions induce the formation of the mouth. The contact with the ectoderm will give rise to the mouth, producing a complete gut: this is the prism stage (Gustafson and Wolpert, 1963).

Unlike PMCs, the other population of mesodermal cells, the Secondary Mesenchyme Cells (SMCs), are a heterogeneous population of non-skeletogenic cells with several different fates, giving rise to at least four populations, including pigment, blastocoelar, coelomic pouch and circumesophageal muscle cells (Gustafson and Wolpert, 1963; Gibson and Burke, 1985; Burke and Alvarez, 1988; Tamboline and Burke, 1992, Zito and Matranga, 2009).

Among the fundamental processes governing development, axis specification and body symmetry are of major importance in the sea urchin model organism. In fact, echinoderm adults, that are radially symmetrical, originate from embryos and larvae that are bilaterally symmetrical (Duboc et al., 2005). During sea urchin embryo development, the transition from a bilateral to a radial body plan relies on an impressive left-right asymmetric process, during which an imaginal disk called the rudiment is formed on the left side of the larva (Duboc et al., 2005; Hibino et al., 2006). The Nodal-Lefty-Pitx2 signaling pathway regulates left-right asymmetry during development of the sea urchin embryo. After an initial phase of bilaterally symmetric expression of *nodal*, which extends from the mesenchyme blastula stage to the late gastrula stage and which is correlated with the early role of *nodal* in formation of the oral-aboral axis of the embryo, the expression of *nodal* is restricted to the right side of the ectoderm and to the right coelomic pouch at the end of gastrulation. Lefty expression starts at the 128-cell stage immediately after that of *nodal*, is rapidly restricted to the presumptive oral ectoderm then shifted toward the right side after gastrulation. Lefty acts as a long-range inhibitor of Nodal signaling, suggesting a key role in the establishment of left–

right asymmetries (Duboc et al., 2005). Another key player is the Bone Morphogenetic Protein (BMP), whose signaling in the endomesoderm is required to establish *nodal* expression in the left-right organizer located on the right side. Furthermore, at the gastrula stage BMP signaling itself is asymmetric, with stronger signaling on the left side of the archenteron (Bessodes et al., 2012). As the skeleton grows, the embryo changes shape into the larval form, called a "pluteus" (Fig. 8I).

1.5 Formation of the endoskeleton in the embryo

The skeleton is deposited within the blastocoel cavity of the developing embryo by primary mesenchyme cells (PMCs), descendants of the large micromeres of the 32-cell stage embryo. The large micromeres divide, forming a cohort of 32-64 cells (depending on the species) located at the vegetal hemisphere of the blastocoel. Later, PMCs ingress into the blastocoel at the beginning of gastrulation and migrate along the ectoderm cells. The PMCs gradually become arranged in a characteristic ring pattern which consists of two ventrolateral clusters of cells linked by cellular chains on the oral (ventral) and aboral (dorsal) surfaces of the blastocoel wall (Fig. 9). As the ring pattern forms, filopodial protrusions of the PMCs fuse, joining the cells in a syncytial network (Hodor and Ettensohn, 1998).

The PMCs in each of the ventrolateral clusters deposit a single rudimental granule in response to local cues from overlying ectodermal cells (Guss and Ettensohn, 1997). The rudimental granule soon develops into a triradiate spicule which in turn develops into the pluteus spicule. The spicules are deposited within a "privileged" space surrounded by the fused filopodial processes of the PMCs.
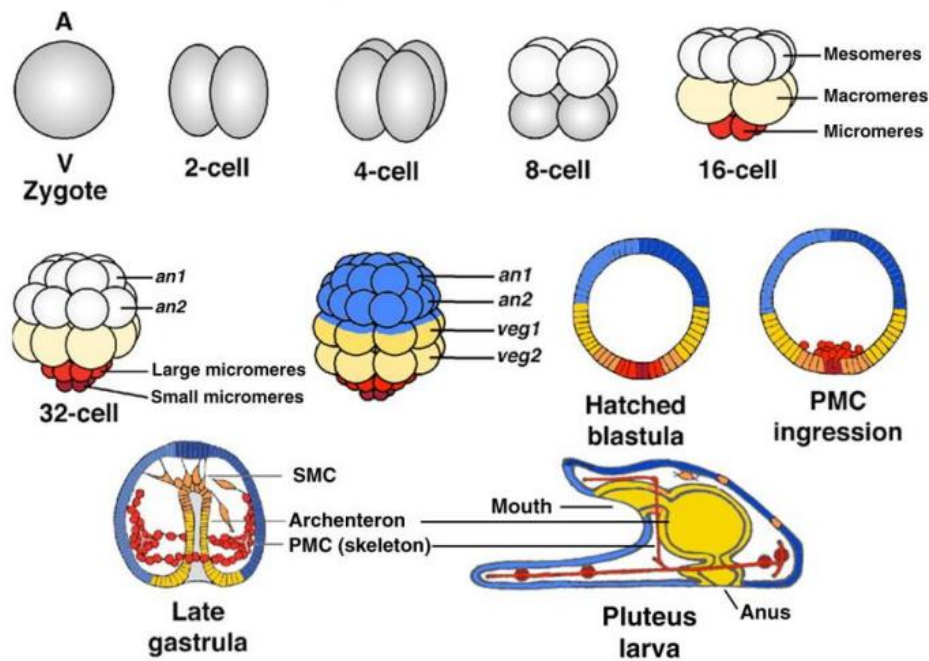
Fig. 9 Chart of sea urchin embryo development and map of the fate of several embryonic districts: blue, ectoderm; yellow, endoderm; red, skeletogenic mesoderm; brown, non-skeletogenic mesoderm (from Gilbert, Develpmetal Biology)

The larval skeleton displays considerable morphological diversity among sea urchin species, including variation in number, structure/shape, and size of rods. Figure 10 shows the skeleton growth during the development of *P. lividus* embryos, identifying the cell chains that will give rise to the different rods. The ventral cell chain will give rise to the ventral transverse rod, the longitudinal chain will form the anterolateral rod, and the dorsal chain will give rise to the body and postoral rods (Matranga et al., 2011).

Some studies demonstrated that the interaction between the PMCs and the ectoderm induces the activation of PMC-specific genes: the inductive signals from the ectoderm control the PMCs distribution within the blastocoel, the growth and dimension of the spicules (Guss and Ettensohn, 1997; Zito et al., 1998, 2003).
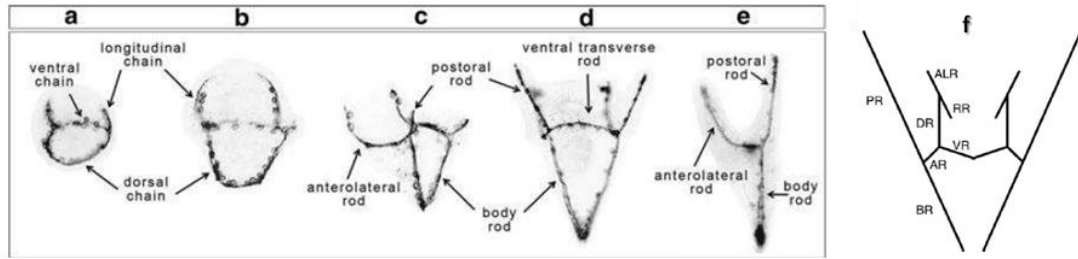
Fig. 10 Development of *P. lividus* skeleton. Skematic drawings of skeleton development observed at (a) late gastrula; (b) prism; (c) early pluteus; (d) pluteus, ventral view; (e) pluteus, lateral view. Ventral chain, longitudinal chain, and dorsal chain indicate set of PMCs which will give raise to the ventral traverse rod, anterolateral rod and postoral rod, respectively; (f) diagram of the major skeletal elements of a four-armed pluteus larva. AR = anonymous rod, ALR = anterolateral rod, BR = body rod, DR = dorsoventral rod, PR = postoral rod, RR = recurrent rod, VR = ventral transverse rod. (adapted from Matranga et al., 2011 and Cheers and Ettensohn, 2005).

The endoskeleton mineral is a high Mg^{2+} (~5%) containing calcite, intensely birefringent, which diffracts X-rays like a single crystal. It contains occluded matrix proteins (about 0.1% by mass). The material properties of the composite are much harder, flexible, and resistant to fracture than pure calcite. The calcium contained in the spicules (and presumably the Mg as well) is obtained from sea water until embryos can feed (Nakano et al., 1963), where it is found at high concentration (~10mM). The calcium is transported from sea water through various layers and is deposited inside cells. PMCs must possess very active Ca^{2+} transporters, presumably with high capacity and low affinity, but they have not yet been identified. Wilt et al. (2008) showed that the Ca^{2+} sensitive fluorescent dye, calcein, when added to cultures of mesenchyme cells derived from 16-cell stage embryos, stained PMCs attached to the elongating spicules initially, and then stained the elongating tips of the spicules. Their results suggest that Ca^{2+} is incorporated into PMCs during spicule formation through Ca^{2+} channels in the PMC membrane before deposition as $CaCO_3$ in the spicules. The manner in which calcium is transported into the PMCs is not known. The calcium and carbonate ions from the sea water have to pass through the various outer layers of the embryo. The cells of these layers thus control the ultrastructural and chemical milieu in which mineralization by the

PMCs occurs and are also involved in the process. The mineral is then translocated to a delimited space inside the syncytium in which the endoskeleton is formed by the PMCs.

1.6 The skeletogenic lineage Gene Regulatory Network

An experiment done by Okazaki in 1975 showed that if fourth-cleavage micromeres are isolated and cultured, they proceed to divide the proper set number of times and then produce biomineral skeletal rods *in vitro*. This demonstrated that the skeletogenic micromeres have all the regulatory inputs required to achieve their autonomous specification (fig. 11).

Specification of an embryonic cell lineage is driven by a network of interactions among genes encoding transcription factors: the Gene Regulatory Network (GRN, fig. 12). GRNs explain developmental phenomenology at the system level, by reference to its source, the genomic control apparatus (Oliveri et al., 2008). The specification of an embryonic cell lineage is traditionally defined as the process by which it achieves its developmental identity. In mechanistic terms specification is the acquisition of a given regulatory state, where regulatory state is the sum of the activities of the transcription factors expressed in the cell nuclei (Oliveri et al., 2008). Therefore, at root the process of specification depends on the regulatory activation (and repression) of genes encoding transcription regulators, that is why a GRN may provide a direct explanation of a specification event at the genomic sequence level. This network is initially deployed through the activity of polarized, maternal inputs that activate a small set of early zygotic regulatory genes selectively in the large micromere-PMC lineage. The transcription factors encoded by the GRN genes engage with additional layers of regulatory genes, resulting in various

feedback and feed-forward interactions to stabilize the transcriptional network and drive it forward (Oliveri et al., 2008). Since gastrulation all the micromere descendants participate in skeletogenesis. They express a distinct suite of genes and carry out no embryological functions other than skeletogenesis.
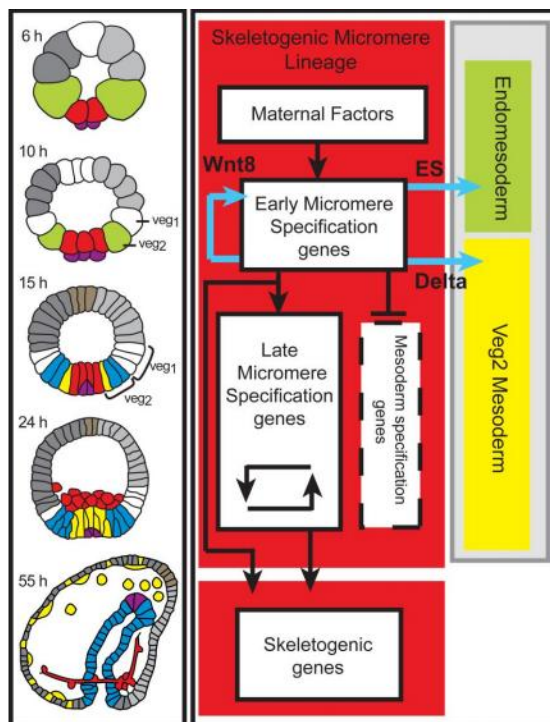
Fig. 11 Territorial components of the sea urchin embryo in lateral view: green, macromeres; red, skeletogenic micromere lineage; purple, small micromeres; yellow, nonskeletogenic mesoderm; blue, gut endoderm; brown, apical neurogenic territory; dark gray, aboral ectoderm; light gray, oral ectoderm. The process diagram summarizes specification functions (from Oliveri et al., 2008).

The most important maternal input is nuclearization of β-catenin, which causes Tcf1 transcriptional activity to be added to the regulatory state in the micromeres, and which activates the expression of *pmar1* gene. The product of the *pmar1* gene is responsible for the first step of micromere specification (Oliveri et al., 2008).

A further function of the skeletogenic micromere lineage is the exclusion of the alternative fate that is assumed by the adjacent non-skeletogenic

mesoderm. This is one of the roles of the micromere lineage regulator *alx-1*, one of the earliest transcription factors defining the definitive zygotic skeletogenic micromere regulatory state. The *alx-1* gene is a primary driver of skeletogenic specification and differentiation in sea urchin embryo and adult development, and it is a member of a family of homeodomain genes also used in vertebrate skeletogenesis (Ettensohn et al., 2003). It acts both as a repressor and an activator on many downstream genes, such as *msp130*, *sm30, p16* and *p19*, as well as on itself having a positive autoregulatory input on its own expression during the dramatic early rise in transcript level, as well as an auto-repression role (Damle and Davidson, 2011).

A major question is what is the molecular nature of the ectoderm signals that regulate skeletal patterning. In the sea urchin embryo, several lines of evidence indicate that ectoderm influences many aspects of skeleton formation, including timing (Ettensohn and McClay, 1986), growth rate (Guss and Ettensohn, 1997), number of spicules and final size (Armstrong et al., 1993). The three-dimensional structure of the skeleton and its bilateral symmetry are foreshadowed and determined by the spatial organization that PMCs can achieve only within the embryo, in intimate contact with the ectoderm wall, suggesting that guidance cues from the ectoderm control the well-defined PMC spatial pattern (Gustafson and Wolpert, 1967; Ettensohn, 1990).
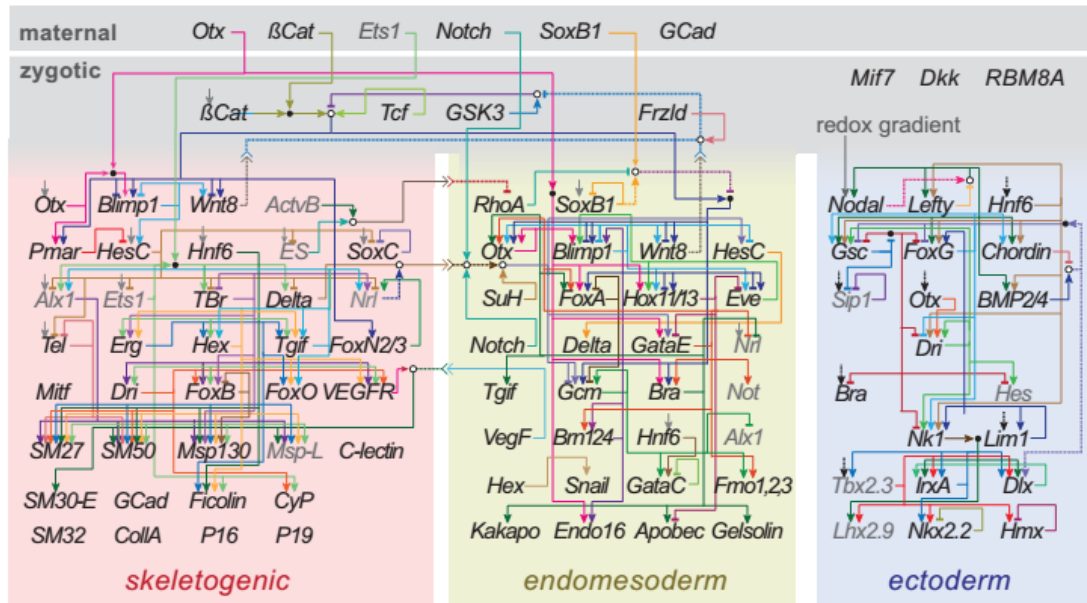
Fig. 12 Developmental gene regulatory network of *S. purpuratus*. The gene regulatory network begins when maternal transcripts and proteins (top) activate a cascade of subsequent gene regulatory interactions (adapted from Garfield et al., 2013).

The directional migration of PMCs is dependent on VEGF (vascular endothelial growth factor) and FGF (fibroblast growth factor) signaling (Duloquin et al., 2007; Röttinger et al., 2008). VEGF and FGF ligands are expressed in localized regions of the ectoderm that serve as PMC target sites, and the cognate receptor tyrosine kinases VEGF receptor (VEGFR) and FGF receptor (FGFR) are expressed exclusively in PMCs. Morpholino knockdowns and mRNA misexpression experiments that disrupt either *fgf* or *vegf* signaling result in aberrant PMC migration and skeletal patterning, and indicate that these pathways play non-redundant roles (Oliveri et al., 2008). In particular, overexpression of *vegf* leads to skeletal abnormalities, whereas inhibition of VEGF/VEGFR signaling results in incorrect positioning of the PMCs, downregulation of PMC-specific genes and loss of skeleton (Duloquin et al., 2007).

Univin is a growth factor of the TGF-β superfamily maternally deposited. It is required early for *nodal* expression during sea urchin development and it probably signals through the same receptor as Nodal, namely Alk4/5/7 (Range et al., 2007). *Univin* gene expression is progressively restricted to areas outlining a circumequatorial band at stages between cleavage and gastrula, and in the growing arms at the pluteus stage in *S. purpuratus* (Stenzel at al., 1994), actually at times and places consistent with a role in promoting skeletogenesis.

Both the regulatory (*alx-1, nodal*) and signaling (*vegf, vegfr, fgf, univin*) genes are necessary for the activation of a set of genes that encode for the skeletal matrix proteins needed for the deposition of the biomineral. These genes include *msp130, sm30, p16* and *p19*.

Msp130 (Mesenchyme Surface Protein 130) belongs to a family of echinoderm-specific proteins, probably involved in the uptake of Ca^{2+} ions from the blastocoelic fluid, facilitating their entrance into the PMCs (Leaf et al., 1987).

The *sm30* gene family of the sea urchin encode for proteins uniquely found in embryonic and adult mineralized tissues. The six *Sp-sm30* family members are strikingly similar, all encoding proteins containing similar c-type lectin domains, signal sequences and proline rich repeats. Five of the six gene transcripts are expressed in PMCs forming the embryonic skeleton (Killian et al., 2010) and encode for proteins occluded within the embryonic endoskeleton and adult mineralized tissues (Killian and Wilt, 1996). Some of the SM30 proteins are among the most abundant of the approximately four-dozen integral matrix proteins of the larval spicule (Killian and Wilt, 1996).

P16 and P19 are two small acidic proteins involved in the formation of the biomineralized skeleton of sea urchin embryos and adults, whose expression is restricted to PMCs throughout embryogenesis and is massively increased specifically from the late gastrula stage (Costa et al., 2012). P16 is required for normal elongation of the initial skeletal primordia but does not appear to be

critical for their formation and was demonstrated to be downstream of *alx1* in the *S. purpuratus* PMC GRN (Cheers and Ettensohn, 2005). Since the *p19* coding region lacks a signal sequence and transmembrane domains, it is supposed that the protein remains localized in the PMCs cytoplasm. The observed localization of the *Pl-p19* mRNA in the cell bodies and filopodial cytoplasm of all PMCs might suggest a role for *Pl*-P19 protein in the regulation of the circumference of the spicules (Costa et al., 2012).

1.7 Ecotoxicological approaches to the study of skeletogenesis

The correct development of the sea urchin embryo relies on an integrated network of genes, proteins and pathways, that also allow sea urchin embryos to defend themselves against various types of stressors, suggesting a function in both regulating defence and development. Genes involved in signal transduction often respond to environmental stress, activating alternative signaling pathways as a defence strategy for survival (Hamdoun and Epel, 2007). Experimental induction of skeleton malformations is a convenient tool to investigate the basic principles of skeleton formation and the signaling pathways involved in the process of skeletogenesis. Sea urchins are exposed to adverse conditions in the environment and they developed strategies to respond to these insults. Harmful ionizing radiation and heavy metals include some of the main environmental stress agents. These stressors impair biomineralization (fig. 13).
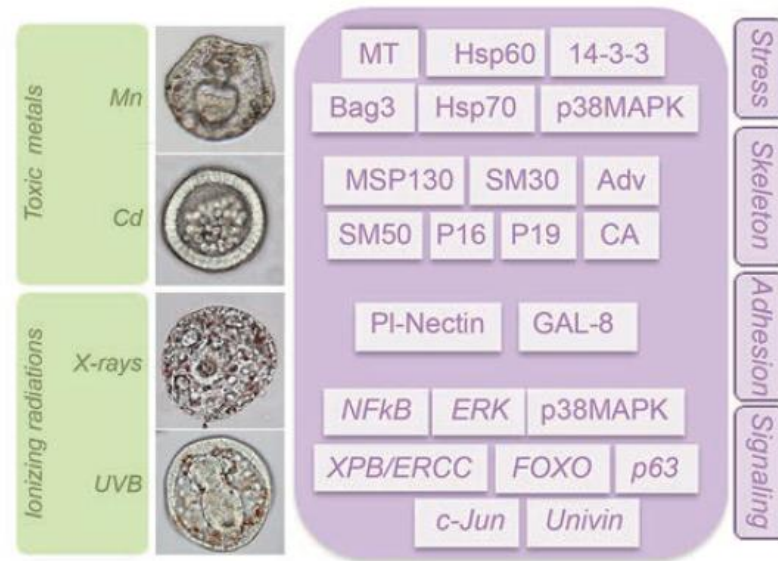
Fig. 13 Summary of skeletogenic genes and signaling pathways studied in P. lividus sea urchin embryos with experimentally induced skeleton malformations. On the left: malformed embryos exposed to manganese, cadmium, UV-B and X-rays. On the right: genes and proteins investigated in our studies were divided into four categories (stress, skeleton, adhesion, signaling) (from Matranga et al., 2013).

1.7.1 Ionizing radiation

In the marine environment, the transmission of solar ultraviolet radiation depends on many variables, as for example the presence of dissolved materials and phytoplankton in the water that in turn affect the amount and wavelength distribution of ultraviolet radiation (Häder et al., 2011). Ultraviolet radiation ionizes molecules inducing chemical reactions that can be harmful to organisms affecting DNA, proteins, and lipids (Dahms and Lee, 2010). The thinning of the atmospheric ozone layer is causing an increase in the levels of UVB rays that reach the Earth (El-Sayed et al., 1996). The UV-B rays can penetrate sea water to a depth of 30m or more (up to 50m in the Antartic Ocean), causing harmful effects on organisms during their embryonic life. Embryos and larvae of several marine organisms, including sea urchins, reside on the water surface and can be exposed to high levels of UVB, causing several developmental defects (Häder et al., 1995).

Several studies demonstrated the harmful effects of exposure to UVB radiation on embryos of different sea urchin species. *P. lividus* embryos irradiated during cleavage using UVB doses ranging from 0.01 to 0.8 kJ/m^2 showed abnormal morphologies at 24 h post irradiation At the highest doses used, i.e. 0.4 and 0.8 kJ/m^2 UVB, about 85.7% and 93.6% were abnormal embryos that lacked an organized epithelium and showed the blastocoelic cavity completely filled with cells (Bonaventura et al., 2006). This morphology was very similar to the so called "permanent" blastula, obtained irradiating *Hemicentrotus pulcherrimus* embryos with UVC at 0.038 and 0.45 kJ/m^2 (Amemiya et al., 1986), and to the so called "packed" blastula, obtained irradiating *S. purpuratus* embryos 20 min after fertilization onwards with PAR + UVA + UVB (with cycles of 12 h light/dark) (Adams and Shick, 2001).

Other natural ionizing radiations are X-rays, components of radionuclide emissions originating from space which do not penetrate the atmosphere. However, X-rays can be released from radionuclides directly and/or indirectly into the air, soil, and water, as for example in the case of nuclear accidents which cause radioactive contamination of the nearby areas, including the marine environment (IAEA-TECDOC-1429 2005). *P. lividus* sea urchin embryos exposed at the cleavage stage to different single doses of X-rays (from 0.1 to 5 Gy) showed a dose-dependent abnormalities (Matranga et al., 2010). When the highest dose was applied, i. e., 5 Gy corresponding to 5 Sv, nearly no embryos were able to develop normally, although no lethal effects were detected.

1.7.2 Heavy metals

Heavy metals, as they are not biodegradable and are persistent in the environment for long periods, cause serious eco-toxicological problems. In addition, some toxic metals may mimic essential metals and thereby gain access to important molecular targets (Chiarelli and Roccheri, 2012). Heavy metals can enter into organisms through food, drinking water and air. These are bio-persistent pollutants that accumulate at the top of the food chain. Heavy metals can enter a water supply by industrial and consumer waste, or even from acidic rain breaking down soils and releasing heavy metals into streams, lakes, rivers, and groundwater (Chiarelli and Roccheri, 2012).

Heavy metals and metalloids are dangerous because they tend to bioaccumulate. Bioaccumulation means an increase in the concentration of a chemical in a biological organism over time compared to its concentration in the environment. Compounds accumulate in living animals any time they are taken up and stored faster than they are broken down (metabolized) or excreted (Chiarelli and Roccheri, 2012).

Manganese-exposed *P. lividus* embryo were do not develop skeleton, although all the other morphological features remained amazingly unperturbed (Pinsino et al., 2011). The defects observed in *P. lividus* embryos continuously exposed to high sublethal Cd concentrations exhibit gut and abnormalities in skeleton elongation and patterning (Russo et al., 2003; Roccheri et al., 2004). After removal of Cd the embryos partially recovered a normal morphology showing a general delay in development, although 30% of the scored embryos showed aberrant skeleton morphologies (Roccheri et al., 2004). Longlasting exposure to Cd concentrations similar to those found in moderately or highly polluted seawaters, caused in *P. lividus* larvae severe developmental delays and abnormalities. This suggests that even very small amounts of Cd, if accumulated in cells, causes significant cytotoxic effects and extensive apoptosis (Filosto et al., 2008).

1.8 Molecular and cellular defense strategies against stress

Marine organisms are exposed to adverse changes in the environment. In response to stress, during evolution, marine organisms have developed various defense mechanisms, including activation of cellular and molecular strategies (synthesis of heat shock proteins, metallothioneins, apoptosis, and autophagy) to survive in adverse conditions (Hamdoun and Epel, 2007; Chiarelli and Roccheri, 2012). Heat shock proteins (HSPs) and metallothioneins produce a detoxifying and antioxidant effect that is not always sufficient to counter the toxic action of the pollutant, depending on the extent of cell damage (Samali and Cotter, 1996; Hamada et al., 1997). In such circumstances, the mechanisms of programmed cell death, such as apoptosis and autophagy, may be triggered, to remove the irreversibly damaged cells in order to maintain the integrity of the tissues.

Cellular death (CD) is defined as the process through which the functional organization of a cell is irreparable damaged: it's the so called "point-of-no-return" (Kroemer et al., 2009). Programmed cell death (PCD) is a physiological event in pluricellular organisms: the cells are able to exploit several methods to self-destroy, that lead to different morphological phenotypes (Bursch et al., 2000). Programmed cell death (PCD) and cell survival are two sides of the same coin. Autophagy and apoptosis are crucial processes during embryo development of invertebrates and vertebrates organisms, as they are necessary for the formation of a new organism, starting from a fertilized egg. Fertilization triggers cell remodeling from each gamete to a totipotent zygote.

Programmed cell death is a key physiological mechanism that ensures the correct development and the maintenance of tissues and organs homeostasis in multicellular organisms. This is classified into two types of PCD, according to the morphology of the dying cells and the molecular machinery involved:

- PCD-I: APOPTOSIS. Morphological signs include blebbing, cell shrinkage, nuclear fragmentation, chromatin condensation and chromosomal DNA fragmentation (Fig. 14). The nuclear envelope becomes discontinuous and the DNA is fragmented in a process referred to as karyorrhexis. The nucleus breaks into several discrete chromatin bodies or nucleosomal units due to the degradation of DNA. The cell then breaks apart into several vesicles called apoptotic bodies, which are then phagocytosed.

- PCD-II: AUTOPHAGY. This process relieves the cell from various stress conditions. Autophagy is a highly conserved cellular degradation process in which portions of cytosol and organelles are sequestered into a double-membrane vesicle and delivered into a degradative organelle, the vacuole/lysosome, for breakdown and eventual recycling of the resulting macromolecules (Klionsky et al., 2005).

1.8.1 Apoptosis

Apoptosis is a cellular phenomenon that orchestrates cell suicide following two main pathways: cytochrome *c* liberation from the mitochondria or activation of death receptors. This genetically controlled process is highly conserved during the evolution from nematodes to mammals, playing critical roles in both homeostasis and development during the morphogenesis and metamorphosis of invertebrates and vertebrates.

Cells undergoing apoptosis show a series of physical and biochemical changes such as plasma membrane blebbing (Fig. 15), loss of mitochondrial membrane potential, caspase-activation, DNA fragmentation and, finally, cell disintegration into apoptotic bodies subsequently engulfed by specialized cells. Phosphatidylserine (PS), a phospholipid normally asymmetrically expressed in the inner leaflet of the plasma membranes in living cells, during the final stages of apoptosis is actively extruded from the internal face of the

cell membrane of the dying cell; its exteriorization represents one of the markers that identify the cell as a target for phagocytosis (Hengartner, 2000).

It is well known that PCD-I is required to remove transitory structures, to sculpt tissues and to eliminate damaged cells that can be harmful to the organism (Agnello et al., 2015). On the other hand, apoptosis is also employed in response to environmental stimuli to remove cells damaged by chemical, physical and mechanical stress.
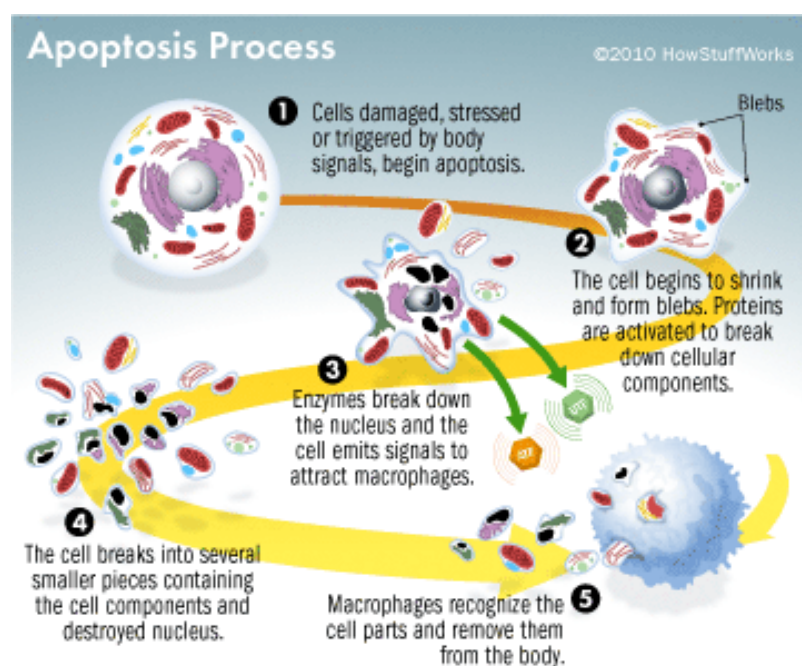
Fig 14 Main steps of the apoptotic process.

Embryos of different species, exposed to various toxicants or to physical or chemical stresses, temporarily slow down or suspend their development, eliminating the affected cells throughout apoptosis and thus altering the normal developmental program (Agnello et al., 2015). Sea urchin embryos use apoptosis both physiologically in the larvae undergoing metamorphosis and in response to chemical or physical stress (Agnello and Roccheri, 2010; Chiarelli et al., 2014).
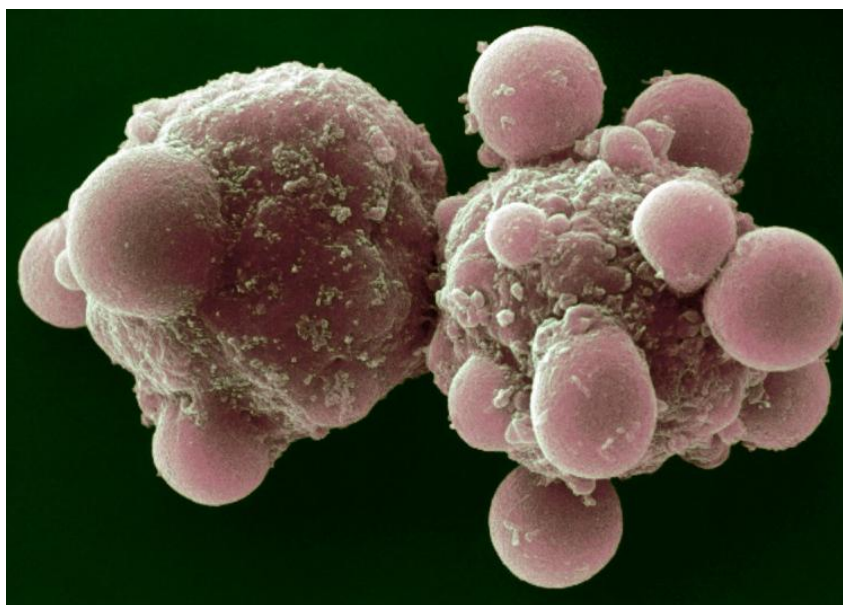
Fig. 15 Liver cells blebbing and undergoing apoptosis

1.7.2 Autophagy

Autophagy is the most important intracellular process by which eukaryotic cells sequester and degrade cytoplasm portions and organelles via the lysosomal pathway (Klionsky and Emr, 2000). It is essential for development, growth, and maintenance of cellular homeostasis in multicellular organisms and is able to prevent the accumulation of malfunctioning cellular structures.

There are three major types of autophagy in eukaryotic cells, mechanistically different from each other: macroautophagy, microautophagy, and chaperone-mediated autophagy (Klionsky, 2005; Massey et al., 2004). Microautophagy involves the direct engulfment of cytoplasm at the lysosome surface by invagination and protrusion of the lysosome membrane. In contrast, during macroautophagy, portions of cytoplasm are sequestered into a double-membrane vesicle, the autophagosome. Subsequently, the completed autophagosome fuses with the lysosome/vacuole and the inner single-

membrane vesicle is released into the lumen. On contrast, chaperone-mediated autophagy does not involve a similar type of membrane rearrangement; instead, it translocates unfolded, soluble proteins directly across the limiting membrane of the lysosome.

The macroautophagic process includes several steps (fig. 16): induction, cargo recognition and packaging, vesicle nucleation, vesicle expansion and completion, Atg (autophagy related gene) protein cycling, vesicle fusion with the vacuole/lysosome, vesicle breakdown, and recycling of the resulting macromolecules (Huang and Klionsky, 2007).
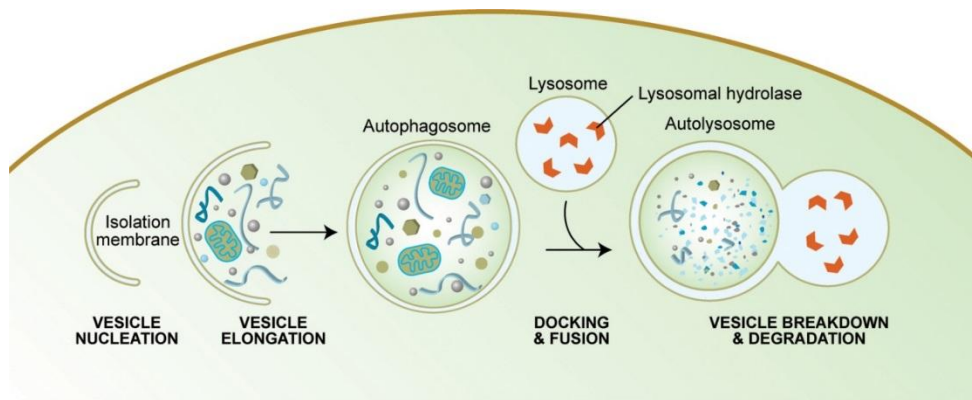
Fig. 16 Representations of the principal steps in macroautophagy
(adapted from Melendez and Levine, 2009)

During the engulfment of cytoplasmic components, the cytosolic form of the LC3 protein (LC3-I) is conjugated to phosphatidylethanolamine, forming LC3-phosphatidylethanolamine conjugate (LC3-II), which is then recruited to autophagosomal membranes. During the degradation by lysosomal hydrolases, LC3-II is degraded in the autolysosomal lumen. Thus, detecting an increase of LC3 by immunoblotting or immunofluorescence has become a reliable method for monitoring autophagy (Tanida et al., 2008).

Increased autophagy is usually induced by environmental conditions such as starvation, hyperthermia, hypoxia, salinity increase, bacterial or viral infections, accumulation of misfolded proteins and damaged organelles, toxic stimuli, radiation, and many other stress agents (Cuervo, 2004; Moore and Allen, 2006; Tasdemir et al., 2008). Autophagy can act as a cell survival mechanism if the cellular damage is not too extensive or as a cell death mechanism if the damage/stress is irreversible; in the latter case, it can operate as an independent pathway or together with the apoptotic one.

Since autophagy plays a key role under both physiological and pathological conditions in several animal species, the components of the autophagic machinery are evolutionarily conserved (Di Bartolomeo et al., 2010). The lysosomal-autophagic system appears to be a common target for many environmental pollutants as lysosomes are able to accumulate many toxic metals and organic xenobiotics (Moore et al., 2008).

The role of autophagy as cellular protective mechanism in aquatic invertebrates was investigated in bivalves, corals, and in the sea urchin embryos (Moore et al., 2006; Weis, 2008; Paxton et al., 2013; Chiarelli et al., 2011). Autophagy was reported for the first time in *Paracentrotus lividus* embryos by Chiarelli and colleagues in 2011, and it is now known as one of the most important cellular/molecular pathways triggered by sea urchin embryos both in physiological and stressfull conditions (Chiarelli et al., 2011).

2.   AIM OF THE WORK

The aim of this research is to investigate the effects of gadolinium, a metal of the lanthanide series, on the development of four sea urchin species: two from Europe, *Paracentrotus lividus* and *Arbacia lixula*, and two from Australia, *Heliocidaris tuberculata* and *Centrostephanus rodgersii*. Information of their sensitivity to Gd will aid in the understanding of the hazard posed and of the conserved morphological response across species to provide insights into potential mechanisms of Gd toxicity. Using different Gd concentrations, the dose-dependent responses to this agent were investigated at several different functional levels.

- <u>Development</u>: at the whole morphological level, the teratogenic effects of Gd on the morphogenetic success was determined; abnormal phenotypes were examined, categorised, compared among the four species, and the data analyzed to identify the sublethal concentrations to be used for risk assessment;

- <u>Differentiation</u>: at the cellular level, the localization of the PMCs, the only cells in the embryo involved in skeletogenesis, was investigated in response to Gd to verify their correct differentiation and placement;

- <u>Gd and Ca content</u>: to investigate the relationship between Gd exposure, skeleton growth and Ca uptake, the amount of Ca and Gd endogenous content inside embryos was determined;

- <u>Gene expression</u>: the expression of several genes of the skeletogenic network in embryos treated with Gd compared with control embryos was determined from three functional levels;

- <u>Apoptosis and autophagy</u>: the expression and localization of autophagy- and apoptosis-related proteins were investigated in Gd-exposed embryos compared to controls.

3. MATERIALS AND METHODS

*"Poison is in everything, and no thing is without poison.
The dosage makes it either a poison or a remedy."*

Paracelsus, XVI century

3.1 Embryo cultures, toxicological assays and recovery experiments

Adult *Paracentrotus lividus* and *Arbacia lixula* were collected along the North-Western coast of Sicily, Italy. *Heliocidaris tuberculata* and *Centrostephanus rodgersii* were collected near Sydney, Australia. Gametes were collected by routine methods (Pinsino et al., 2011; Byrne et al., 2013) and used for fertilization. Four independent experiments were performed for *P. lividus*, *H. tuberculata* and *C. rodgersii* and two for *A. lixula* (see Table 1), with gametes obtained from at least two males and two females. Embryos were reared at 18°-2°C in Millipore filtered seawater (MFSW) in the presence of antibiotics only for the European species (30 mg/L penicillin and 50 mg/L streptomycin sulfate). Just after fertilization, embryos were exposed to different concentrations of Gadolinium Acetate Tetrahydrate (GAT, Waco). GAT was freeze-dried before weighing and usage to remove the hydrated surface (Scanvac CoolSafe). To minimize the volumes to be used for the assessments of Gd toxicity, exposures were carried out in 24-multiwell plates (Cellstar, Greiner Bio-One), with 2000 embryos per well in 2 ml.

P. lividus was used in preliminary experiments to assess the Gd concentration range causing developmental abnormalities and with respect to results with *Hemicentrotus pulcherrimus, Pseudocentrotus depressus* and *Heliocidaris crassispina* (Saitoh et al., 2010). Specifically, we used doses increasing by a factor of 5 (from1 to 125 µM) and found about 50% of abnormal embryos at the lowest dose, and 100% lethality at the highest dose tested. A similar approach was used for the other three species under investigation, with final Gd concentrations used ranging from 1 nm to 200 µM. For each experiment 50 embryos from three different wells were sampled at the two developmental stages, gastrula (24 h post fertilization-hpf) and pluteus (48 hpf), as in previous studies (Bonaventura et al., 2005; Pinsino et al., 2011). In some experiments, a total number of 100 or 300 embryos were sampled (see Table 1). Embryos were examined microscopically (Zeiss Axioscop 2 plus or Olympus BX60), photographed using a digital camera and scored for normal/abnormal development (see below).

Embryos at different developmental stages were collected by low-speed centrifugation and either fixed in 4% paraformaldehyde in MFSW for immunofluorescence studies or immediately frozen in liquid nitrogen and stored at −80°C for subsequent protein or RNA extraction.

To obtain information on the reversibility of the exposure in *P. lividus* embryos, Gd was removed after 24h of development/exposure by washing the embryos three times in MFSW by hand centrifugation. Subsequently, embryos were cultured in MFSW and monitored by optical microscopy during the next 24h recovery phase.

Table 1. Summary of experiments performed on the four sea urchin species

Species	N° Exp	Exp	N° of counts	Gd Concentrations																					
				nanoMolar										microMolar										
				0	1	10	25	50	100	125	250	500	800	1	2.5	5	10	20	40	50	80	100	150	200
P.lividus	4	#1	1*	0										1	2.5	5	10	20						
		#2	1*	0										1	2.5	5	10	20						
		#3	1*	0										1	2.5	5	10	20	40					
		#4	3	0							250	500	800	1	2.5	5	10	20	40		80	100		
A.lixula	2	#1	3	0							250	500		1	2.5	5	10	20	40		80	100		
		#2	3	0							250	500		1	2.5	5	10	20	40		80	100		
H. tuberculata	4	#1	1+	0										1	2.5	5	10	20						
		#2	1+	0						125	250	500	800	1	2.5	5	10	20						
		#3	1+	0	1	10	25	50	100															
		#4	1+	0	1	10	25	50	100	125	250	500	800											
C. rodgersii	3	#1	3	0										1	2.5	5	10	20						
		#2	3	0										1	2.5	5	10	20	40	50	80	100		
		#3	3	0															40	50	80	100	150	200
		#4	3	0																			150	200

1*: for *P.lividus*, a total number of 300 embryos were scored for normal/abnormal development.
1+: for *H. tuberculata*, a total number of 100 embryos scored for normal/abnormal development.

3.2 Toxicity criteria

The four species were chosen because of their comparable developmental timeline. At 48 hpf, embryos of all species have reached the pluteus stage, where a tri-partite gut and larval arms could be observed in control embryos. Exposure to Gd resulted in major alterations or inhibitions of skeleton growth at the final endpoint (48 hpf). Thus, abnormal embryos were categorized into five morphotypes, as sketched in Fig. 17: CS, complete skeleton: larvae with a regular skeleton; NS, no skeleton; SS, shorter skeleton: skeleton arm rods shorter than controls; AS, asymmetrical skeleton: larvae with a left-right (LR) asymmetry in skeleton rods. For *H. tuberculata* and *C. rodgersii* we identified one additional category, called LP, lost pattern, characterized by an incorrect growth and branching of the skeletal rods. The percentage of each skeleton category in the larvae examined from each of the three wells (per fertilization) was determined and used as the datum for statistical analysis.
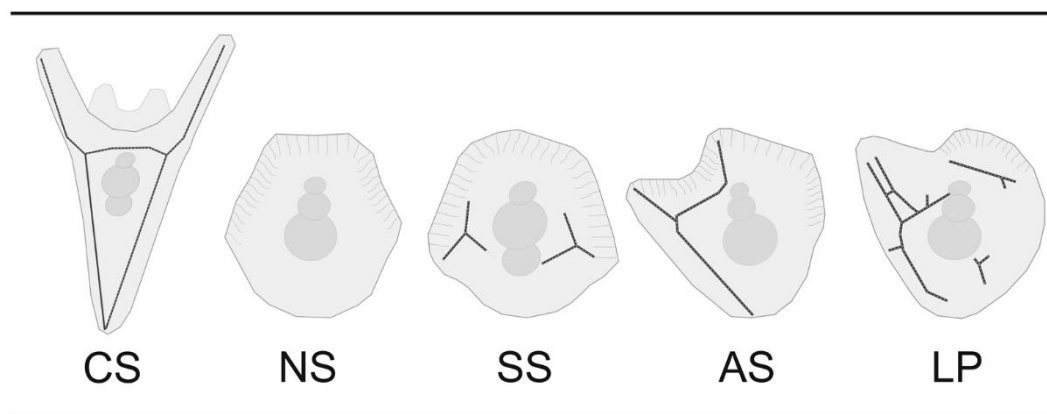
Fig. 17 Sketches of the five morphotypes observed and categorised on the basis of skeleton occurrence, abnormality and asymmetry. CS, Complete Skeleton; NS, No Skeleton; SS, Shorter Skeleton; AS, Asymmetrical Skeleton; LP, Lost Pattern (from Martino et al., 2016).

3.3   Statistical analysis

The dose-response curves of the four species were calculated plotting the percentages of embryos bearing an abnormal skeleton (Fig. 6: NS, SS, AS and LP embryos) across increasing Gd concentrations. Two ecotoxicological parameters were determined: EC50, the half maximal effective concentration, that represents the concentration where 50% of Gd maximal effect is observed, and the NOEC, no observed effect concentration, the highest concentration of a substance at which no adverse effect is found in exposed organisms. The EC50 values for each Gd-experiment performed were determined using the SigmaPlot 13.0 analysis software (Systat Software, Inc., San Jose, California, USA). The EC50 values were analyzed by the one-way ANOVA on the data for three species (except for *H. tuberculata* due to insufficient replication) with species as the fixed factor. The analyses were performed using the OriginPro 8.1 (OriginLab Corp., Northampton, MA, USA), and the level of significance was set to P ≤ 0.05. The percentage data determined for each of the morphological categories observed were analysed by the one-way analysis

of variance (ANOVA) with Gd concentration as the fixed factor and individual skeletal morphology as the response variable. Tukey's HSD test was used as Post-hoc test for mean comparison. Additionally, two-way ANOVAs were run with Gd concentration and species as the fixed factor and individual skeletal morphology as the response variable. Homogeneity of variance and normality were checked using the Levene's and Shapiro-Wilk tests, respectively. The Shapiro-Wilk normality test showed that all data was significantly drawn from a normally distributed population, except for the concentrations corresponding to percentages all equal to zero or very similar. The data for the skeleton categories of *H. tuberculata* were not analyzed by ANOVA tests as there were only two replicates for each Gd concentration (see Table 1).

3.4 Gadolinium and Calcium determination

Frozen embryos were prepared for metal determination by acid digestion in 70% HNO_3/30% H_2O_2 (v/v 2:1) at 150°C in oil bath. The dried residues were reconstituted in 0.2% HNO_3 and analyzed for metal contents by Flame Atomic Absorption Spectrometry using a Perkin Elmer Analyst 800 apparatus.

3.5 SDS-PAGE and Western Blot

At 24 and 48 hours of development the *P. lividus* embryo cultures from Petri dishes were collected in 50mL centrifugation tubes. The centrifugation tubes were spun at 1000rpm at 4°C for 2 minutes. The pellets were resuspended in 1mL of the supernatant in 1.5mL microtubes. The microtubes were span at 1000rpm at 4°C for 2 minutes. The supernatant was discarded, and the pellets were frozen in liquid nitrogen. The pellets were stored at -20°C or -80°C for long term storage. Pellets of control and Gd-exposed embryos were homogenized in lysis buffer (7 M urea, 1% IPG, 2% CHAPS and 10 mM

DTT) containing protease inhibitors cocktail tablets (Roche, 1836170). Protein concentration was evaluated using the Bradford method and 40 µg of samples were analyzed by SDS-PAGE (13% gel). The molecular masses were evaluated by comparison with a set of standard proteins (Fermentas, SM0671). After electrophoretic separation, the proteins were transferred and immunoreacted. Specifically, the antibodies adopted were: rabbit polyclonal anti-LC3 (Sigma-Aldrich, L8918) and anti-actin (Sigma-Aldrich, A5060) diluted respectively 1:1000 (overnight incubation) and 1:500 (1 h incubation) in 5% nonfat dried milk powder (EuroClone, EMR180500)/TBS-T (20 mM Tris, pH 7.6, 137 mM NaCl, 0.1% Tween 20). As secondary antibody we used an anti-rabbit IgG (Fc) horseradish peroxidase-conjugated (Promega, S373B), diluted 1:2,500 in TBST (1 h incubation). Bands were detected by ChemiDoc Imaging System (BioRad), analyzed by the ImageJ software (BioRad) and normalized with respect to the corresponding values obtained with the anti-actin antibody reaction.

3.6 Immunofluorescence

Immunofluorescence was performed on *P. lividus* whole-mount control and exposed fixed embryos. Each sample was incubated for 1 h at room temperature in blocking solution: 0.5% albumin from bovine serum (Sigma-Aldrich, A7906) and 5% heat inactivated goat serum (Sigma-Aldrich, G9023) in PBS-T (phosphate-buffered saline, 0.1% Tween 20) and overnight at 4°C with the following antibodies: anti-LC3, 1:125 diluted in blocking solution; anti-cleaved caspase 3, 1:100 diluted in blocking solution. In the negative controls, the primary antibody was omitted. After rinsing with PBS-T, embryos were incubated with a fluorescein conjugated secondary antibody anti-rabbit IgG (whole molecule)-FITC, developed in goat (Sigma-Aldrich, F0382 and F0257 resp.), 1:50 diluted in blocking solution. The nuclei were stained with propidium iodide for 5 min. Samples were mounted on glass in 80% glycerol/PBS-T. The observations were performed using a Confocal

Laser Scanning Microscopy (Olympus FV10i). Several optical sections (10μm thick) of embryos were acquired using a Nikon camera. Image acquisition was performed measuring the intensity of autofluorescence in the negative control; this value becomes the threshold level for the capture of other samples.

For immunostaining with fluorescein isothiocynate conjugated wheat germ agglutinin (WGA-FITC), embryos were incubated with WGA-FITC (SIGMA 2 mg/mL, 1:400 in MFSW) for 30 min at room temperature, in the dark, then washed three times in MFSW, and finally observed under a Zeiss Axioskop 2 Plus microscope, equipped for epifluorescence and recorded by a digital camera system.

3.7   Acridine orange vital staining

Acridine Orange (AO) is a metachromatic, fluorescent cationic dye, which moves freely across biological membranes, emitting green fluorescence in the monomeric form while interacting with nucleic acids, and red fluorescence in the bi/oligomeric form, related to the protonation of acidic vesicular organelles (AVOs). To detect AVOs on whole-mount embryos, *P. lividus* control and Gd-exposed embryos at different development times were incubated with AO (SIGMA-ALDRICH, A-6014) at 5 μM final concentration, for 1 min. Then, the embryos were washed twice with Millipore filtered sea water to remove the excess dye and observed using a CLSM (Olympus FV10i). Image acquisition and analysis were performed as described by Morici and colleagues (2007).

3.8 One Step RT-PCR

RNA from the control and the gadolinium-exposed embryos was extracted from previously frozen pellets, collected in three different experiments and at three developmental endpoints: 6, 24 and 48h. The extraction of the RNA from the *P. lividus* embryos was performed using the GenElute Mammalian Total RNA Miniprep Kit™ (Sigma), while the extraction of the RNA from the Australian species was performed using the RNeasy Mini Kit (Qiagen). Residual DNA was eliminated by DNase I (Sigma) digestion. The RNA was then quantified by readings at 260 nm using an Eppendorf bio-photometer or a NanoDrop Spectrophotometer (Thermo Scientific).

The Superscript One-Step RT-PCR kit (Invitrogen) was used for comparative single-step reverse transcription-polymerase chain reactions (RT-PCR) (Bonaventura et al, 2011).

For *P. lividus,* nine different cDNA fragments were amplified by specific primers from total RNA. The cDNA fragments have the following sizes: 364nt-VEGF, 356nt-vegfr, 415nt-alx1, 543nt-p16, 515nt-p19, 517nt-msp130, 446nt-univin, 174nt-nodal, 159nt-fgf and 220nt-s24. The primers for vegf, vegfr, alx1, p16, p19, msp130, univin, and s24 were kindly provided by Dr. Caterina Costa (Istituto di Biomedicina e Immunologia Molecolare, Consiglio Nazionale delle Ricerche, Palermo), while the primers for nodal and fgf were kindly provided by Dr. Vincenzo Cavalieri (Dipartimento STEBICEF, Università degli Studi di Palermo). S24 is a transcript that encodes a ribosomal protein of the *P.lividus* embryo (Sgroi et al, 1996) and it was used as internal reference as it is constantly expressed during development (Zito et al, 2003; Bonaventura et al, 2011).

For *H. tuberculata,* eight different cDNA fragments were amplified from total RNA: 548nt-vegf, 824nt-fgf, 847nt-nodal, 829nt-lefty, 835nt-bmp, 771nt-msp130, 600nt-sm30, 771nt-z12. Z12 mRNA, which encodes a zinc-finger

transcription factor, was used as the internal endogenous reference gene, as it was found to be constant during development (Costa et al., 2012).

The One Step RT-PCR was performed for 30 min at 50°C (reverse transcriptase), then a denaturation step for 2 minutes at 94°C followed by a specific number of cycles (26 to 35) keeping a logaritmic trend in every reaction: 94°C, 15 sec; 54-55°C, 30 sec; 72°C, 30 sec. After amplification, a final extension step for 10 min at 72°C was performed. The analysis of the whole RT-PCR reactions was done by electrophoresis on agarose gel: 2% for *P. lividus* PCR products, 1.5% for *H. tuberculata* PCR products; stained respectively with Ethidium Bromide and EZ-VISION dye (Amresco). Quantification of the band intensities of each amplification product was done by respectively the GelDoc1000 imaging detection system (BioRad) and the FluorChem E digital imaging system (Alpha Innotech). Densitometric analysis was then performed using the Quantity One image analysis software, version 1.1 (BioRad). The comparison of relative expression levels of the genes between control and Gd-exsposed embryos were obtained after normalizing measurements of amplicon band intensities to the values of S24 for *P. lividus,* and of Z12 for *H. tuberculata*.

4. RESULTS

The Elegance of the Sea Urchin

4.1 Gd toxicity dose-response curves in phylogenetically distant species show divergent levels of sensitivity

This study determined the response to Gd in the four sea urchin species (two from the Mediterranean, *P. lividus* and *A. lixula*, and two from Australia, *H. tuberculata* and *C. rodgersii*). The morphology of control embryos raised in normal seawater was compared with that of embryos raised in seawater containing different concentrations of Gd. Control embryos developed through the gastrula stage (24 hpf) and subsequently reached the pluteus larvae (48 hpf), characterized by the presence of a fully-developed skeleton.

In response to Gd, a decrease in the percentage of CS embryos (complete skeleton, see Fig. 17 in section 3.2) was observed in all four species, in parallel with the increase of the Gd concentration tested, with species-specific differences in sensitivity. The dose-response curves showing the response with respect to skeleton formation are shown in Figure 18. The EC50 values were: 56 nM for *H. tuberculata*; 1.18 µM for *P. lividus*; 2.1 µM for *A. lixula* and 132 µM for *C. rodgersii*. Thus, there was a three-order magnitude of difference between the EC50s of *H. tuberculata* and *C. rodgersii* values and a two-order magnitude of difference between the EC50s of *P. lividus*/*A. lixula* and *H. tuberculata*.
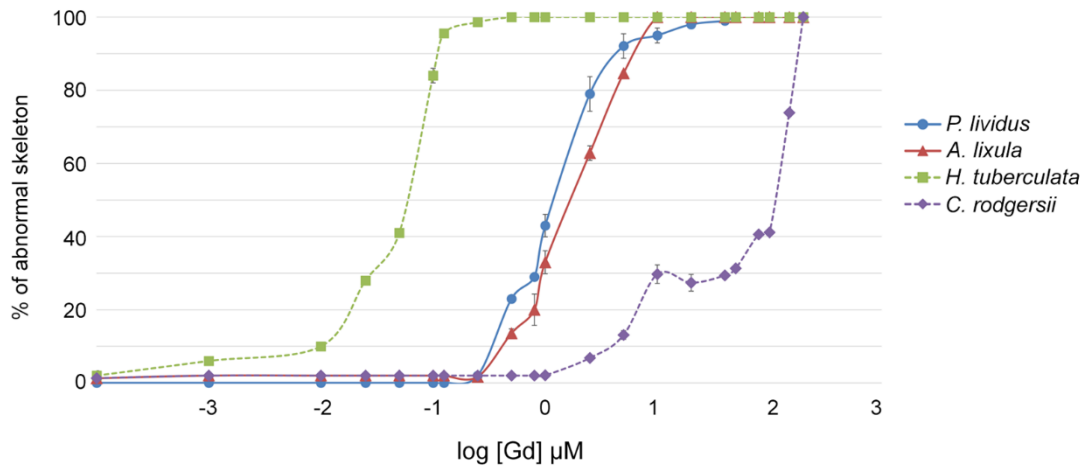
Fig. 18 Concentration-dependent effects of 48 h Gd exposure on abnormal skeleton formation. Percentages of embryos bearing an abnormal skeleton are plotted across increasing Gd concentrations in seawater (from Martino et al., 2016).

The NOEC values, calculated empirically on the basis of the observed effects, were: 1 nM for *H. tuberculata*; 250 nM for *A. lixula*; 250 nM for *P. lividus* and 1 μM for *C. rodgersii*.

One-way ANOVA revealed significant differences for the EC50 of *P. lividus, A. lixula* and *C. rodgersii* (F = 482,27; P = 2,32·10^{-14}).

There were significant differences in the percentage of the CS embryos in the control and Gd-exposed embryos (Table 2). The pair-wise comparisons (Tukey HDS Post-hoc Test) showed that the mean percentages of CS embryos for 5, 10 and 20 μM Gd concentrations to 0 μM Gd (control embryos), differed (P < 0.05, data not shown). Gd concentrations among sea urchin species had significant effects on the categorized skeletal morphologies (Two-way ANOVA, Table 3).

Species	Morph.	DF	F Value	P Value
P.lividus	CS	11	262.60	0
	NS	11	39,49	0
	SS	11	25,95	$1{,}887 \cdot 10^{-15}$
	AS	11	20,27	$1{,}469 \cdot 10^{-13}$
A.lixula	CS	10	763,08	0
	NS	10	171,01	0
	SS	10	91,03	0
	AS	10	37,54	0
C.rodgersii	CS	11	464,65	0
	SS	11	717,87	0
	AS	11	67,99	0
	LP	11	37,40	0

Table 2: Effects of Gd concentrations on the categorized skeletal morphologies (One-way ANOVA). P value < 0.05 indicated that Gd concentrations had significant effects on skeleton morphologies. DF, degree of freedom: number of Gd concentrations to which embryos were exposed, including zero concentration (control embryos), minus 1.

4.2 Gadolinium exposure perturbs skeleton growth and pattern

Control embryos of the four species were gastrulae after 24 hr of development, with visible triradiate rudiments (fig. 19 A-C, see arrows), except for *C. rodgersii* (fig. 19 D) that forms the rudiments a few hours later. Embryos continuously exposed to Gd from fertilization showed no major effects until gastrulation, with timing of endoderm invagination and gut formation equal to controls (fig. 19, see asterisk), correct PMCs migration and clustering and a slight delay in biomineral deposition, with either no visible deposition or only the first calcite crystal (fig. 19 E-H, see arrows). In both controls and Gd-exposed embryos, the cells of the aboral ectoderm flatten from their original cuboidal shape to form a squamous epithelium, while the cells of the oral

ectoderm remain thickened. These morphogenetic features, taken as cues to identify the correct differentiation of the ectoderm (Cameron et al,. 1993), were correctly observed in Gd-exposed embryos.
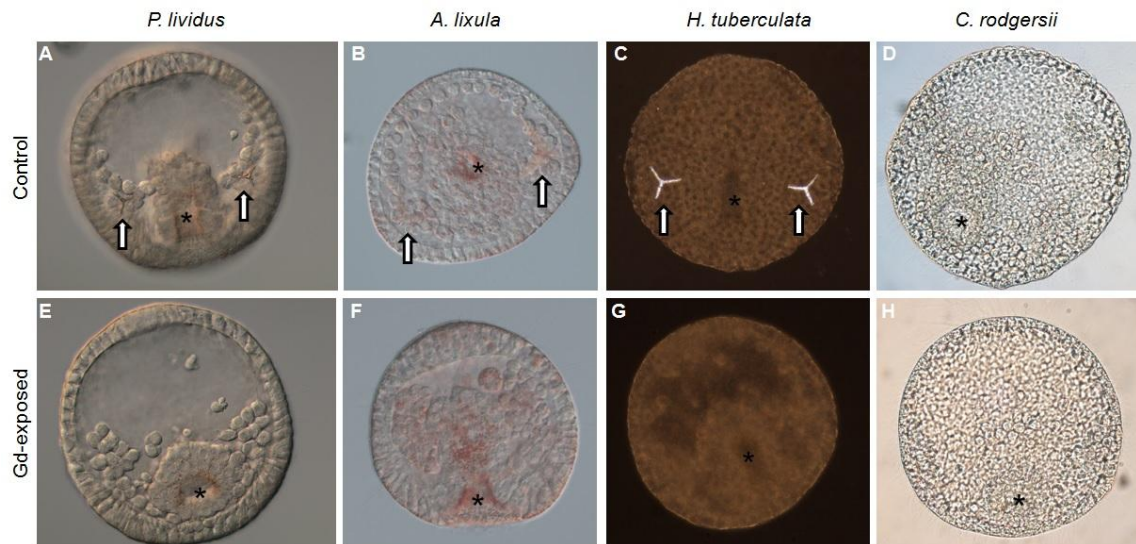
Fig. 19 Control (A-D) and Gd-exposed (E-H) embryos of the four species after 24 h of development. Arrows and asterisks indicate triradiate rudiments and gut formation, respectively.

At 48 hpf, control embryos of all the four species were plutei with a tri-partite gut and well-developed skeleton, with species specific evident differences (Fig. 20 A-D). Specifically, *P. lividus* plutei (Fig. 20 A) have an elongated body, with unfenestrated skeletal rods typical of Echinidae (Emlet, 1982; Zito et al., 2015). *A. lixula* plutei (Fig. 20 B) have fenestrated postoral rods and a robust apical dentate rostrum with a variable number of 7-9 teeth. The plutei of *H. tuberculata* (Fig. 20 C) are more truncated and their skeleton forms a robust and intricate basket-structure, with solid ladder-like fenestrated rods typical of the Echinometridae (Kinjo et al., 2008). The plutei of *C. rodgersii* (Fig. 20 D) are generally referred to as two-armed larvae (Soars and Byrne,

2015) because of their very long postoral arms in comparison to the short anterolateral arms, characteristic form of many diadematids (Emlet et al., 2002).

At 48 hpf, differentiation of ectoderm territories into the columnar epithelium at the animal pole and the squamous epithelium at the vegetal pole also appeared normal in Gd-exposed embryos (see Fig. 20 E, F, K, P). Gd also had no apparent effect on normal tripartite gut development, as shown for *P. lividus* (Fig. 20 E, H, L) and *C. rodgersii* embryos (Fig. 20 K, O, Q).

Morph.	Factors	DF	F Value	P Value
CS	Gd Conc.	14	96.55	0
	Species	2	320.70	0
NS	Gd Conc.	14	16.86	0
	Species	2	103.64	0
SS	Gd Conc.	14	13.00	0
	Species	2	94.90	0
AS	Gd Conc.	14	73.42	0
	Species	2	118.14	0

Table 3. Effects of Gd concentrations among sea urchin species on the skeletal morphologies (Two-way ANOVA). DF: Degrees of Freedom. P value < 0.05 indicated that among species, Gd concentration had significant effects on the categorized skeletal morphologies.

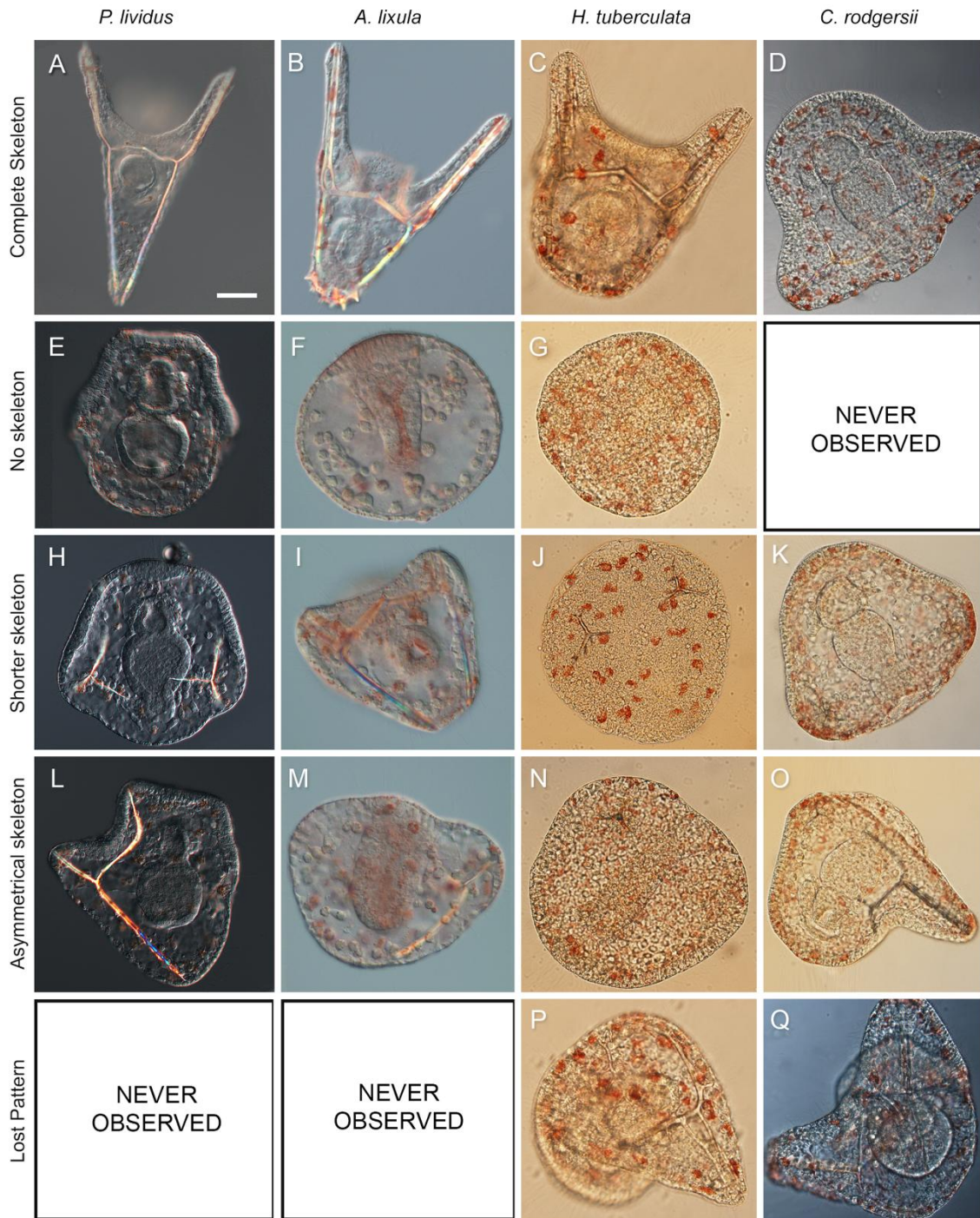| | *P. lividus* | *A. lixula* | *H. tuberculata* | *C. rodgersii* |

Fig. 20 Representative pictures of the morphotypes occurring after Gd exposure show severe impairments of skeleton growth and patterns. Control (A-D) and Gd-exposed (E-Q) embryos after 48 h of development. Bar = 50 μm in A-D, G, J, K, N-Q; 25 μm in E, F, H, I, L, M (from Martino et al., 2016).

After 48 hpf of Gd exposure, impaired skeleton development was evident with a range of skeletal abnormalities (Figs. 17 and 20), including complete skeleton (CS, Fig. 20 A-D), no skeleton (NS, Fig. 20 E-G), shorter skeleton (SS, Fig. 20 H-K) and asymmetrical skeleton (AS, Fig. 20 L-O). The lost pattern category was only seen in *C. rodgersii* and *H. tuberculata* (LP, Fig. 20 P-Q). A summary of the occurrence of the morphotypes observed in the presence of different concentrations of Gd is shown in Fig. 21. There was a significant effect of Gd concentration on the percentage of the skeletal morphologies observed (Table 2).

Morph.	Species	Mean Diff	SEM	q Value	Prob	Sig
CS	Al-Cr	-31.73	2.15	20.84	0	1
	Pl-Cr	-34,81	2.28	21.58	0	1
	Pl-Al	-3,07	2.36	1.83	0.39	0
NS	Al-Cr	1.09	1.32	1.17	0.68	0
	Pl-Cr	17.85	1.39	18.10	0	1
	Pl-Al	16.75	1.44	16.38	0	1
SS	Al-Cr	6.79	1.54	6.20	$5.70 \cdot 10^{-5}$	1
	Pl-Cr	12.24	1.62	10.63	0	1
	Pl-Al	5.45	1.68	4.56	0.0042	1
AS	Al-Cr	1.09	1.32	1.17	0.68	0
	Pl-Cr	17.85	1.39	18.10	0	1
	Pl-Al	16.75	1.44	16.38	0	1

Table 4. Tukey HSD Post-hoc Test, Pair-Wise comparison between species considering the effects of Gd concentrations on the categorized skeletal morphologies by the Anova two-way analysis. SEM: standard error of the mean. Sig equals 1 indicates significant that the means difference is at the 0.05 level.
Sig equals 0 indicates that the means difference is not significant at the 0.05 level.
Pl: *P. lividus*
Al: *A. lixula*
Cr: *C. rodgersii*
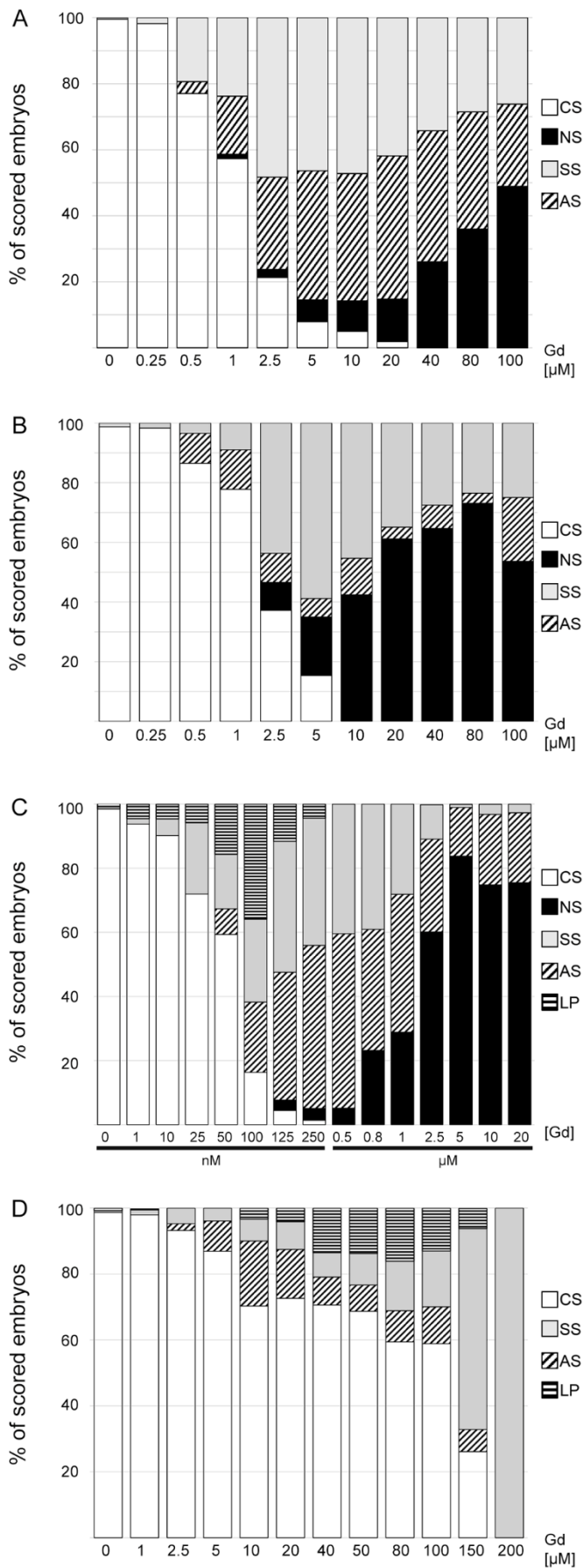
Fig. 21. Impairment of skeleton growth and pattern correlates with the exposure to increasing Gd concentrations. *P. lividus* (A), *A. lixula* (B), *H. tuberculata* (C) and *C. rodgersii* (D) embryos after 48 h of development. Bars in the histograms show the percentages of observed phenotyes: white: CS (complete skeleton); black: NS (no skeleton); grey: SS (shorter skeleton); oblique strips: AS (asymmetrical skeleton); horizontal strips: LP (lost pattern). Standard deviation values ranged from 0.0004 to 0.06 for all samples (from Martino et al., 2016).

For *P. lividus*, the SS category initially increased with the increase of Gd concentration (48.30% ± 0.06 SD at 2.5 μM), as for *A. lixula* (58.82% ± 0.03 SD at 5.0 μM) (Fig. 21 A and B). At Gd concentrations higher than 2.5 μM (*P. lividus*) and 5.0 μM (*A. lixula*) the SS category decreased, in parallel with the increase of the NS morphotypes, probably occurring because of the high Gd dose used. The AS morphotype was infrequent in *A. lixula* (Fig. 21 B), but common in *P. lividus* with a peak percentage of 43.41% (±0.05 SD) at 20 μM (Fig. 21 A). At higher concentrations (100 μM), the incidence of the most severe phenotype (NS) increased (48.85% ± 0.01 SD) in *P. lividus*.

The most sensitive species to Gd exposure was *H. tuberculata* (Fig. 21 C). Beyond the 250 nM threshold there were no CS larvae and the skeleton was absent at concentrations above 5 μM (NS embryos). The peak percentages of the SS, AS and LP morphotypes were reached at 40.80% (±0.03 SD) at 125 nM, 54.38% (±0.03 SD) at 0.5 μM, and 36.00% (±0.0015 SD) at 100 nM, respectively, and decreased at higher Gd doses tested. In contrast, *C. rodgersii* was far less sensitive than the other three species (Fig. 4D). Very low amounts of SS (4.72% ± 0.01 SD) and AS (2.07% ± 0.007 SD) morphotypes were observed at 2.5 μM. The amount of CS embryos decreased in a dose-dependent manner, but as much as 26.14% (±0.02 SD) of the normal morphologies were present even at high Gd concentration (150 μM). Differently from what observed in the other species, in *C. rodgersii* the AS category was represented by embryos with a completely full-sized spicule on one side only, never shorter than that of controls, with the highest percentage of 19.74% (±0.01SD) at 10 μM. The LP morphotype reached the amount of 16.10% (±0.02 SD) at 80 μM and then gradually decreased at higher doses. In contrast with what we observed in the other three species, the NS phenotype was never observed in *C. rodgersii* even at the highest concentration tested (200 μM). In this latter treatment, the SS category was 100% (Fig. 21 D).

The effects of Gd concentration with respect to each morphological category for *P. lividus, A. lixula* and *C. rodgersii* were significant (Table 2). For *P.*

lividus, the data of skeletal morphologies analyzed by ANOVA included values of 0.8 μM Gd concentration (see Table 2) not shown in Fig. 21. The effects of Gd concentrations per each morphological category and across the three species were significant ($P < 0.05$). The pair-wise tests between species (Tukey HSD, Table 4), revealed significant differences. For two species, *P. lividus* and *A. lixula* the responses to Gd of the CS category was not significantly different (Table 4), because the percentage of CS embryos in these species was similar (Figs. 18 and 21, Table 4).

4.3 Asymmetric spicule formation occurs on either left or right side

At this point, we had to select a concentration that would be used for all the further experiments in *P. lividus* embryos. We chose to use from now on the 20 μM concentration as it is the dose at which we observed the highest percentage of AS embryos (43.41% ±0.05 SD), but also all the other morphotypes are present (see Fig. 21 A).

To understand if in AS embryos the growing spicule was formed always on the same side of the blastocoel, three experiments were carried out during which about 100 *P. lividus* AS embryos were examined after 48 hours of development. Asymmetric spicule formation was observed on both sides, with an occurrence of ~45% right-sided embryos and ~55% left-sided embryos (fig. 22).

This result demonstrate that the side of the asymmetric spicule formation is random in Gd-exposed embryos.

Fig. 22 Asymmetric spicule formation occurs on either side of left (A) or right (B). *P. lividus* embryos were cultivated in 20μM gadolinium containing seawater for 48 hours. The blastopore can be seen in the centre of each embryo (see arrows).

4.4 Embryos show partial reconstitution of spicules growth after Gd removal

It was important to determine whether Gd removal at the time of triradiate formation (24hpf) could lead to the complete recovery of skeleton growth. To investigate this hypothesis, we performed a recovery experiment in which *P. lividus* embryos exposed to 20μM Gd for 24h were transferred and cultured in fresh seawater for further 24h. Embryos were then scored for the morphological analysis at 48 hpf.

Results indicate that recovered embryos partially resume skeleton elongation, presenting longer spicules than embryos continuously exposed to Gd for 48h. However, the skeleton patterns were strongly perturbed (fig. 23): after 24h of recovery, only 5% of the embryos developed a complete skeleton with the correct pattern (CS morphotype, against 0.83% of embryos continuously exposed to Gd for 48h, see Fig. 21 A), 10% were AS embryos, 2.5% were NS embryos, and 82.5% had longer spicules with incorrect pattern (LP category).
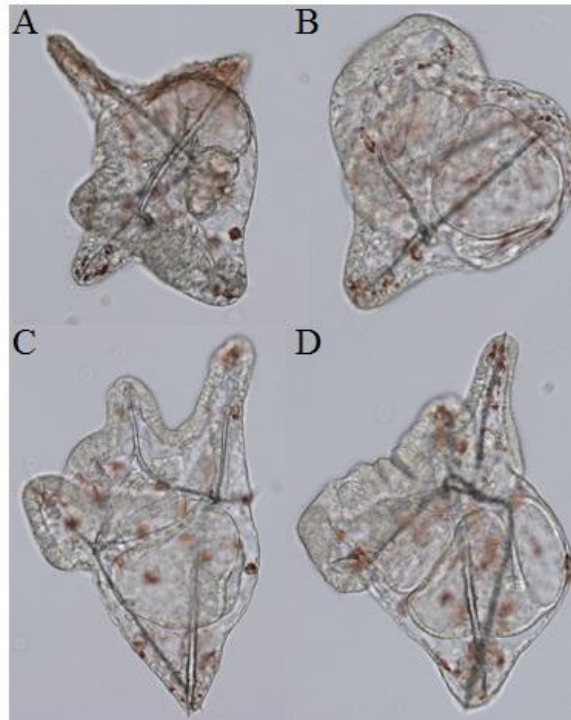
Fig. 23 Representative *P. lividus* embryos exposed to 20μM Gd for 24h, and then cultured in fresh MFSW for a following period of 24 h and microscopically inspected.

4.5 PMCs differentiation and migration occur normally in Gd-exposed embryos

To investigate the PMCs differentiation and migration in Gd-exposed embryos, *P. lividus* embryos were stained with WGA-FITC, a fluorochrome-conjugated lectin that specifically recognizes a PMC-specific cell surface protein. Immunostaining showed that at 24hpf, PMCs maintained the capacity to migrate and correctly pattern inside the blastocoel, as they do in control embryos (compare fig. 24 A with fig. 24 B). At 48 hpf, when in control embryos (pluteus stage) the PMCs were localized along the developing spicules (fig. 24 C), in SS Gd-exposed embryos these cells were mostly distributed around the immediate ring area similarly to what observed in controls at the previous gastrula stage (fig. 24 D). On the contrary, in AS embryos PMCs were found along the growing spicule, while on the other side

(the site of the lacking spicule) they were still found forming a cell cluster (see fig. 24 E). Immunostaining showed that the total number of PMCs present at 48 hpf in Gd-exposed embryos of all morphotypes was equal to the number of PMCs found in controls (~38 cells, Table 5).
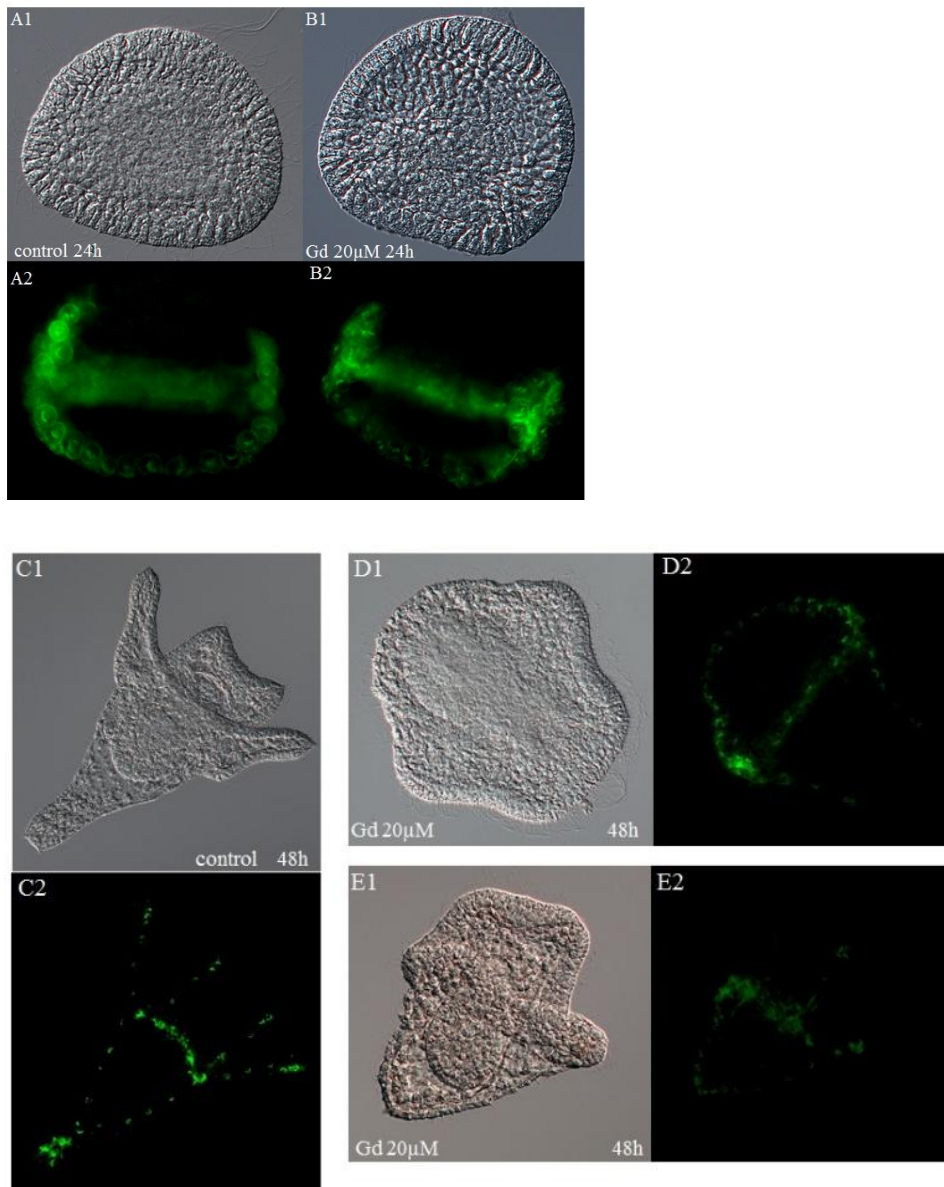
Fig. 24 Localization of PMCs by immunofluorescence with WGA-FITC. In Gd-exposed embryos, PMCs maintained the capacity to migrate and pattern inside the blastocoel, as they do in control embryos (A, C), but at later developmental stages, they were mostly distributed around the immediate ring area (compare C with D and E). A, C) control embryos, 24h and 48h resp.; B) 20μM Gd-exposed embryo, 24h; D, E) 20μM Gd-exposed embryo, 48h. A1, B1, C1, D1, E1) bright-field images; A2, B2, C2, D2, E2, F2) Immunofluorescence with WGA-FITC.

	Controls	Gd-exposed embryos
Mean	37.5	36.6
SD	1.8	1.9

Table 5. Number of PMCs 48 hpf in controls and in *P. lividus* Gd-exposed embryos.

4.6 Gadolinium-induced inhibition of spicules growth correlates with calcium uptake during development

Skeletal spicules are calcareous structures composed of magnesium calcite, secreted by primary mesenchyme cells (PMCs) in the blastocoel of the embryo (Matranga et al., 2011). Sea urchin embryos obtain calcium directly from sea water until they can feed (Nakano et al., 1963). The calcium is transported from the sea water through various outer layers and is deposited inside cells. The manner in which calcium is transported to the PMCs is still not known (Wilth FH, 2002). To investigate the relationship between Gd exposure, skeleton growth and Ca uptake, the amount of Ca and Gd endogenous content was analysed by Flame Atomic Absorption Spectrometry (FAAS).

The histogram in figure 25 shows the relative calcium amount in *P. lividus* Gd-exposed embryos as fold change compared to control embryos. After 24 hpf, there was an 45.36% reduction in the Ca amount in Gd-exposed embryos if compared to controls, while at 48 hpf there was a 67.12% reduction. Considering just the controls, the total Ca amount was 10-fold higher at 48 hpf than at 24 hpf; this is potentially due to the fact that the biomineralization process is just starting at 24 hpf with the rudimental granule deposition (Fig. 25 A) and so just a little amount of Ca is needed.

Between 24 and 48 hpf embryos greatly increase the skeleton size, forming the complex structure that characterizes the pluteus stage. Being the endoskeleton

mineral a high Mg^{2+} containing calcite, Ca is needed to construct the skeleton. In Gd-exposed embryos, the total Ca amount was ~4-fold higher at 48 hpf than at 24 hpf. Recovered embryos showed an intermediate value between 48 hpf-controls and embryos continuously exposed to Gd for 48 hr, with a 26.46% reduction with respect to controls.

Fig. 25 Relative calcium (A) and gadolinium (B) content determined by Flame Atomic Absorption Spectrometry (FAAS), measuring the total amount in *P. lividus* embryo pellets from controls and 20μM Gd-exposed embryos. The histograms show the mean relative levels, expressed in arbitrary units as fold increase compared to the control sample. Values are the mean of three independent experiments; standard deviations are indicated.

Figure 25 B shows results about the total Gd amount; no Gd was detectable in controls (<5ng, the resolution limit of the instrument), while in Gd-exposed embryos there was a 3456-fold increase at 24 hpf and a 5457-fold increase at 48 hpf. Strikingly, also in this case recovered embryos showed an intermediate value between 48 hpf-controls and embryos continuously exposed to Gd for 48 hr, with a 2236-fold increase.
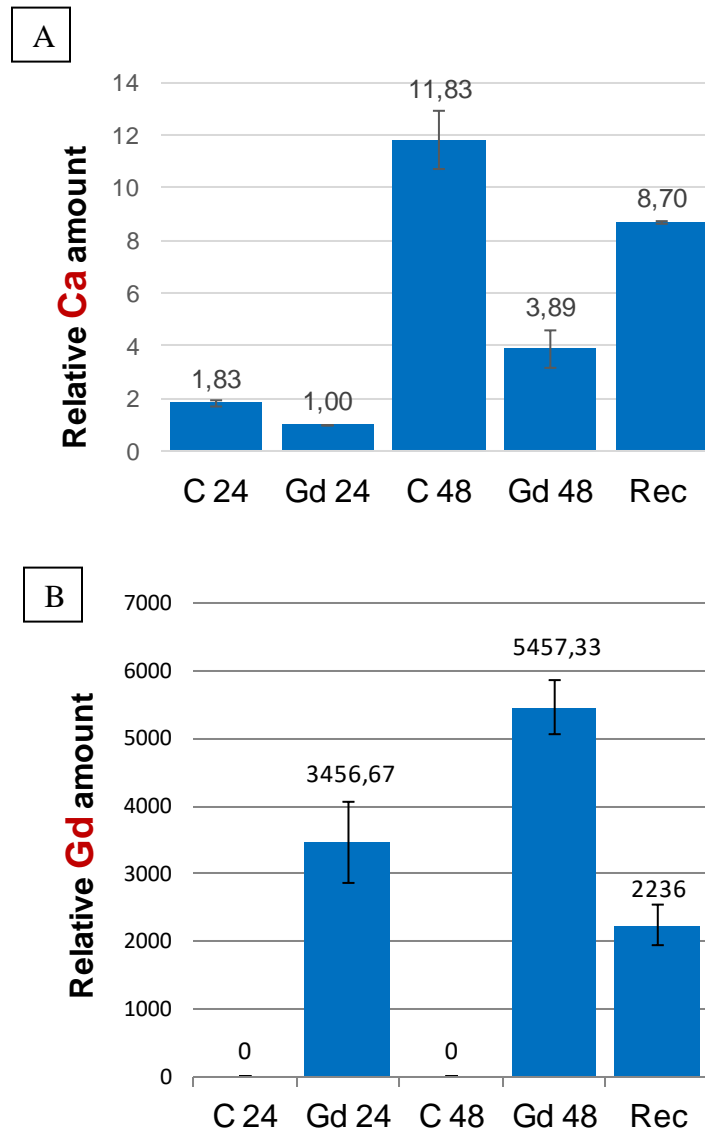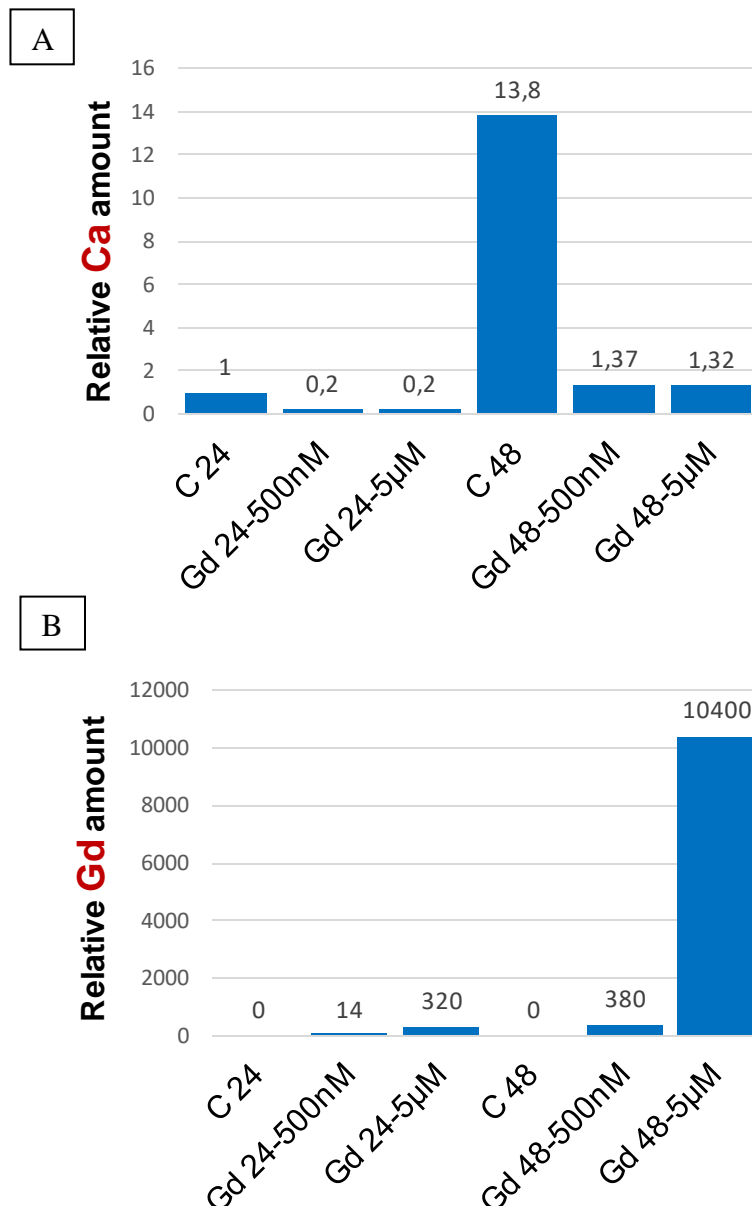

Fig. 26 Relative calcium (A) and gadolinium (B) content determined by Flame Atomic Absorption Spectrometry (FAAS), measuring the total amount in *H. tuberculata* embryo pellets. The histograms show the relative levels, expressed in arbitrary units as fold increase compared to the control sample.

Results on *H. tuberculata* embryos showed a very similar trend (Fig. 26). To see if a dose-response effect was present, we used two different Gd concentrations: 500 nM, at which we observed the highest percentage of AS embryos, and 5 μM, the concentration with the highest percentage of NS embryos (see fig. 21 C). After 24 hpf, there was an 80% reduction in the Ca amount in Gd-exposed embryos at both doses if compared to controls, while at 48 hpf there was a ~90% reduction at both doses (fig. 26 A). This means that the lowest Gd dose tested (500nM) is sufficient to block the Ca channels.

As seen in *P. lividus* embryos, in control *H. tuberculata* embryos the total Ca amount was 13-fold higher at 48 hpf than at 24 hpf. No Gd was detectable in controls (<5ng, the resolution limit of the instrument), while a dose-response effect can be observed in Gd-exposed embryos, with a greater Gd-amount at the highest dose tested both at 24 hpf (14-fold increase at 500 nM and 320-fold increase at 5 μM) and at 48 hpf (380-fold increase at 500 nM and 10400-fold increase at 5 μM) (Fig 26 B).

4.7   Gd-exposure causes the misregulation of the skeletogenic Gene Regulatory Network

Both *P. lividus* and *H. tuberculata* embryos showed a severe impairment of skeleton formation and patterning after Gd-exposure, with species-specific levels of sensitivity and percentages occurrence of the different morphotypes (Fig. 18 and 21).

P. lividus recovered embryos were able to partially resume skeleton elongation, presenting longer spicules than embryos continuously exposed to Gd for 48h. However the skeleton pattern was abnormal. Strikingly, recovered embryos display the same morphotypes observed in embryos continuously exposed to Gd for 48h (Fig. 23), even if with different percentages occurrence (see section 4.4). Recovered embryos may be able to resume skeleton

elongation because they have a greater amount of calcium available for spicules growth than embryos continuously exposed to Gd for 48h, as indicated by the higher levels of Ca quantified in these embryos using FAAS (see section 4.6). If the limited availability of calcium is the major obstacle to spicule growth, then why is the skeleton pattern strongly perturbed in Gd-exposed embryos? It appears that a developmental process is perturbed. This may involve modified expression of genes of the skeletogenic network. As a developmental program must ultimately rely on the genomic regulatory code, we decided to focus our attention on the expression of genes involved in the regulation of skeletogenesis. Significant insights have emerged from the analysis of some genes of the gene regulatory network (GRN) that underlies the development of the endoskeleton of the *P. lividus* and *H. tuberculata* sea urchin embryos. Our comparative studies have revealed ways in which this GRN has been modified by Gd-exposure in both species, providing interesting hypothesis to understand what prevents the correct skeleton pattern formation in these two species.

4.7.1 *P. lividus*

To determine the temporal expression of several transcripts involved in the regulation of skeletogenesis, we carried out semi-quantitative measurements of mRNA levels by relative One Step RT-PCR analysis. Candidate genes were chosen on the basis of three different hierarchical levels, those encoding for: i) early expressed genes (*alx-1, nodal*), ii) signaling molecule genes (*univin, vegf, vegf-r, fgf*) and iii) skeletal matrix protein genes (*p16, p19 and msp130*).

Figures 27, 28 and 29 show the results of semi-quantitative analyses of mRNA levels in embryos exposed to 20μM Gd after 6, 24 and 48h of development, in comparison to an unexposed control. Values obtained from band intensity measurements for each amplification product were normalized to the *Pl*-S24

values, a transcript encoding a ribosomal protein expressed at similar levels in all stages, used as endogenous reference gene (Zito et al., 2003).

The histogram in fig. 27 shows the relative quantity of *alx-1* and *nodal* transcripts, two transcription regulators expressed early in development. After 6h of development there is only a modest decrease in their relative transcription levels, if compared to controls; specifically, 38% decrease for *alx-1* and 30% for *nodal*.

Fig. 27 Relative quantities of *alx-1* and *nodal* determined by RT-PCR during development in Gd-exposed *P. lividus* embryos. The histogram shows the semi-quantitative analysis of RT-PCR products. Mean relative levels are expressed in arbitrary units as fold change compared to the control sample, assumed as 1 in the histogram, using the endogenous gene *Pl*-S24 for normalization.

After 24 hours of development, *alx-1* and *nodal* show respectively 40% and 60% reduction of their relative transcriptional levels (fig. 27). After 48 hours of development, *nodal* expression is close to control levels, showing only 20% reduction, while *alx-1* expression is still found greatly reduced, being 60% less than controls (fig. 27).

The histogram in figure 28 shows the relative quantity of *univin, vegf, vegf-r* and *fgf* transcripts, after 24 and 48 hours of development. All these genes encode signaling molecules involved in the ectoderm–mesoderm induction that regulates skeletogenesis. *vegf* and *vegf-r* mRNAs have transcription levels comparable to control embryos, suggesting that this signaling pathway is not affected by Gd-exposure. On the contrary, a significant down-regulation of *univin* and *fgf* transcripts is observed at 48h, with reduced levels of 50% and 60%, respectively.
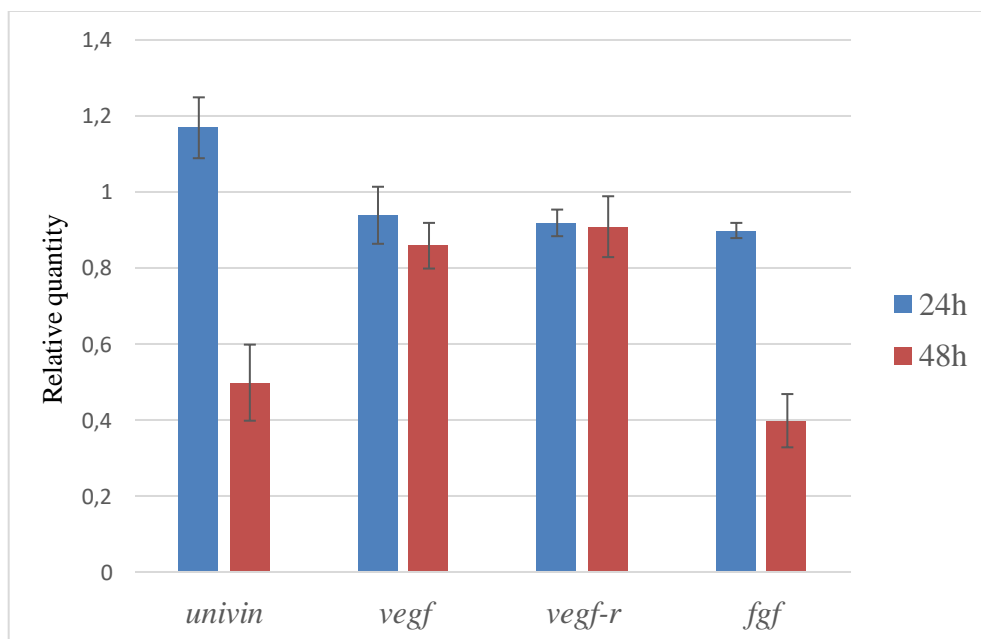
Fig. 28 Relative quantities of *univin, vegf, vegf-r* and *fgf* determined by RT-PCR during development in Gd-exposed *P. lividus* embryos. The histogram shows the semi-quantitative analysis of RT-PCR products. Mean relative levels are expressed in arbitrary units as fold change compared to the control sample, assumed as 1 in the histogram, using the endogenous gene *Pl*-S24 for normalization.

Finally, we looked at the expressions levels of three genes encoding spicule matrix proteins: *msp130, p16* and *p19*. While only a modest variation in their relative transcription levels is observed at 24h, all these skeletal structural genes are down-regulated after 48 hours of development; specifically, we

found a ~50% reduction for *msp130* and *p16* and a modest one (23%) for *p19* (fig. 29).
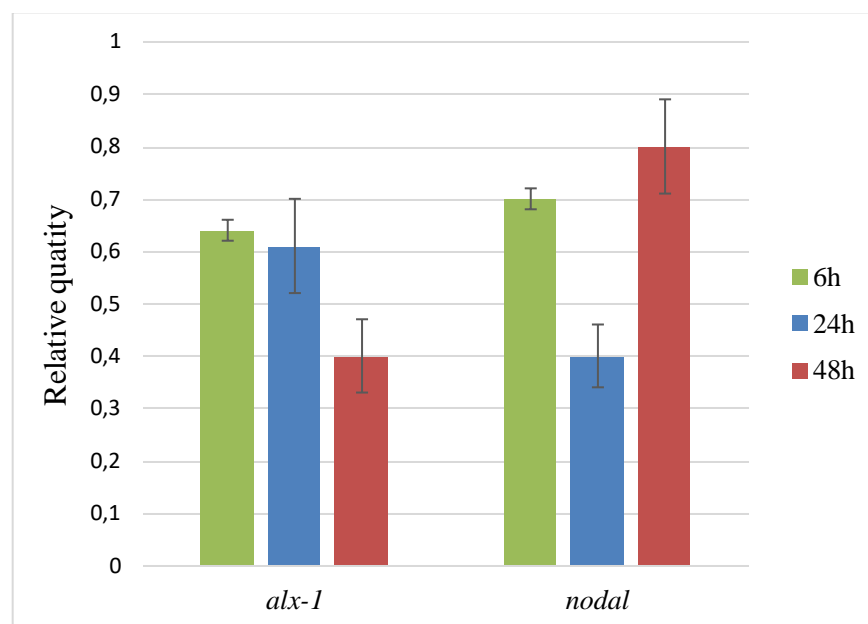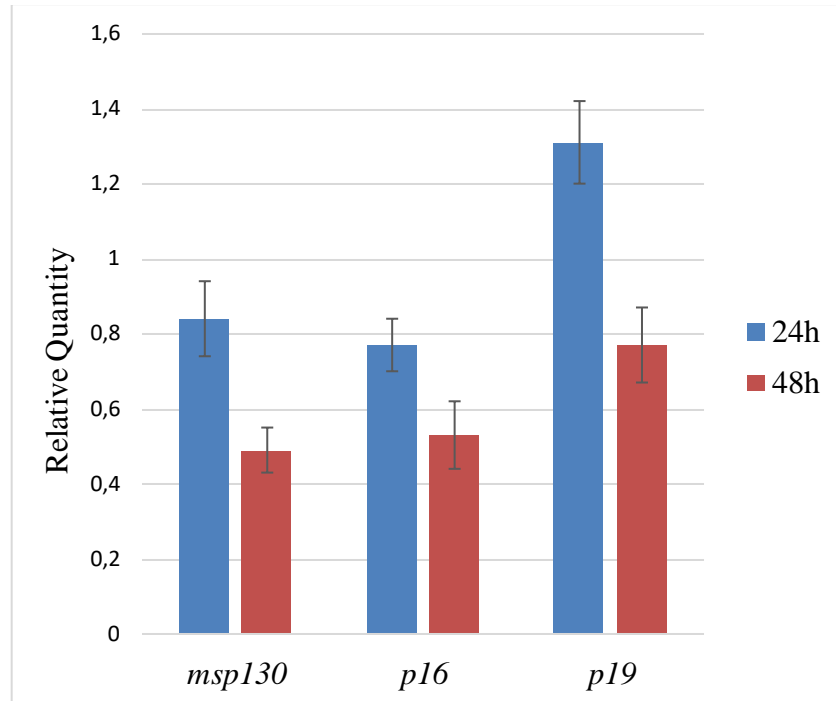

Fig. 29 Relative quantities of *msp130, p16* and *p19* determined by RT-PCR during development in Gd-exposed *P. lividus* embryos. The histogram shows the semi-quantitative analysis of RT-PCR products. Mean relative levels are expressed in arbitrary units as fold change compared to the control sample, assumed as 1 in the histogram, using the endogenous gene *Pl*-S24 for normalization.

4.7.2 *H. tuberculata*

To investigate the effect of Gd-exposure on the temporal expression of several genes involved in the skeletogenic network of the *H. tuberculata* embryo, we carried out semi-quantitative measurements of mRNA.

To understand if there is a dose-dependent response not only at the morphological level, but also at the gene expression level, two different Gd concentrations were analysed: 500nM and 5μM. These candidate doses were

chosen on the basis of their morphological effect on skeleton growth: 500nM being the concentration resulting in the highest percentage of AS (54,38 ± 0,03 %), while the 5µM treatment resulted in the highest level of NS embryos (84 ± 0,02 %) (see Fig. 21 C). These coud also be useful to for an attempt to associate a morphotype with a specific gene expression alteration within the skeletogenic GRN.

Fig. 30 Relative quantities of *nodal, lefty* and *bmp* determined by RT-PCR during development in *H. tuberculata* Gd-exposed embryos. The histogram shows the semi-quantitative analysis of RT-PCR products. Mean relative levels are expressed in arbitrary units as fold change compared to the control sample, assumed as 1 in the histogram, using the endogenous gene *Ht-*Z12 for normalization.

We analyzed the same suites of genes as for *P. lividus*, belonging to three different hierarchical levels of the skeletogenic gene regulatory network: i) early expressed genes involved in the left/right specification axis (*nodal, lefty, bmp*), ii) signaling molecule genes (*vegf, fgf*), and iii) skeletal matrix protein genes (*msp130, sm30*).

The histogram in fig. 30 shows the relative quantity of three transcripts encoding for key players in the left/right specification axis: Nodal, Lefty and BMP. A ~25% and ~35% decrease in *nodal* expression can be observed in embryos exposed for 24h to 500nM and 5 µM Gd, respectively, while only a very slight reduction (< 25%) can be observed at 48 hpf at both concentrations. No significant variation could be observed in the mRNA levels of *lefty* and *bmp*, both at 24 and 48h and at either concentrations, indicating that the Lefty-BMP signalling pathway is not affected at the transcriptional level in Gd-exposed *H. tuberculata* embryos.

Figure 31 shows the relative transcription levels of *fgf* and *vegf*, two genes encoding signaling molecules involved in the ectoderm–mesoderm induction that regulates skeletogenesis directing PMCs migration and skeleton patterning. The histogram shows that both signaling pathways are greatly affected in Gd-exposed embryos. The *vegf* expression is greatly up-regulated at 24 hpf, with a ~2 fold increase of the mRNA levels at 500 nM and an almost 3 fold increase at 5 µM Gd, showing a consistent dose-dependent response, while at 48 hpf the transcription levels are comparable to controls.

In contrast, at 24h, there is a 40% reduction in the mRNA levels of *fgf* at both concentrations, while at 48h the transcript expression is restored at levels comparable to control embryos (Fig. 31).

These results indicate that these two pathways are misregulated at the transcriptional level in *H. tuberculata* Gd-exposed embryos at 24h, while there is no difference at 48h.

Finally, we looked at the expression levels of two genes encoding spicule matrix proteins: *msp130* and *sm30* (Fig. 32). We found a ~20% reduction reduction in the mRNA levels of *msp130* at both concentrations at 24 hpt, while at 48 hpf there was a bigger decrease (30%) at 5 µM Gd if compared to the lower dose (~20% reduction).
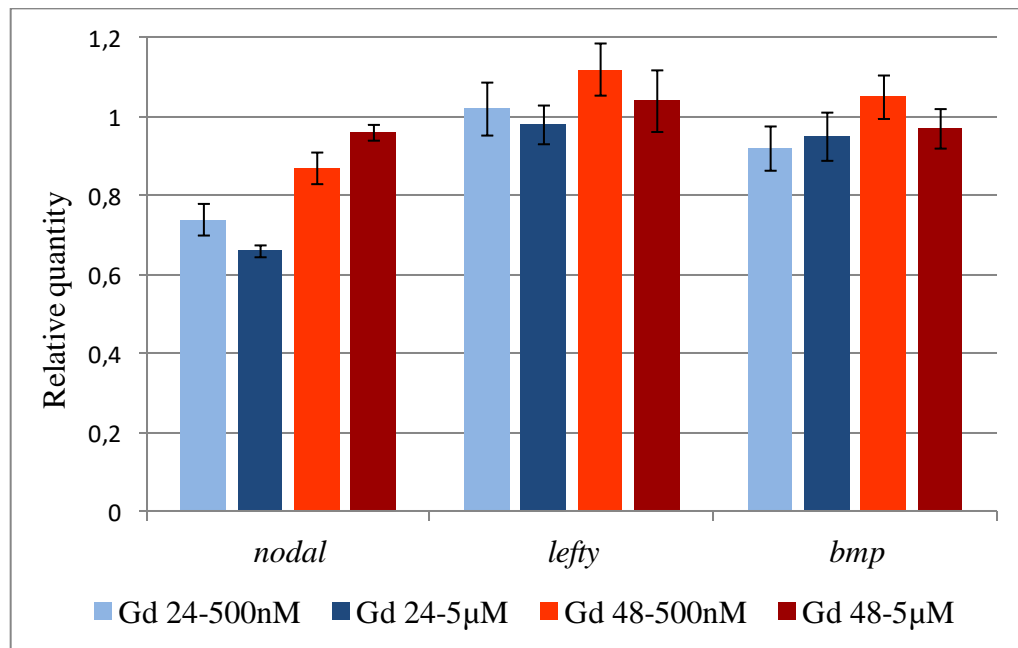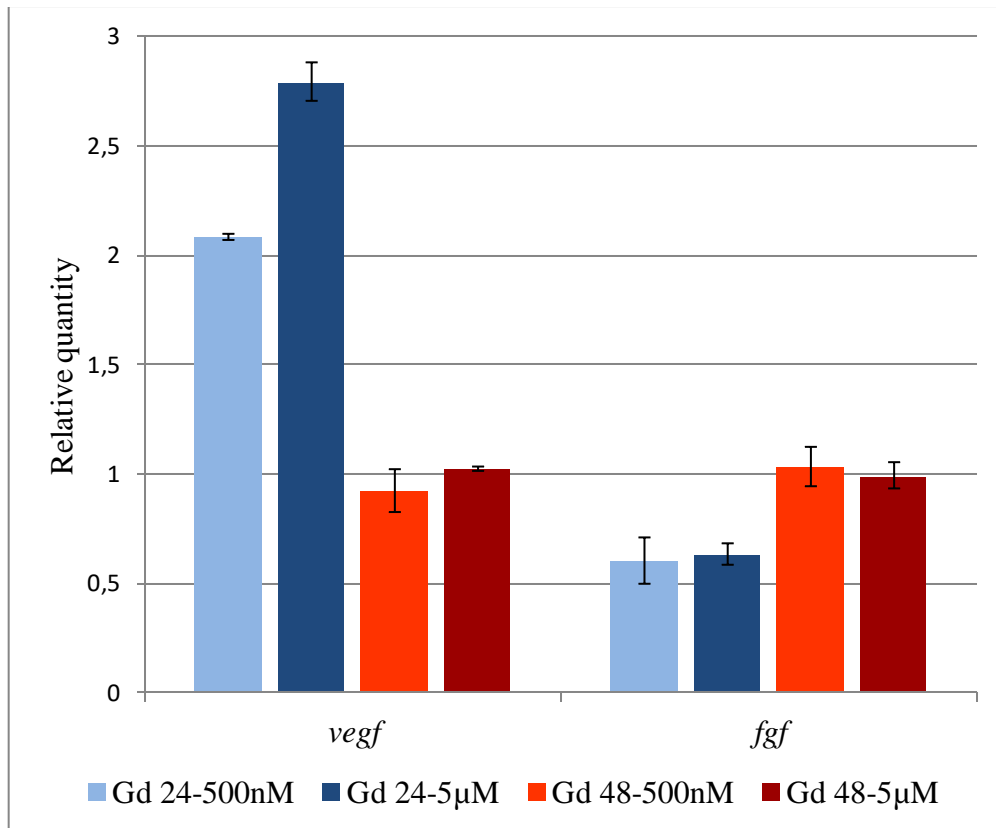
Fig. 31 Relative quantities of *vegf* and *fgf* determined by RT-PCR during development in *H. tuberculata* Gd-exposed embryos. The histogram shows the semi-quantitative analysis of RT-PCR products. Mean relative levels are expressed in arbitrary units as fold change compared to the control sample, assumed as 1 in the histogram, using the endogenous gene *Ht*-Z12 for normalization.

A significant ~50% decrease in *sm30* expression was observed in embryos exposed to Gd for 24h, and a ~40% and ~30% decrease in the expression of these genes in embryos exposed for 48h to 500nM and 5 µM Gd, respectively (Fig. 32). No significant dose dependent response was observed.
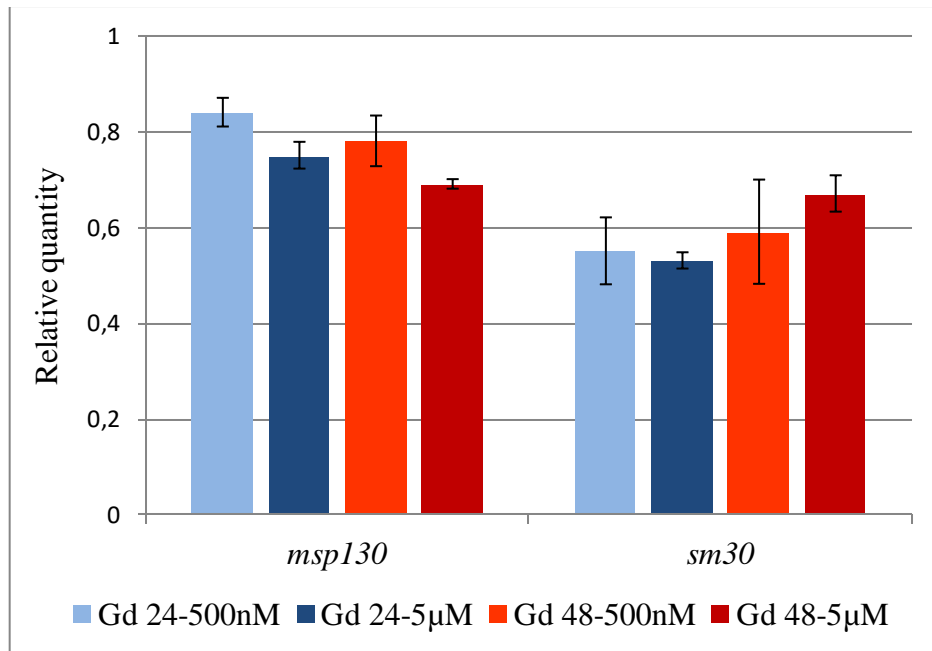
Fig. 32 Relative quantities of *msp130* and *sm30* determined by RT-PCR during development in *H. tuberculata* Gd-exposed embryos. The histogram shows the semi-quantitative analysis of RT-PCR products. Mean relative levels are expressed in arbitrary units as fold change compared to the control sample, assumed as 1 in the histogram, using the endogenous gene *Ht*-Z12 for normalization.

4.8   Gd-exposed embryos do not undergo apoptosis

Apoptosis is a mechanism to remove cells whose DNA has been heavily damaged. Execution of programmed cell death (PCD) is operated by a proteolytic cascade that involves caspases activation. Since caspase-3 activation is one of the main events that leads to apoptosis, we performed immunofluorescence assays on *P. lividus* whole-mount embryos exposed to 20μM Gd for 48h, using an anti-cleaved-caspase-3 antibody. As a positive control, we used cadmium-exposed embryos, as it is known that cadmium induces an apoptotic response after 24 hours of treatment (Chiarelli et al., 2013).

Figure 33 shows that Cd-treated embryos exhibited higher levels of green fluorescence (fig. 33 B), related to cleaved caspase-3 protein, than control (fig.

33 C and E) and Gd-exposed embryos (fig. 33 D and F), suggesting that the exposure to gadolinium ions does not induce any apoptotic process. It appears that Gd^{3+} do not provoke any DNA damage in the cells, that are probably using other defence strategies. To investigate this hypothesis, we used specific markers of the autophagic process.
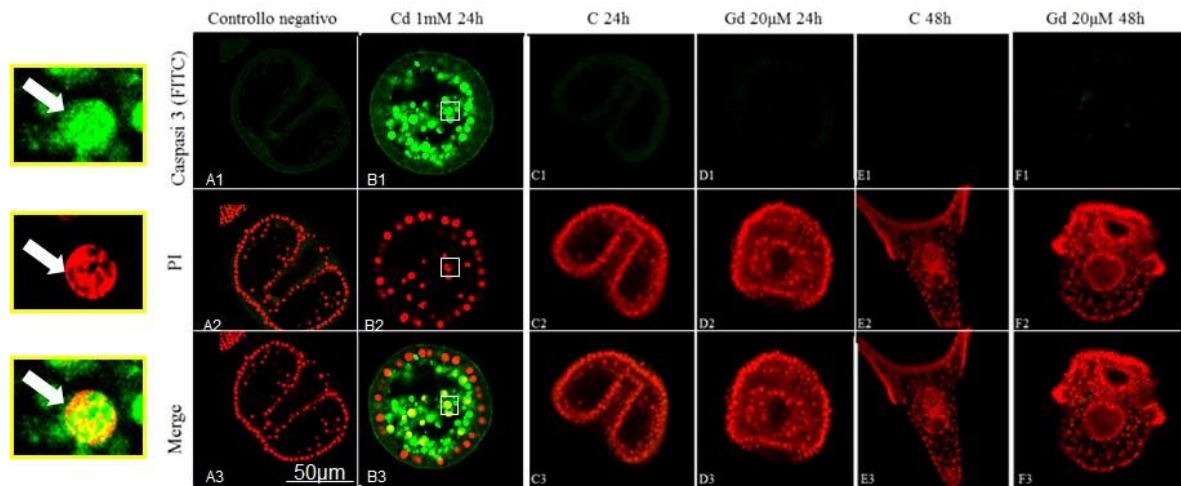
Fig. 33 Immunofluorescence assay on whole-mount embryos at gastrula and pluteus stage. Equatorial optical sections of embryos observed under Confocal Laser Scanning Microscopy (CLSM). Top row: Cleaved-caspase-3 (FITC, green channel); middle row: totality of nuclei by propidium iodide (red channel); bottom row: merging of the two channels. On the left: magnification of the areas highlighted in B1, B2 and B3.

4.9   Autophagy induction in Gd-exposed embryos

4.9.1 Acidic Vesicular Organelles staining

Autophagy is used by several organisms as a defense strategy to face environmental stress. This mechanism has been described as the most important intracellular pathway responsible for degradation and recycling of proteins and organelles (Klionsky and Emr, 2000). It can act as a cell survival mechanism if the cellular damage is not too extensive, or as a cell death mechanism if the damage/stress is irreversible. The autophagic process occurs

constitutively at basal levels and appears to be activated as an adaptive response to a series of intracellular and extracellular stimuli. The chemicals of anthropogenic origin are of considerable interest for their ability to induce the activation of defence systems or interrupt the developmental program. To investigate the possibility that embryos are trying to safeguard the developmental program taking advantage of the autophagic pathway, we used different methods to detect the occurrence of autophagy in *P. lividus* embryos.

Using the acridine orange (AO) vital dye, we studied the acidic vesicular organelles (AVOs) in whole embryos, monitoring controls and 20μM Gd-exposed embryos at 24 and 48h of development. As described, AO enters in acidic compartments such as lysosomes and autophagolysosomes, and is consequently sequestered and protonated. In these low pH cellular compartments, the dye emits the red fluorescence, while the cytoplasm and nucleus fluorescence is green. The intensity of the red fluorescence is proportional to the degree of acidity and/or the volume of the cellular acidic compartments (Traganos and Darzynkiewicz, 1994).

While 24h control embryos show basal autophagy levels (Fig. 34 A, B), embryos at the pluteus stage (48h) have no acidic vesicular organelles (AVOs, Fig. 34 G, H). The external and equatorial optical sections show that Gd-exposed embryos have a considerable higher number of red dots than controls, both at 24 hpf (compare fig. 34 A, B and fig. 34 C, D) and at 48 hpf (compare fig. 34 G, H and fig. 34 I, L). In addition, Gd-exposed embryos displayed not only a higher number, but also a larger size of AVOs, if compared to control, indicative of several cytosolic elements destined to be eliminated through autophagy. These results also revealed important spatial features about the localization of AO granules: at the gastrula stage, we found a major localization of AVOs in the ectoderm of Gd-exposed embryos (see enlargements in fig. 34 C, D), probably due to the direct exposure of this layer of cells to Gd. The localization of AVOs at 48 hpf was no more restricted to the ectoderm, but also found in the gut cells (fig. 34 I). Recovered embryos

showed a reduction in AVOs occurrence if compared to embryos continuously exposed to Gd for 48 hours (Fig. 34 M, N).
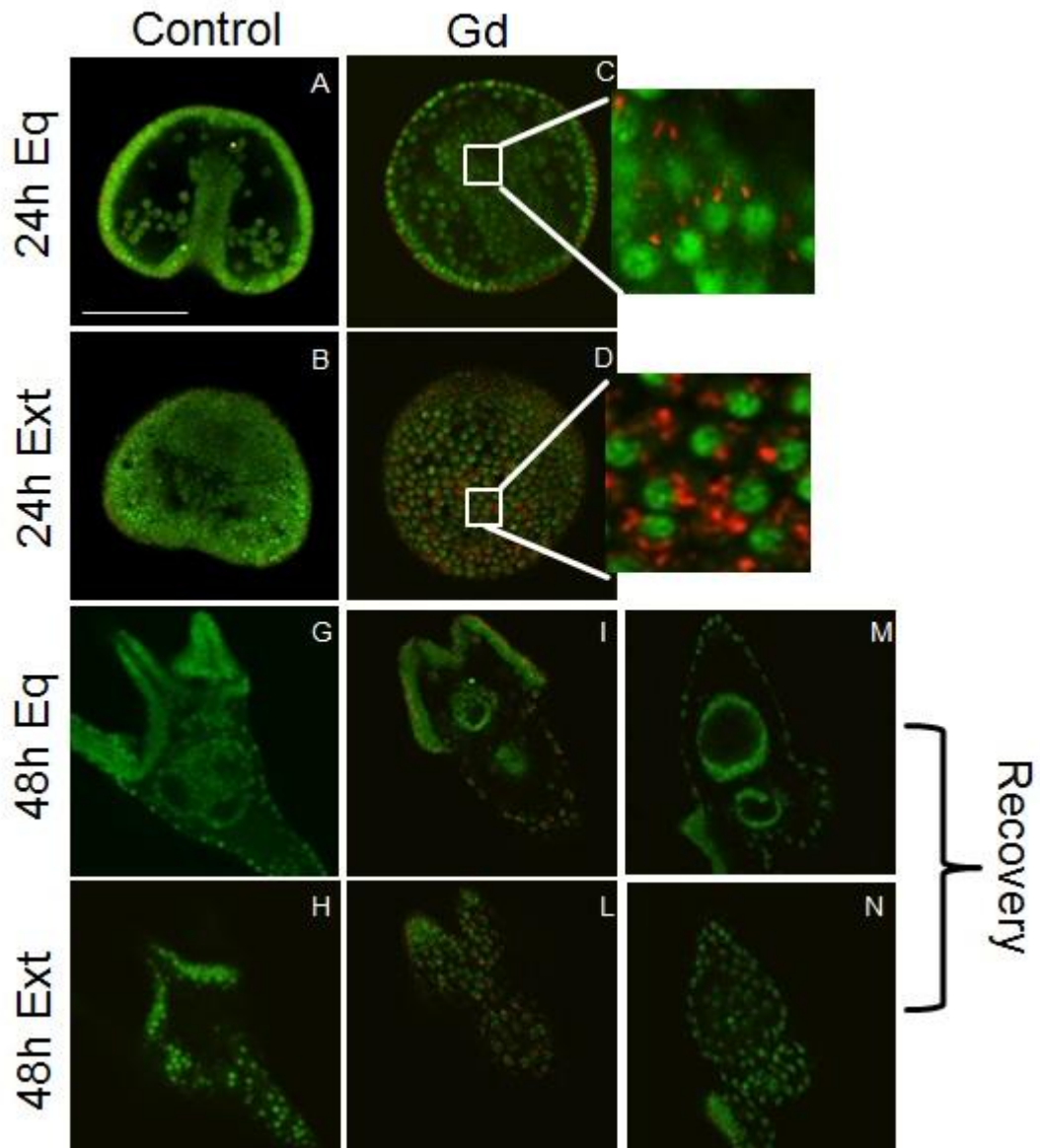
Fig. 34 AO vital staining on whole-mount embryos. The images were captured by Confocal Laser Scanning Microscopy (CLSM). Embryos after 24h of growth: (A-B) control, (C-D) 20μM Gd. Embryos after 48h of growth: (G-H) control, (I-L) 20μM Gd, (M-N) recovered.

4.9.2 LC3 detection by gel blot analysis

Protein gel blot analysis to detect LC3, a specific autophagic marker, was used to asses the occurrence of the autophagic process. The antibody is able to recognize both the LC3-I (16-18 kDa) and –II (14-16 kDa) forms of the protein (fig. 35 A). LC3-I is the cytosolic and inactive form; when conjugated to phosphatidylethanolamine, the complex LC3-phosphatidylethanolamine conjugate (LC3-II), is recruited to autophagosomal membranes and represents the active form of the LC3 protein.
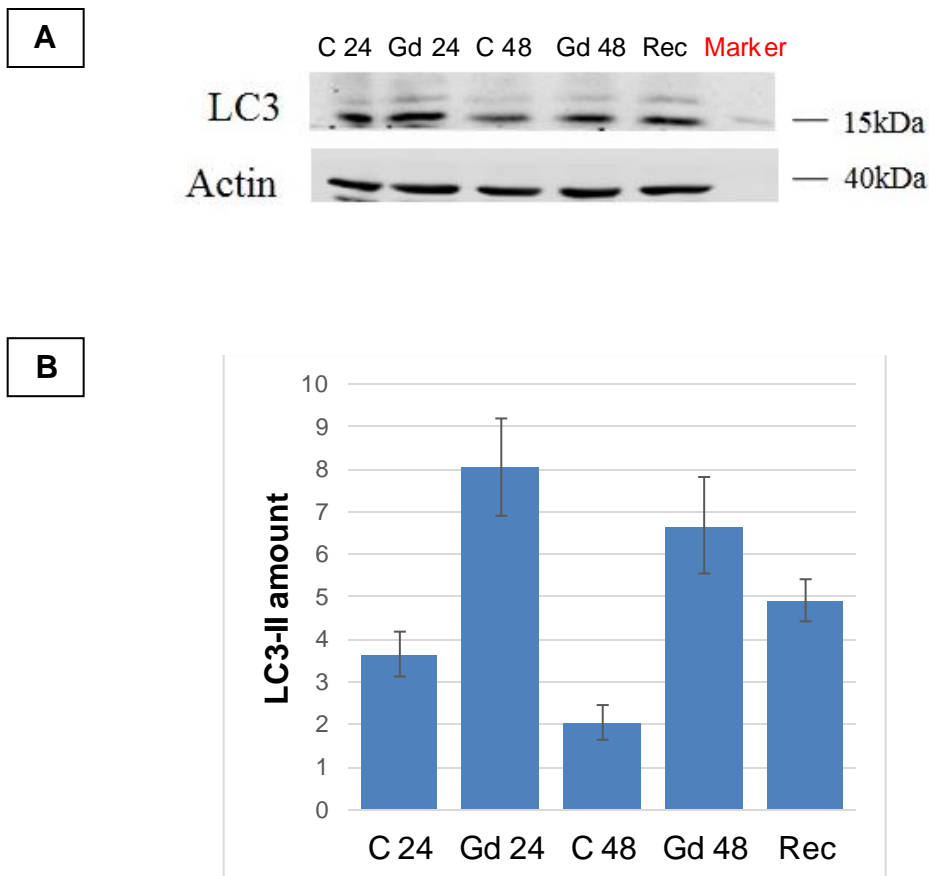
Fig. 35 Immunoblotting detection of LC3. A) A representative WB shows total lysates from controls and Gd-exposed embryos (20 μM) after 24 and 48 h of development, reacted with anti-LC3 antibody. The same membranes were incubated with anti-actin antibody; B) Densitometric analysis of the bands visualized by immunoreaction. Results were obtained from the analysis of LC3-II band intensities normalized by comparison to actin and reported as arbitrary units. Values are the mean of three independent experiments. Bars are SD.

The histogram (fig. 35 B) summarizes the quantitative analysis performed on the bands from three different experiments and plotted as the mean (±SD). There is a 2.2-fold increase in LC3 in treated embryos relative to controls at 24h, a 3.4-fold increase at 48h, and a 2.4 fold increase in recovered embryos, suggesting that the autophagic process is involved as a cellular defensive strategy.

4.9.3 LC3 staining and localization by immunofluorescence

Immunofluorescence cytochemistry of LC3 using the same antibody confirmed a higher level of autophagosomes in embryos treated for 24 and 48h with 20μM Gd, compared with controls (Fig. 36). Furthermore, the same technique was applied to embryos exposed to 20μM for 24h, and then recovered in fresh sea water for 24h. This supports the result of the immunoblotting. Gd-treated embryos have a higher number of autophagosomes than control embryos, but a lower number if compared to embryos continuously exposed to Gd for 48h (compare fig. 36 D and 36 E-F with fig. 36 G-H).

The signal of the cytosolic form (LC3-I) can be observed widespread in the cytoplasm (fig. 36 A1), while the signal of the active form of the protein (LC3-II) is punctate (fig. 36 B3, E3, H3), as the protein is anchored at the membrane of the autophagosomes. Through CLSM analysis, the cellular localization of the autophagosomes was confirmed: cytoplasmic and perinuclear (fig. 36, see magnifications). The CLSM analysis of LC3 also confirmed the localization results obtained by AO staining: at 24 hpf, we found a major localization of both AVOs and the LC3 protein in the ectoderm, while at 48 hpf the autophagic signal was no more restricted to the ectoderm, but also found in the gut cells.
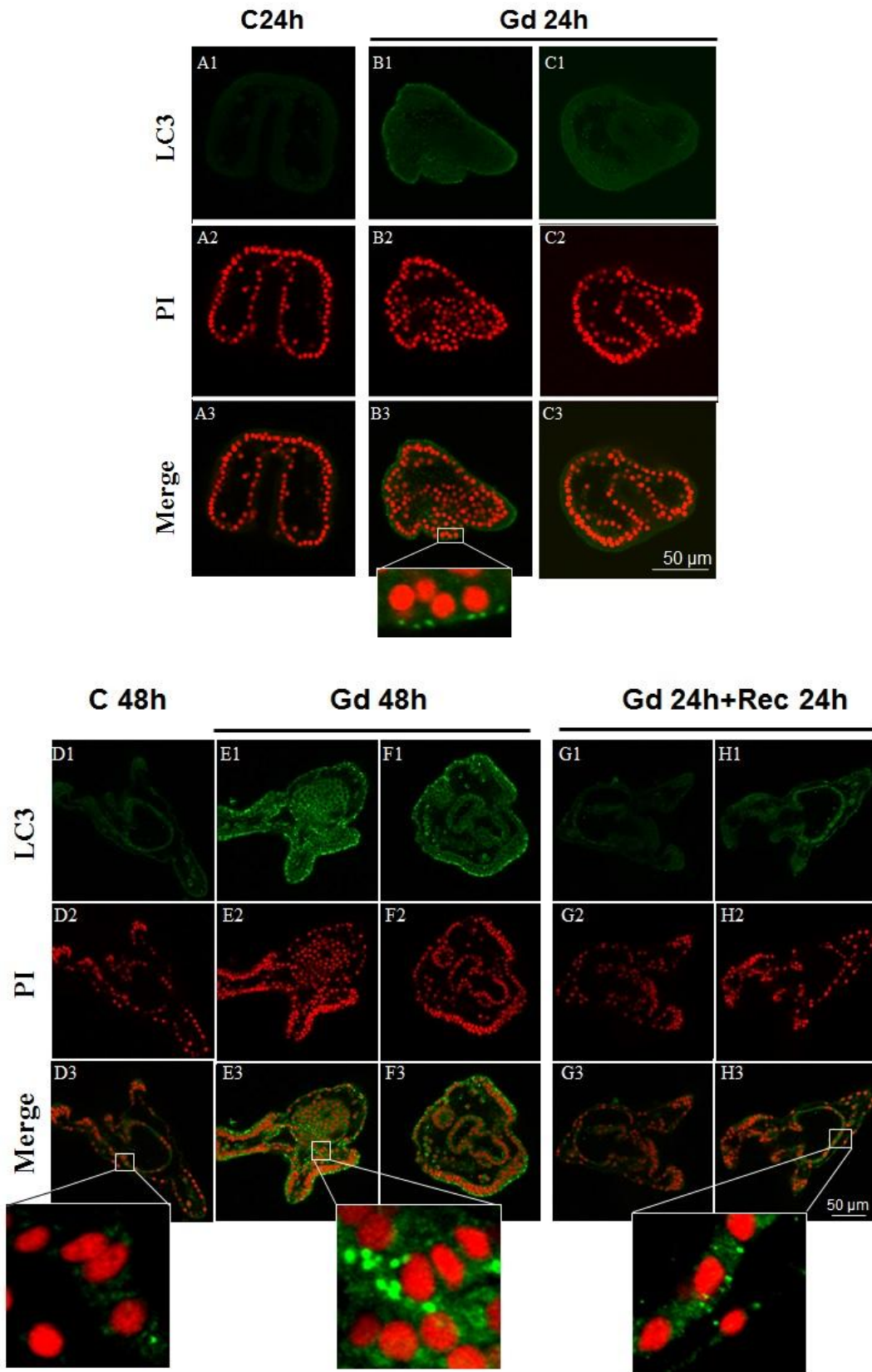
Fig. 36 Immunofluorescence analysis of LC3 protein in whole embryos, after 24 and 48h of development. Equatorial optical sections captured by CLSM. (A1-H1) green: LC3 protein; (A2-H2) red: totality of nuclei stained with propidium iodide; (A3-H2) merge of the two channels.

5. DISCUSSION

"The whole is more than the sum of its parts"
Aristotele, Metaphysics, IV century B.C.

5.1 Effects of exposure to gadolinium on the development of geographically and phylogenetically distant sea urchins species

Gadolinium, along with a plethora of medically used agents released into the marine environment, is an emerging pollutant (Telgmann et al., 2013). Gd pollution is measured as "the Gd anomaly", calculated as the ratio of the measured Gd concentration in a sample with respect to the background levels of Gd due to geological processes. Positive Gd anomalies were observed in several rivers, lakes and in seawater from different locations (Bau and Dulski, 1996; Nozaki et al., 2000; Elbaz-Poulichet et al., 2002; Zhu et al., 2004; Ogata and Terakado, 2006; Kulaksiz and Bau, 2007). The Gd anomaly is determined using only the total Gd concentration, without information about the speciation of the Gd present in the sample (Bau and Dulski, 1996). Strikingly, the Gd anomalies in seawater around urban areas with large human populations have increased greatly over time, all over the world, demonstrating that Gd anomalies are caused by the release from anthropogenic sources (Zhu et al., 2004). Here we show the toxic effects of Gd on development of four sea urchin species living in coastal areas around big cities (Palermo, Italy: >1 million inhabitants; Sydney, NSW: >4 million inhabitants) and, in particular, the perturbation of bio-mineralization. As many marine species make a skeleton during their planktonic developmental stage, the

strong negative effects of Gd, for some of the sea urchin species at very low concentrations, highlights that Gd pollution is an issue that needs to be addressed.

The four species investigated included European (*Paracentrotus lividus* and *Arbacia lixula*) and Australian (*Heliocidaris tuberculata* and *Centrostephanus rodgersii*) species that all develop through an echinopluteus larva producing a complex three-dimensional skeleton. As the mechanism of skeletogenesis and digestive tract formation in echinoplutei is conserved across the Echinoidea (Arnone et al., 2015), we expected that the four species would have a similar response to Gd, exhibiting similar phenotypes. On the other hand, due to differences in the extent of skeletogenesis between the species we expected that there might be some differences in absolute sensitivity levels. As expected, the phenotypic response to Gd of impaired skeleton formation was similar across the four species, indicating a similar response mechanism, albeit with different levels of sensitivity with respect to the concentrations used. The response observed for the four species investigated here is similar to that reported for three Japanese species, *Hemicentrotus pulcherrimus, Heliocidaris crassispina* and *Pseudocentrotus depressus* (Saitoh et al., 2010), providing further evidence of a conserved mechanism of toxicity of Gd to sea urchin embryos.

Pharmaceuticals are designed to specifically act on biological systems, the mechanism underlaying their high toxicity. Gd ions (Gd^{3+}) toxicity appears to be associated with its action as a blocker of Ca^{2+} channels because its ionic radius is nearly equal to that of divalent Ca^{2+} (Sherry et al., 2009). Some studies suggested that Gd ion concentrations in the micromolar range (between 1 and 200 μM) are able to block Ca^{2+} channels in the membrane of sea urchin eggs (David et al., 1988), *Xenopus* oocytes (Yang and Sachs, 1989) and mammalian cell lines (Broad et al., 1999; Lansman, 1990; Luo et al., 2001). As the skeleton is a calcium carbonate structure, potential blockage of Ca^{2+} channels by Gd may be particularly toxic to the calcification response.

There was several orders of magnitude difference in the EC50 for the most sensitive (*H. tuberculata*) and most tolerant (*C. rodgersii*) species. For all species we observed a strong concentration-dependent impairment of skeletogenesis. The sensitivity to Gd might reflect the differences in the amount of calcite deposited in the spicules, with the species that produce more robust and complex skeletons (eg. *H. tuberculata* and *A. lixula*) being more sensitive than species that produce a simpler, lower calcite skeleton (e.g. *P. lividus*). It may be that species that normally produce more calcite are more affected by Gd-impaired uptake of Ca^{2+}. The requirement of Ca^{2+} for the sea urchin biomineralization requires the supply of bicarbonate or carbonate ions, by the formation of an oversaturated micro-environment at the calcification compartment in the embryo (Stumpp et al., 2012; Karakostis et al., 2016a), and a molecular toolkit for mineral deposition in adult tests (Karakostis et al., 2016b) which might be the same in the larvae.

As predicted, *H. tuberculata* embryos were much more sensitive to the Gd exposure than the other three species, suggesting that the need to deposit more calcite and construct a robust larval skeleton may be an indication of sensitivity. The differences in the sensitivity of the species to Gd may also be related to their different habitats and perhaps pollution history of the parental population, a transgenerational effect as seen for the progeny of other sea urchins from polluted sites (Lister et al., 2015). This is a form of developmental plasticity through the influence of environment on gamete quality (Ghalambor et al., 2015; Hamdoun and Epel, 2007). The epigenome may also be involved (Vandegehuchte and Janssen, 2014). The different ability to activate defence strategies, such as the autophagic program (Chiarelli and Roccheri, 2012) and stress proteins induction (Matranga et al., 2011), may also contribute to the resilience of the species. Chemical pollutants have been a persistent source of evolutionary challenges throughout the life history of living organisms (Whitehead, 2014). Human-introduced pollutants greatly increased the rate of change of contemporary environment, severely challenging the adaptive potential of many species. Empirical data on the

evolutionary potential of a wide range of species are needed to determine their adaptation to the changing world (Hoffmann and Sgro, 2011). Geographically separated populations within the same species have been shown to differ in their tolerance to climatic conditions, indicating that past selection has resulted in local adaptation to temperature (Kelly et al., 2011) and pH (Langer et al., 2009; Hammond and Hofmann, 2010). The same trends may be seen in response of sea urchins from areas differing in pollutant loads, a suggestion that would need to be addressed though testing resilience to toxic stressors in populations from clean and polluted sites, as Lister et al. (2015) did for *Sterechinus neumayeri*.

The two European species collected from the same environment, *P. lividus* and *A. lixula*, showed similar sensitivities in response to Gd exposure, in agreement with a previous work where these two species were found equally sensitive to several chemicals (Carballeira et al., 2012). In contrast, a recent article on the effects of silver nanoparticles (Ag-NPs) on the development of three sea urchin species demonstrated the species-specific effects of Ag-NPs low concentrations (from 100 down to 1 mg/L) (Burić et al., 2015). These authors found that the three species, *A. lixula*, *P. lividus* and *Sphaerechinus granularis*, differ in their sensitivity to Ag-NPs. The most sensitive species is *A. lixula* whose embryos show an impaired development at the lowest Ag-NP concentrations (1-10 mg/L) tested. For *S. granularis* the effective Ag-NP concentration range was 10-50 mg/L, while for *P. lividus* was 50-100 mg/L. Thus, sympatric species living in the same environment can have different sensitivities to toxicants, as shown here for the two Australian species and as observed by Saitoh and colleagues (2010) for Japanese sea urchin species in response to Gd. This indicates that different species, despite having a similar environmental history and potential exposure to pollution, might have similar sensitivities to some toxicants and different sensitivities to others.

The differences in sensitivity between the sea urchin species investigated here may also be influenced by their phylogenetic relationships. Phylogenetic trees,

based on molecular data, show that *C. rodgersii* is a member of the oldest sea urchin lineage among the four examined (Lawrence, 2013), while *H. tuberculata* and *P. lividus* are more recent and more closely related (Fig. 37). The key strategies for developmental success are cellular mechanisms providing robustness and buffering embryos from changes in the environment, as well as regulatory pathways able to alter the developmental path in response to the conditions encountered. These defenses and pathways have evolved to permit optimal development in the environment likely to be encountered, with limits adapted to the historical environment of the embryos (Hamdoun and Epel, 2007). The hypothesis that *C. rodgersii* is the most robust to the Gd insult may be due to being of a more ancient lineage needs to be assessed. A quantitative genetics study showed the presence of tolerant genotypes in response to concurrent warming and acidification, contributing to the adaptive capacity and resilience of *C. rodgersii* in a changing ocean (Foo et al., 2012). Comparative data on Gd toxicity from the Mediterranean species, *Centrostephanus longispinus* would help discern the potential influence of phylogeny or geographic environment on sensitivity. To understand the relative influence of environmental or phylogenetic history on the different sensitivities of the embryos and larvae of different sea urchins to Gd and other stressors, data from many other sea urchin species are needed.

The comparison of the effects of Gd on development of the larval skeleton of different species can be used to address important evolutionary questions from a developmental biology perspective, to understand how these differences are generated, and from an ecotoxicological perspective, to investigate how such differences between species sensitivities influence the response to environmental contaminants.
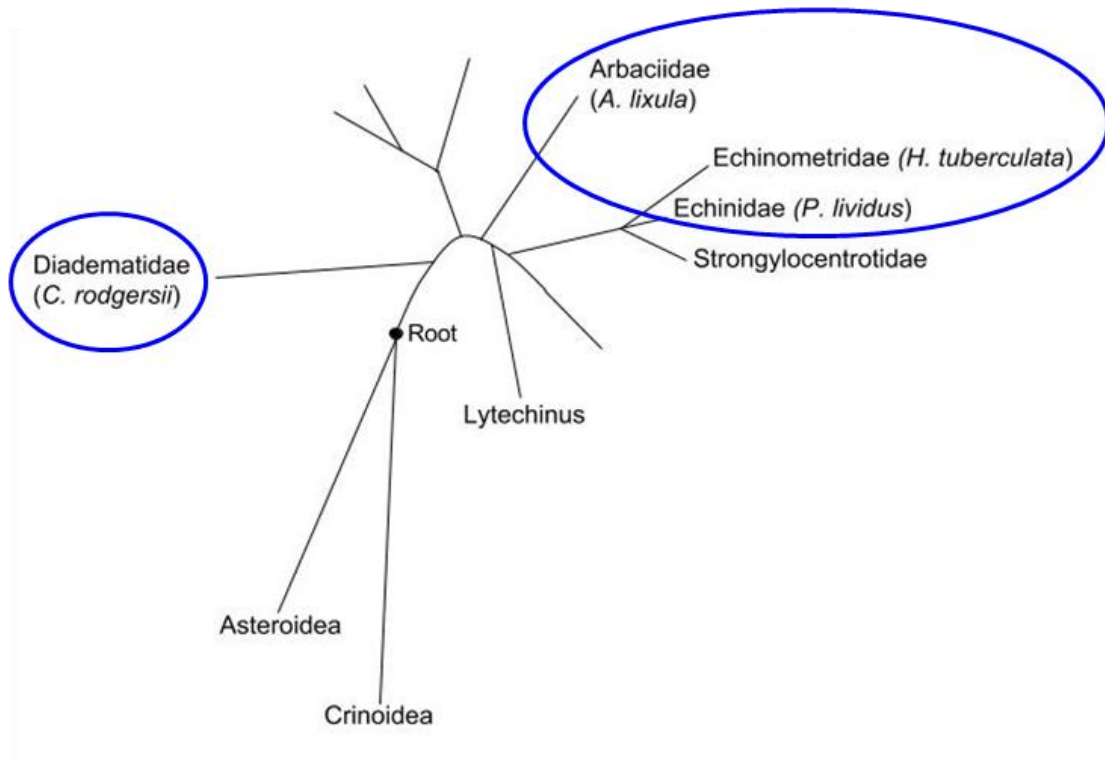
Fig. 37 Phylogram of higher-level echinoid relationships derived from maximum likelihood analysis of partial gene sequences of the nuclear 18S-like small subunit and 28S-like large subunit rRNA (adapted from Lawrence, 2013).

5.2 The relevant implications of asymmetric skeleton formation

Body plan symmetry is an essential feature of development. Echinoderms have a unique position in metazoan phylogeny as deuterostomes, which include the chordates and the hemichordates, making them an interesting phylum to study left-right asymmetry and the conservation of mechanisms used to build the body plan of deuterostomes. Adult sea urchins are radially symmetrical (Fig. 38), a derived feature as echinoderms evolved from an ancestor that had bilateral symmetry (Davidson et al., 1998). Indeed, the embryos and larvae are bilaterally symmetrical, as are the larvae of animals belonging to most extant phyla. During sea urchin development, the transition

from a bilateral to a radial body plan relies on an impressive left-right asymmetric process (Davidson et al., 1998; Arenas-Mena et al., 2000). During metamorphosis most larval tissues are replaced by adult tissues generated from the rudiment, that forms exclusively on the left side of an otherwise bilaterally symmetric larva (Fig. 38).
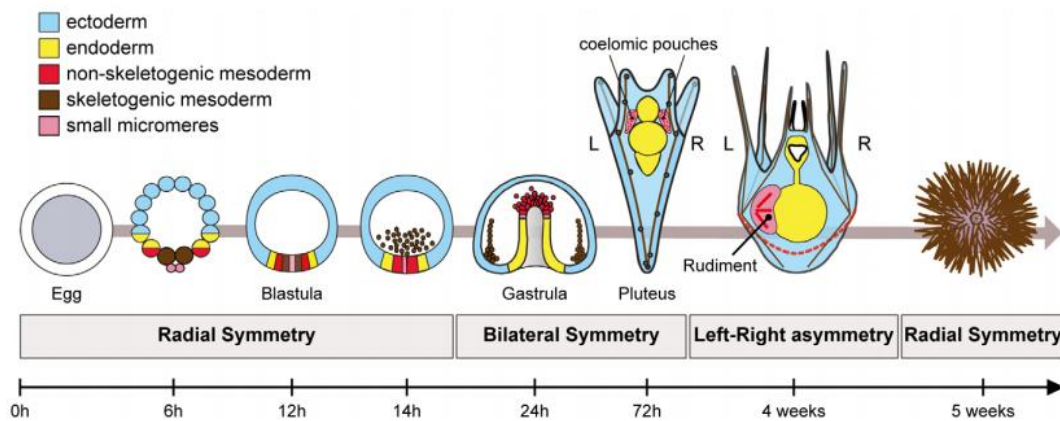
Fig. 38 Establishment of left-right asymmetry in echinoderms. Left-right asymmetry in echinoderms is characterized by the asymmetric positioning of the imaginal rudiment on the left side of the bilateral pluteus larva. The adult emerges from this imaginal rudiment through metamorphosis (adapted from Bessodes et al., 2012).

Left-right asymmetry is an essential feature of development in most bilaterian animals. In vertebrates, the morphology and positioning of many internal organs as well as development of the nervous system is left-right asymmetric and failure to establish these asymmetries can result in pathological disorders (Levin, 2005).

The skeleton of the sea urchins was the embryonic structure most affected by Gd exposure. Embryos of the four species investigated here displayed a significant inhibition of skeleton elongation and patterning. A significant percentage of Gd-exposed embryos displayed asymmetric spicule formation, with a variable occurrence at different Gd concentrations (AS morphotype, see fig. 21 in section 4.2).

In *P. lividus* embryos, asymmetrical spicule formation was observed on both sides; this shows that abnormal spicules formation on the right or left side of the embryo is accidental in Gd-exposed embryos, in agreement with results obtained in Japanese species (Saitoh et al., 2010). A deeper insight into the mechanism underlying this response may be obtained through investigation of the Nodal-Lefty-Pitx2 signaling pathway, that regulates left-right asymmetry during development of the sea urchin embryo. The function of Nodal on the right side is also to restrict formation of the rudiment to the left side (Duboc et al., 2005). The effect of Gd on *nodal* expression is discussed below.

5.3 Gadolinium interferes with calcium uptake during embryo development

In experiments where *P. lividus* embryos were treated with Gd and then removed from this toxicant, these embryos had longer spicules than embryos continuously exposed to Gd for 48h, but the skeleton pattern was abnormal. As Gd is a known inhibitor of Ca channels, this disruption of spicule formation may be due to the action of Gd as a blocker of Ca^{2+} channels. If this hypothesis is correct, it is reasonable to suggest that transferring the embryos after a 24h Gd-exposure time to fresh seawater for a further 24h time would allow for some restoration of Ca channels functionality by Gd dissociation away from the channel pore. If so, the Ca uptake would be partially restored, and this would explain the presence of longer spicules in recovered embryos than in embryos continuously exposed to Gd.

To investigate the relationship between skeleton growth and calcium uptake by Gd-exposed embryos, we analyzed the Gd and Ca content by flame atomic absorption spectrophotometry (FAAS) in *P. lividus* and *H. tuberculata* embryos. Results showed a similar trend in the two species. While no Gd was detectable in control embryos, Gd-exposed embryos showed a significant increase in the Gd content both at 24 hpf (3456-fold increase in *P. lividus*; 14-

fold increase at 500 nM and 320-fold increase at 5 μM in *H. tuberculata*) and at 48 hpf (5457-fold increase in *P. lividus*; 380-fold increase at 500 nM and 10400-fold increase at 5 μM in *H. tuberculata*). Strikingly, for *H. tuberculata* there was a dose-dependent effect in the Gd accumulation inside the embryo. Recovered *P. lividus* embryos showed an intermediate value between 48 hpf-controls and embryos continuously exposed to Gd for 48 hr, with a 2236-fold increase.

In parallel with the increase of the Gd content, results show the decrease of the Ca content. Specifically, there was an 45.36% reduction in the Ca amount in *P. lividus* Gd-exposed embryos if compared to controls after 24 hpf and a 67.12% reduction at 48 hpf, while in *H. tuberculata* Gd-exposed embryos there was an 80% reduction in the Ca amount at both doses if compared to controls after 24 hpf and a ~90% reduction at both doses at 48 hpf. Recovered *P. lividus* embryos showed an intermediate value between 48 hpf-controls and embryos continuously exposed to Gd for 48 hr, with a 26.46% Ca reduction with respect to controls.

The results demonstrate that Gd interferes with Ca uptake and internalization and, consequently, with biomineral formation, indicating that Gd^{3+} competes with Ca^{2+} for binding to the Ca channels; being a trivalent ion, Gd^{3+} binds with much higher affinity (Sherry et al., 2009), competing Ca^{2+} and thus passing through the Ca channels, where it accumulates into embryos in a time- and dose- dependent manner.

During the 24 hr rescue period of embryos removed from Gd treatment, Ca^{2+} ions, having now a higher concentration in seawater than Gd^{3+} ions, appear to compete with Gd^{3+} potentially leading to the removal of Gd ions from the Ca channels thus allowing Ca to start again to enter the cells. Thus recovered embryos were able to accumulate a higher amount of Ca and grow longer spicules than embryos continuously exposed to Gd, supporting the hypothesis.

At the same time, recovered embryos were not able to extend their spicules with the correct skeleton pattern, showing the same aberrant morphotypes displayed by embryos continuously exposed to Gd. There are several potential explanations. One is that the differentiation of the PMCs was corrupted and this was not repaired by removal of Gd.

Considering that the explanation of a process of development must ultimately be couched in the terms of the genomic regulatory code, another hypothesis could be found in the network of interactions among genes encoding transcription factors that drive the specification of an embryonic cell lineage. We attempted to address this question investigating these two hypothesis, first observing the PMCs migration and patterning inside embryos, second analysing the expression levels of some genes involved in the skeletogenic gene regulatory network.

5.4 PMCs migration and localization occur normally in Gd-exposed embryos

Cell migration is a fundamental process for the maintenance of adult life as well as for development of the embryo, and its alteration leads to severe pathological states or congenital defects. One of the fundamental events during gastrulation in the sea urchin is the directional migration of mesodermal primary mesenchyme cells (PMCs), which produce the embryonic endoskeleton (Matranga et al., 2013). PMCs, after undergoing an epithelial-to-mesenchymal transition, migrate directionally within the blastocoel by means of filopodia and form a characteristic ring pattern (the subequatorial PMC ring), which consists of two ventrolateral clusters of PMCs joined by oral and aboral cell strands. The PMCs fuse as they migrate, forming a single continuous syncytium within which an elaborate calcium carbonate endoskeleton is secreted. Spiculogenesis begins by the formation of a tri-radiate spicule rudiment in each ventrolateral cluster. Later, the two rudiments

elongate and branch to form the two symmetrical halves of the skeleton. From specification to terminal differentiation, the process takes about two days, and although the number of cells implicated is small, the spatial patterning is stereotypical. The three-dimensional structure of the skeleton and its bilateral symmetry are foreshadowed and determined by the spatial organization that PMCs can achieve only within the embryo, in intimate contact with the ectoderm wall, suggesting guidance cues from the ectoderm control the well-defined PMC spatial pattern (Armstrong et al., 1993; Guss and Ettensohn, 1997; Gustafson and Wolpert, 1967).

We analysed the migration and patterning of the PMCs in *P. lividus* embryos to understand if some errors in these processes may be associated with the abnormal skeleton formation in Gd-exposed embryos. We found that, in Gd-exposed embryos at 24 hpf, PMCs maintained the capacity to migrate and pattern inside the blastocoel, as they do in control embryos, excluding the possibility that the abnormalities in skeleton formation could be caused by PMCs mislocalization. When observed 48h after fertilization, in embryos where Gd caused the formation of an asymmetric skeleton, PMCs were found along the growing spicule, while on the other side of the blastocoel (the site of the lacking spicule) they were still distributed forming a cell cluster (see Fig. 24). This is the result of the failure of cells to build the skeleton and therefore to distribute themselves around a supporting biomineral.

If we consider the correct migration and localization of PMCs in Gd-exposed embryos, the primary cause of the abnormal skeleton formation or its absence may be upstream, in genes involved in the control of skeleton morphogenesis.

5.5 Abnormal skeleton formation relies on changes to the genetic control of bio-mineralization

Developmental plasticity is the notion that the genome enables the organism to produce a range of phenotypes (Gilbert, 2001). The dynamic anatomical changes that characterize embryogenesis are encoded in the genome. The genomic regulatory control of development can be understood in terms of transcriptional gene regulatory networks (GRNs). These are models that explain the causal sequence of combinatorial interactions among genes encoding transcription and signalling factors. The architecture of a GRN gives the map of functional interactions among these genes and provides a direct guide to the regulatory logic of developmental control (Oliveri and Davidson, 2004). GRNs explain developmental phenomenology at the system level, by reference to its source, the genomic control apparatus (Oliveri et al., 2008). Here we address the question if changes in the skeletogenic GRN caused by Gd may be involved in the abnormal skeleton formation by investigating a suites of genes in this GRN.

Significant insights have emerged from the analysis of some genes of the sea urchin skeletogenic gene regulatory network (GRN). The analysis of expression levels of genes in this GRN, carried out by relative One Step RT-PCR, was performed to evaluate the effects of Gd on three hierarchical classes of genes, encoding for: early expressed factors, signalling molecules, and skeleton matrix proteins. The organization of the GRN is inherently hierarchical, because each phase of development has progressive stages with more fine-scale terminal processes, so that network linkages operating earlier at the regulatory level have more pleiotropic effects than those controlling terminal events. The earlier stages of formation of every body part involve specification of the domain of the developing organism that will become that part, followed by pattern formation, which determines its morphological structure. Only at the end of this process are deployed the differentiation gene

batteries that encode the detailed functional properties of the body part (Davidson, 2001).

In *P. lividus*, two early expressed genes, *alx-1* and *nodal*, were investigated. These genes are transcription factors that function in the nucleus controlling expression of downstream genes. Upstream components of this network include several maternal proteins as well as early zygotic transcription factors. One key transcription factor is the Paired-class homeodomain protein, Alx1 (Ettensohn et al., 2003). *Alx1* is expressed selectively in the large micromere lineage and is essential for PMC specification. *Alx-1* expression peaks twice during physiological embryogenesis in *S. purpuratus*: at first sharply at the pre-hatching blastula stage, later at the mesenchyme blastula stage. Its level is then maintained high till the gastrula stage (Damle and Davidson, 2011).

As Alx-1 is one of the essential regulators acting upstream of the skeletogenic process and triggering the cascade of events leading to the expression of downstream structural genes, its reduced levels observed at 6, 24 (~40% reduction) and 48 hours (60% reduction) can be one of the reasons for the lowered mRNA levels of all the structural genes encoding for spicule matrix proteins that were investigated, namely *msp130, p16* and *p19*. The expression of these genes was significantly reduced after 48 hours of development.

Nodal has been intensively studied in vertebrates due to its essential and multiple roles in germ layer formation and dorsoventral patterning (Whitman, 2001). The Nodal-Lefty-Pitx2 signaling pathway regulates the establishment of both the left-right asymmetry and the oral-aboral polarity during development of the sea urchin embryo. Results in *P. lividus* show a 30% decrease in *nodal* expression at 6 hours and a 60% reduction of its relative transcriptional level at 24 hours, while at 48 hpf the transcriptional level is almost restored to the control level, with a modest 20% reduction. Results in *H. tuberculata* show a ~25% and ~35% decrease in *nodal* expression in embryos exposed for 24h to 500nM and 5 μM Gd, respectively, while only a very slight reduction (< 25%) was observed at 48 hpf at both concentrations.

The maximal reduction of *nodal* expression was observed in both species at 24 hpf, corresponding to the gastrula stage, at which stage, in control embryos, a second domain of *nodal* expression appears at the right tip of the archenteron and the ectodermal expression is shifted towards the right side of the embryo (Duboc et al., 2005). This is the crucial moment when Nodal starts acting for the establishment of the left-right asymmetry. This indicates that the observed reduced transcriptional levels of *nodal* at 24 hpf might be critical for the left-right larval symmetry, and it is probably involved in the asymmetrical spicule growth in Gd-exposed embryos.

The other functional level of the GRN considered relates to genes encoding signaling molecules involved in the ectoderm–mesoderm induction that regulates skeletogenesis: *univin, vegf, vegfr* and *fgf.*

Classical experiments demonstrated that spicules formed in vitro from isolated micromeres are linear and lack the complex branches observed in vivo (Okazaki, 1975). They are also much longer than the spicules present in normal embryos, suggesting that isolated PMCs lack signals that regulate growth of the spicules. Recent studies have implicated the *vegf* and *fgf* pathways in providing guidance and differentiation cues to primary mesenchyme cells (PMCs) during sea urchin gastrulation, so controlling the directional migration of PMCs and the formation of the embryonic skeleton (Duloquin et al., 2007; Röttinger et al., 2008). Duloquin et al. (2007) showed that a VEGF receptor (VEGFR-10-Ig) is expressed selectively by migrating PMCs in the sea urchin *P. lividus*, and a VEGF ligand (VEGF3) is expressed in the ectoderm overlying the ventrolateral clusters. Perturbation of *vegf* signaling in this species led to defects in PMC migration and skeletogenesis. Röttinger et al. (2008) identified a similar, complementary pattern of expression of an FGF ligand and receptor (FGFA and FGFR2, respectively) in *P. lividus* and showed that blocking the *fgf* pathway also led to defects in skeletogenesis. These studies suggest that *fgf* and *vegf* might have essential

(and non-redundant) functions in mesoderm cell migration and skeletogenesis in the sea urchin.

Establishment of left-right asymmetry in the sea urchin embryo involves reciprocal signaling between the ventral ectoderm that expresses *nodal* and a left-right organizer of endodermal origin and that this long-range signaling requires the activity of several signaling pathways including the Notch, FGF-ERK, BMP2/4 and Univin/Vg1 (Bessodes et al., 2012).

In *P. lividus* Gd-exposed embryos the PMCs ability to correctly migrate and pattern was not affected by Gd, as well as the expression of *vegf/vgfr*, with levels similar to controls. On the contrary, in *H. tuberculata* Gd-exposed embryos the *vegf* expression was greatly up-regulated at 24 hpf, with a 2 fold increase of the mRNA levels at 500 nM and an almost 3 fold increase at 5 μM Gd, showing a dose-dependent response, while at 48 hpf the transcription levels are comparable to controls. Information about the PMCs ability to migrate and pattern in *H. tuberculata* Gd-exposed embryos is still needed.

At 48 hpf treated *P. lividus* embryos exhibited a down-regulation of *univin* and *fgf* trancripts. It is known that, under physiological conditions, *Pl-univin* transcript levels increase from the beginning of gastrulation through the late pluteus stage, coinciding with the time of spicule elongation (Zito et al., 2003). Exposure to Gd ions seems to perturb the *univin* expression, leading to a significant misregulation of its normal temporal expression at 48 hpf. For *H. tuberculata* Gd-exposed embryos there was a 40% reduction in the *fgf* expression at both concentrations at 24hpf, while at 48h the transcript expression was found restored at levels comparable to control embryos.

Expression of *fgf* in sea urchin embryos begins at the hatching blastula stage in an equatorial belt of ectodermal cells surrounding the embryo; at the gastrula stage, intense expression of *fgf* is observed in the ectodermal regions where one of the three arms of the tri-radiate spicule rudiment branches to form the body rods and the post-oral (or anal) rod and where PMCs accumulate to form

the bilateral clusters (Röttinger et al., 2008). Novel domains of expression appear near the animal plate; finally, at the pluteus stage, the *fgf* transcripts are restricted to the region surrounding the stomodeum and to three to four PMCs located at the tips of the growing spicule rods. Concomitantly with the onset of *fgfA* expression, the migrating PMCs start to express *fgfr2* (Röttinger et al., 2008).

FGF signaling plays a key role in regulating the formation of the ramified respiratory system of Drosophila and vertebrates (Min et al., 1998; Metzger and Krasnow, 1999). Despite the fact that the skeleton of the sea urchin larva does not form from an epithelium as the lung of vertebrates and the tracheae of flies, but from a syncytium of mesenchymal cells, *fgfA* and other genes (*sprouty, pea, ets1 and fgfr2*) are expressed selectively in all regions where the spicules will branch, allowing formation of the oral arms of the pluteus larva (Röttinger et al., 2008). In the sea urchin *fgf* is involved in the regulation of the formation of the complex three-dimensional structure of the skeleton, reinforcing the idea that the function of this pathway in regulating formation of ramified organs and structures is highly conserved between species.

The down-regulation of *fgf* expression in *P. lividus* Gd-exposed embryos at 48 hours may be involved in the inhibition of spicule elongation. On the other hand, the down-regulation observed at 24 hpf in *H. tuberculata* Gd-exposed embryos may result in abnormal branching of the skeleton, as observed in many embryos.

It was demonstrated by Cavalieri and colleagues (2011) that the gene *strim1*, involved in the epithelial-mesenchymal signaling network, is expressed in ectoderm regions adjacent to the bilateral clusters of PMCs and that its misexpression leads to severe skeletal abnormalities. *Strim1* is probably not required for PMCs specification but it is necessary for proper positioning of PMCs into the blastocoel. Furthermore, *strim1* indirectly participates in the transcription of the *fgfA* gene to achieve the maximum expression in ectoderm cells. This genes is probably essential for turning on the expression of terminal

differentiation genes, such as *sm30*, that are associated with the inception of the skeletal morphogenesis (Cavalieri et al., 2011). It is interesting to note that the Strim1 protein needs calcium ions to work properly. Thus the lack of Ca^{2+} in Gd-exposed embryos could provoke the abnormal functioning of Ca-dependent proteins such as Strim1 and the misexpression of the genes requiring its regulatory activity, i.e. *fgfA* and *sm30*.

Finally, the last functional level considered relates to genes encoding spicule matrix proteins, and specifically *msp130, p16* and *p19* in *P. lividus*, *msp130* and *sm30* in *H. tuberculata*. All these genes were down-regulated in Gd-exposed embryos of both species. Strikingly, in *P. lividus* we found a greater reduction at 48 hpf, as it would be expected for these genes encoding for occluded matrix proteins, considering the massive reduction in the skeleton size at this time.

5.6 Changes in gene interactions within the skeletogenic GRN

Considering that evolution and development are both manifestations of the heritable genomic regulatory programs that determine how the morphological characters of each species are built, the detected differences in gene expression in response to Gd treatment in the two species are not surprising, despite their similar phenotypes. Changes in regulatory gene interactions during development play a major role in the evolution of phenotypic differences between species. The detailed anatomy of this structure differs widely among the euechinoids (Wray, 1992), reflecting changes in the patterning inputs over time.

The two species of sea urchin analyzed in this study have contrasting investment in skeleton production: *H. tuberculata* produces mechanically robust ladder-like fenestrated arm rods, typical of the Echinometridae (Kinjo

et al., 2008), while *P. lividus* produces thin unfenestrated rods as typical of the Echinidae (Emlet, 1982). Evolutionary change in morphological features may also involve modulation of the gene expression levels in the gene regulatory networks (GRNs), just as true conservation of morphological features must imply retention of ancestral developmental GRN features.

For example, while both the *vegf* and *fgf* expression is affected by Gd exposure in *H. tuberculata* embryos, only *fgf* is mis-regulated in *P. lividus* embryos, as the vegf and *vegf-r* genes are correctly expressed. In *P. lividus* Gd-exposed embryos, *fgf* is correctly expressed at 24h, and a 60% reduction was observed at 48h. In contrast, in *H. tuberculata* Gd-exposed embryos, there is a 40% reduction at 24h, while normal levels of the transcript can be observed at 48h. The difference between species may be influenced by the differences in the structure of the skeleton and the mass of the spicules produced. The larval skeleton of *H. tuberculata* embryos is more complex and robust than the skeleton of *P. lividus embryos*. Thus, *H. tuberculata* embryos may require higher levels of *fgf* by 24h to support skeleton growth. In addition, some *H. tuberculata* Gd-exposed embryos had skeletons that were more branched than in controls. It is known that VEGF is involved in spiculogenesis and that its concentration controls the spicules shape and their branching (Knapp et al., 2012). So, the comparatively higher increase in the *vegf* mRNA levels at 24h in *H. tuberculata* Gd-exposed embryos may be the cause for the increased branching of the spicules in these embryos.

Due to the fabrication of a more extensive skeleton, *H. tuberculata* may have higher endogenous levels of spicule matrix proteins than *P. lividus*, and this could explain why we found higher levels of *msp130* at 48 hpf in *H. tuberculata* Gd-exposed embryos than in *P. lividus* Gd-exposed embryos. Similar implications were suggested in a recent work that compared the effects of acetazolamide on carbonic anhydrase activity in these two species (Zito et al., 2015).

Several studies found that divergence in gene expression on the transcriptome scale is positively correlated with phylogenetic distance (Kalinka et al., 2010; Irie and Kuratami, 2011). Living echinoids, members of the phylum Echinodermata, belong to either the Cidaroidea or Euechinoidea, and these two subclasses comprise the crown group echinoids (Kroh and Smith, 2010). A large-scale reorganization of echinoid gene regulatory networks (GRNs) underlay the initial divergence of cidaroids and euechinoids. For example, in the euechinoid *Strongylocentrotus purpuratus* the *alx1* gene is a primary driver of skeletogenic specification and differentiation in sea urchin embryo, while the *alx1* gene is not an initial regulatory mediator of skeletogenic specification in the cidaroid *Eucidaris tribuloides* micromeres (Erkenbrack and Davidson, 2015).

A comparative network analysis between two closely related species, the lecithotroph direct-developing *Heliocidaris erythrogramma* and the planktotroph *H. tuberculata* showed major changes in the expression profiles of several genes related to skeletogenic cell fate specification, morphogenesis, and biomineralization, indicating a relevant rewiring of the GRN even within the same genus (Israel et al., 2016).

5.7 Gd-exposed embryos use autophagy as a defence mechanism

Aquatic organisms are exposed to adverse changes in their environment and are able to sense these deleterious changes and activate several defense mechanisms. The developmental success relies on cellular mechanisms providing robustness and buffering embryos from changes in the environment. These mechanisms provide potent, although not unassailable, defenses against developmental stressors including changes in temperature, hypoxia, pathogens, UV radiation, free radicals, and toxicants (Hamdoun and Epel, 2007). Anthropogenic changes of the environment are beyond the range of

these protective mechanisms. When the cellular impairment is too extensive, the mechanisms of programmed cell death, such as apoptosis and autophagy, may be triggered (Yuan and Kroemer, 2010), contributing to remove the irreversibly damaged cells to maintain tissues homeostasis and integrity. Autophagy can act as a cell survival mechanism if the cellular damage is not too extensive or as a cell death mechanism if the damage is irreversible. In this latter case, it can operate as an independent pathway or together with the apoptotic one (Chiarelli et al., 2016).

Some toxicants can be sequestered in cellular vesicles and granules, activating the autophagic process. Lysosomal membrane integrity or stability appears to be an effective indicator of cellular well-being as seen in bivalve mollusks and fish where lysosomal stability is correlated with many toxicological responses and pathological reactions (Moore et al., 2006).

It has been hypothesized that repeated triggering of autophagy can protectively minimize the production of reactive oxygen species (ROS) and so the cellular stress. Consequently, animals living in fluctuating environments, in which autophagy is repeatedly stimulated by natural stressors, seem to be generically more tolerant to pollutant stress. Moore and colleagues (2006, 2008) speculated that organisms making up functional ecological assemblages in fluctuating environments, where up-regulation of autophagy should provide a selective advantage, may be preselected to be tolerant of pollutant-induced oxidative stress.

Two studies reported the activation of the autophagy-lysosome pathway in zebrafish embryos exposed to nanoparticles. Cheng and colleagues (2009) observed the appearance of lysosome-like vesicles after multi-walled carbon nanotubes exposure of zebrafish embryos at single-cell stage. Simultaneous treatment of embryos with S-doped TiO_2 nanoparticles and simulated sunlight irradiation caused receptor-mediated autophagy and vacuolization, indicating entrance of the nanoparticles via endocytosis rather than diffusion (He et al., 2014).

Recent studies with sea urchin embryo demonstrated that autophagy is required for sea urchin oogenesis and early development (Agnello et al., 2016), this suggests that autophagy could act: (i) during oogenesis, as a mechanism of survival and maturation, acting respectively in the recycling of cellular components and in the breakdown of the germinal vesicle; (ii) after fertilization, to direct correct development; (iii) during early embryogenesis, for yolk digestion and/or for removal of obsolete proteins and organelles; and (iv) in the micromeres, probably for mechanisms linked to the subsequent gastrulation process (Agnello et al., 2016). Treatment with the autophagic inhibitor bafilomycin A_1 just after fertilization, even just for 2 h, caused developmental delays and malformations. Removal of the inhibitor and the following recovery of embryos restored the autophagic signals. It was also observed a strong activation of the apoptotic process, indicating a close relationship between autophagy and apoptosis and suggesting the activation of apoptosis to eliminate the cells irreversibly compromised by damage caused by autophagic inhibition (Agnello et al., 2016).

The crosstalk between apoptosis and autophagy has been shown in sea urchin embryos under stressful conditions (Chiarelli et al., 2014), demonstrating that they are able to activate different defense strategies after Cd exposure thus providing a clear structure of the hierarchically triggered defense strategies at the cellular and molecular levels. It appears that the exposure of the developing embryo to sublethal Cd concentrations first induces the activation of the early defense mechanisms, such as the synthesis of HSPs and metallothioneins (Russo et al., 2003; Roccheri et al., 2004), but if this is not sufficient to safeguard the developmental program, embryos will trigger the autophagic and/or apoptotic processes (Chiarelli et al., 2011; Agnello et al., 2007). A further study showed that induction of autophagy in sea urchin embryos has a maximum peak after 18 hours of Cd exposure, when apoptosis is just beginning (Chiarelli et al., 2011). It was also shown that the cells differently activate the autophagic mechanism depending on their position in

the embryo, as a major localization of autolysosomes were observed in the ectoderm (Chiarelli et al., 2011).

A hypothetical model of cellular defense was proposed, suggesting that the first response to the Cd insult is the induction of HSPs and metallothioneins. Subsequently, the embryo activates the autophagic process as a cell survival mechanism. Finally, if the damage is too extensive, the apoptotic program is massively activated leading to the death of the embryo. The results demonstrated that autophagy temporally anticipates the massive apoptotic response and the inhibition of autophagy produces a concomitant reduction of apoptosis (Chiarelli et al., 2016).

Starting from this model of cellular defense supporting the homeostatic relationship between autophagy and apoptosis during sea urchin development, we investigated the possibility that such mechanisms were also acting in Gd-exposed embryos. Embryos undergoing massive apoptotic processes after Cd exposure also showed morphological features typical of dying embryos, such as the loss of cells and the complete block of development (Roccheri et al., 2004). These features were never observed in the Gd-exposed embryos investigated here. In all species treated embryos were alive after 72 hours, indicating that apoptotic processes were not triggered. This was confirmed by data from immunofluorescence examination on *P. lividus* embryos at the gastrula and pluteus stage using an anti-cleaved-caspase-3 antibody. No apoptotic processes were observed.

The activation of autophagy in Gd-exposed embryos was demonstrated using three different methods, including AO vital staining on whole mount embryos and LC3 detection, Western blot and *in situ* immunofluorescence. Quantitative analysis of LC3 showed an increase in the protein amount relative to controls both at 24 and 48h, confirmed by a higher number of autophagosomes. Results indicate that autophagy is acting as a cell survival strategy in Gd-exposed embryos, and that removal of Gd and recovery in fresh sea water reduce the

need of cells to recycle damaged cell components or remove stressed organelles by autophagic processes.

Using confocal microscopy the cells involved in the autophagic processes were identified. At 24 hpf, we found a major localization of both AVOs and the LC3 protein in the ectoderm, probably because this is the first cellular layer exposed to and damaged by Gd. At 48 hpf the autophagic signal was no more restricted to the ectoderm, but also found in the gut cells, indicating that during development the Gd-caused cellular damage was broadening throughout the embryo. The confocal microscopy on whole embryos allowed us to investigate the autophagic phenomenon in cells in their natural position, avoiding the disadvantage of the investigation of isolated cells, deprived of their normal network of cell-cell interactions.

6.   Conclusions

"Contrary to the view that embryos and larvae are the most fragile stages of life, development is stable under real-world conditions. Adaptive responses to the environment either buffer stress or produce alternative developmental phenotypes. Rapid anthropogenic changes to the environment are beyond the range of these protective mechanisms."

Hamdoun and Epel, 2007

In conclusion, the morphological and comparative results from this thesis show that four sea urchin species, geographically and phylogenetically distant, differed in their sensitivity to Gd, but that the effect of this agent on larval phenotype was similar. The similar morphological response to Gd in the four species indicates a similar mechanism underlying abnormal skeletogenesis. Sensitivity to Gd greatly varied, with the EC50 ranging from 56 nM to 132 μM across the four species. These different sensitivities highlight the importance of testing toxicity in several species for risk assessment. That the same pollutant can have very different toxicity levels on marine organisms, even within the same taxonomic group, shows that using only one model organism to test the effects of pollutants on the marine environment is not sufficient. Results of pollution assays based on one species within a taxon can be misleading with respect to hazard risk assessment.

Exposure to Gd from fertilization resulted in inhibition or alteration of skeleton growth in the plutei of the four species tested. The strong negative effects of Gd on calcification in plutei, in consideration of the plethora of marine species that have calcifying larvae, indicates that Gd pollution is urgent issue that needs to be addressed.

The increase in the Gd content inside developing embryos inversely correlated with the decrease in the Ca content, strongly suggesting that Gd ions are able to compete for the Ca channels, thus altering the calcium availability and leading to abnormal skeletal morphogenesis. This effect was partially reversible as embryos removed from Gd showed an increase in the Ca content and subsequently in the spicules size. This suggests that the removal al Gd from the culture medium restored skeleton elongation by increasing the calcium availability. The perturbation of skeleton pattern observed both in Gd-exposed embryos and in recovered embryos is probably due to changes in the genetic regulation of bio-mineralization, as several genes involved in the skeletogenic GRN were found misexpressed.

Sea urchin embryo develops in a fast-changing envorinment and, although they may be buffered for expected environmental changes, rapid anthropogenic changes, as occurring due to climated change and increasing pollution, can overwhelm their intrinsic robustness. Gadolinium is one of the man-made chemicals that evades the embryo defence mechanisms that are triggered in response to environmental stressors. Results of this thesis highlight the key role that the autophagic pathway plays as one of the cellular defence mechanisms activated in sea urchin embryos after Gd-exposure.

In the new Anthropocene age, the influence of humans on the global environment is arguably greater than that of any other species. Rapid global changes and human population growth hasten the need to achieve human wellbeing by combining economic benefit with environmental protection. The ocean is neither inexhaustible nor immune to damage, as well as its inhabitants. The assessment of impacts of environmental disturbances on ecosystems and organisms (including humans) requires an understanding of stress effects throughout the hierarchy of biological organization, from the molecular and cellular to the organism and population levels, as well as the community and ecosystem levels. The implications are far-reaching for human, environmental and global fitness.

REFERENCES

Adams NL, Shick JM. Mycosporine-like amino acids prevent UVB-induced abnormalities during early development of the green sea urchin *Strongylocentrotus droebachiensis*. Mar. Biol. (2001) 138: 267-280.

Agnello M, Filosto S, Scudiero R, Rinaldi AM, Roccheri MC. Cadmium induces an apoptotic response in sea urchin embryos. Cell Stress Chaperones. (2007) 12(1):44-50.

Agnello M, Roccheri MC. Apoptosis: Focus on sea urchin development. Apoptosis (2010), 15: 322-330.

Agnello M, Bosco L, Chiarelli R, Martino C, Roccheri MC. The Role of Autophagy and Apoptosis During Embryo Development, Cell Death - Autophagy, Apoptosis and Necrosis, Dr. Tobias Ntuli (Ed.), InTech (2015) DOI: 10.5772/61765.

Agnello M, Chiarelli R, Martino C, Bosco L, Roccheri MC. Autophagy is required for sea urchin oogenesis and early development. Zygote (2016) 24(6):918-926.

Amemiya S, Yonemura S, Kinoshita S, Shiroya T.. Biphasic stage sensitivity to UV suppression of gastrulation in sea urchin embryos. Cell Differ (1986) 18: 45-49.

Arenas-Mena C, Cameron AR, Davidson EH. Spatial expression of Hox cluster genes in the ontogeny of a sea urchin. Development (2000) 127, 4631–4643.

Armstrong N, Hardin J, McClay DR. Cell-cell interactions regulate skeleton formation in the sea urchin embryo. Development (1993). 119, 833-840.

Arnone I, Byrne M, Martinez P. Echinodermata. In: Wanninger, A. (Ed.), Evolutionary Developmental Biology of Invertebrates, (2015) vol. 6. Springer-Verlag, Wien, pp. 1-58.

Badger D, Kuester RK, Sauer JM, Sipes IG. Gadolinium chloride reduces cytochrome P450: relevance to chemical-induced hepatotoxicity. Toxicology (1997) 121(2), 143–53.

Bau M, Dulski P. Anthropogenic origin of positive gadolinium anomalies in river waters. Earth and Planetary Science Letters (1996), 143(1-4), 245–255.

Bau M, Knappe A, Dulski P. Anthropogenic gadolinium as a micropollutant in river waters in Pennsylvania and in Lake Erie, northeastern United States. Chem. Erde - Geochem. (2006) 66 (2): 143–152

Bessodes N, Haillot E, Duboc V, Röttinger E, Lahaye F, Lepage T. Reciprocal signaling between the ectoderm and a mesendodermal left-right organizer directs left-right determination in the sea urchin embryo. PLoS Genet (2012) 8(12):e1003121.

Bonaventura R, Poma V, Costa C, Matranga V. UVB radiation prevents skeleton growth and stimulates the expression of stress markers in sea urchin embryos. Biochem Biophys Res Commun. (2005) 328:150-7.

Bonaventura R, Poma V, Russo R, Zito F, Matranga V. Effects of UV-B radiation on development and hsp70 expression in sea urchin cleavage embryos. Marine Biology (2006) 149:79-86.

Bonaventura R, Zito F, Costa C, Giarrusso S, Celi F, Matranga V. Stress response gene activation protects sea urchin embryos exposed to X-rays. Cell Stress Chaperones (2011) 16(6):681-7.

Bonaventura R, Russo R, Zito F, Matranga V. Combined effects of cadmium and UVB radiation on sea urchin embryos skeleton impairment parallels p38 MAPK activation and stress genes overexpression. Chem. Res. Toxicol (2015) 28 (5), 1060-1069.

Boudouresque CF, Verlaque M. *Paracentrotus lividus*. In: Lawrence, J.M. (Ed.), Sea Urchins: Biology and Ecology, third ed. (2013) Elsevier B.V., London, pp. 297-327.

Broad LM, Cannon TR, Taylor CW. A non-capacitative pathway activated by arachidonic acid is the major Ca2+ entry mechanism in rat A7r5 smooth muscle cells stimulated with low concentrations of vasopressin. J. Physiol. (1999) 517, 121–134.

Brodin T, Piovano S, Fick J, Klaminder J, Heynen M, Jonsson M. Ecological effects of pharmaceuticals in aquatic systems—impacts through behavioural alterations. Philos Trans R Soc Lond B Biol Sci. (2014) 369(1656).

Burić P, Jaksić Z, Stajner L, Dutour Sikirić M, Jurasin D, Cascio C, Calzolai L, Lyons DM. Effect of silver nanoparticles on Mediterranean sea urchin embryonal development is species specific and depends on moment of first exposure. Mar. Env. Res. (2015) 111: 50-59.

Burke RD, Alvarez CM. Development of the esophageal muscles in embryos of the sea urchin *Strongylocentrotus purpuratus*. Cell Tissue Res (1988) 252, 411-417.

Bursch W, Ellinger A, Gerner C, Fröhwein U, Schulte-Hermann R. Programmed cell death (PCD). Apoptosis, autophagic PCD, or others? Ann N Y Acad Sci. (2000) 926:1-12.

Byrne M, Andrew N. *Centrostepharnus rodgersii*. In: Lawrence, J.M. (Ed.), Sea Urchins: Biology and Ecology, third ed. (2013) Elsevier B.V., London, pp. 243-256.

Byrne M, Lamare M, Winter D, Dworjanyn SA, Uthicke S. The stunting effect of a high CO2 ocean on calcification and development in sea urchin larvae, a synthesis from the tropics to the poles. Philos Trans R Soc Lond B Biol Sci. (2013) 368(1627):20120439.

Cameron RA, Britten RJ, Davidson EH. The embryonic ciliated band of the sea urchin *Strongylocentrotus purpuratus* derives from both oral and aboral ectoderm. Dev Biol (1993) 160, 369-376.

Carballeira C, De Orte MR, Viana IG, Delvalls TA, Carballeira A. Assessing the toxicity of chemical compounds associated with land-based marine fish farms: the sea urchin embryo bioassay with *Paracentrotus lividus* and *Arbacia lixula*. Arch. Environ. Contam. Toxicol. (2012) 63 (2): 249-261.

Cavalieri V, Guarcello R, Spinelli G. Specific expression of a TRIM-containing factor in ectoderm cells affects the skeletal morphogenetic program of the sea urchin embryo. Development (2011) 138(19):4279-90.

Chapman PM. Determining when contamination is pollution e weight of evidence determinations for sediments and effluents. Env. Int. (2007) 33: 492-502.

Cheers MS, Ettensohn CA. P16 is an essential regulator of skeletogenesis in the sea urchin embryo. Dev Biol. (2005) 283(2):384-96.

Cheng J, ChanCM, VecaLM, PoonWL, Chan PK, Qu L, Sun YP, Cheng SH. Acute and long-term effects after single loading of functionalized multi-walled carbon nanotubes into zebrafish (*Danio rerio*). Toxicol Appl Pharmacol (2009) 235:216–25

Chiarelli R, Agnello M, Roccheri MC. Sea urchin embryos as a model system for studying autophagy induced by cadmium stress. Autophagy (2011) 7:9.

Chiarelli R, Roccheri MC. Heavy metals and metalloids as autophagy inducing agents: focus on cadmium and arsenic. Cells. (2012) 27;1(3):597-616.

Chiarelli R, Agnello M, Bosco L, Roccheri MC. Sea urchin embryos exposed to cadmium as an experimental model for studying the relationship between autophagy and apoptosis. Mar Envl Res (2014) ; 93: 47–55.

Chiarelli R, Martino C, Agnello M, Bosco L, Roccheri MC. Autophagy as a defense strategy against stress: focus on *Paracentrotus lividus* sea urchin embryos exposed to cadmium. Cell Stress Chaperones (2016) 21(1):19-27.

Costa C, Karakostis K, Zito F, Matranga V. Phylogenetic analysis and expression patterns of p16 and p19 in *Paracentrotus lividus* embryos. Dev Genes Evol (2012) 222(4)245-251

Cowper SE, Robin HS, Steinberg SM, Su LD, Gupta S, LeBoit PE. Scleromyxoedema-like cutaneous diseases in renal-dialysis patients. Lancet (2000) 356(9234):1000-1.

Cowper SE, Boyer PJ. Nephrogenic systemic fibrosis: an update. Curr. Rheumatol. Rep. (2006) 8(2): 151–157.

Cuervo AM. Autophagy: in sickness and in health. Trends Cell Biol (2004) 14:70–77

Dahms HU, Lee JS. UV radiation in marine ectotherms: molecular effects and responses. Aquat. Toxicol. (2010) 97: 3-4.

Damle S, Davidson EH. Precise cis-regulatory control of spatial and temporal expression of the alx-1 gene in the skeletogenic lineage of *S. purpuratus*. Dev Biol (2011) 357(2):505-17.

David C, Halliwell J, Whitaker M. Some properties of the membrane currents underlying the fertilization potential in sea urchin eggs. J. Physiol. (1988) 402: 139–154.

Davidson EH, Cameron RA, Ransick A. Specification of cell fate in the sea urchin embryo: Summary and some proposed mechanisms. Development (1998) 125: 3269–3290.

Davidson EH. Gene Regulatory Systems. Development and Evolution. Academic Press, San Diego, 2001.

Depledge MH. Rapid assessment of marine pollution (RAMP). In: Proceedings of the Vietnam-UK Joint Workshop on Marine Pollution Assessment. – Hanoi, June 8, 2000. Publi.National Centre for Natural Science and Technology of Vietnam, Hanoi, Vietnam, pp.5-16.

Di Bartolomeo S, Nazio F, Cecconi F. The role of autophagy during development in higher eukaryotes. Traffic (2010) 11:1280–1289

Duboc V, Röttinger E, Lapraz F, Besnardeau L, Lepage T. Left-right asymmetry in the sea urchin embryo is regulated by nodal signaling on the right side. Dev Cell. (2005) 9(1):147-58.

Duloquin L, Lhomond G, Gache C. Localized VEGF signaling from ectoderm to mesenchyme cells controls morphogenesis of the sea urchin embryo skeleton. Development (2007) 134, 2293-2302.

EC (2008). DIRECTIVE 2008/56/EC OF THE EUROPEAN PARLIAMENT AND OF THE COUNCIL of 17 June 2008 establishing a framework for community action in the field of marine environmental policy (Marine Strategy Framework Directive).

Elbaz-Poulichet F, Seidel JL, Othonie, C. Occurrence of an anthropogenic gadolinium anomaly in river and coastal waters of Southern France. Water Res. (2002) 36 (4), 1102–1105.

El-Sayed SZ, Van Dijken G, Gonzales-Rhodas G. Effects of ultraviolet radiation on marine ecosystems. Int J Environ Stud (1996) 51:199-216.

Emlet RB. Echinoderm calcite: a mechanical analysis from larval spicules. Biol. Bull. (1982) 163, 264–275.

Emlet RB, Young CM, George SB. Phylum Echinodermata: Echinodea. In: Atlas of Marine Invertebrate Larvae, Young, C.M., Sewell, M.A., Rice, M.A. (eds.), Academic Press, London. (2002) 532–551.

Erkenbrack EM, Davidson EH. Evolutionary rewiring of gene regulatory network linkages at divergence of the echinoid subclasses. Proc Natl Acad Sci USA (2015) 112(30):E4075-84. doi: 10.1073/pnas.1509845112

Ettensohn CA, McClay DR. The regulation of primary mesenchyme cell migration in the sea urchin embryo: transplantations of cells and latex beads. Dev. Biol (1986). 117: 380-391.

Ettensohn CA. The regulation of primary mesenchyme cell patterning. Dev. Biol. (1990). 140: 261-271.

Ettensohn CA, Illies MR, Oliveri P, De Jong DL. Alx1, a member of the Cart1/Alx3/Alx4 subfamily of Paired-class homeodomain proteins, is an essential component of the gene network controlling skeletogenic fate specification in the sea urchin embryo. Development (2003) 130(13):2917–2928.

European Marine Board. Linking Oceans and Human Health: a Strategic Research Priority for Europe, pp. 27e30. Position Paper 19 of the European Marine Board (2013), Ostend, Belgium.

Fent K, Weston AA, Caminada D. Ecotoxicology of human pharmaceuticals. Aquat Toxicol. (2006) Feb 10;76(2):122-59.

Filosto S, Roccheri MC, Bonaventura R, Matranga V. Environmentally relevant cadmium concentrations affect development and induce apoptosis of *Paracentrotus lividus* larvae cultured in vitro. Cell Biol Toxicol (2008) 24(6):603–610

Fink RD, McClay DR. Three cell recognition changes accompany the ingression of sea urchin primary mesenchyme cells. Dev Biol. (1985) 1:66-74.

Foo SA, Dworjanyn SA, Poore AGB, Byrne M. Adaptive capacity of the habitat modifying sea urchin *Centrostepharnus rodgersii* to ocean warming and ocean acidification: performance of early embryos. PLoS ONE (2012) 7 (8), e42497.

Franco Jr A, Lansman JB. Stretch-sensitive channels in developing muscle cells from a mouse cell line. J. Physiol. (1990) 427, 361–380.

Garfield DA, Runcie DE, Babbitt CC, Haygood R, Nielsen WJ, Wray GA. The impact of gene expression variation on the robustness and evolvability of a developmental gene regulatory network. PLoS Biol. (2013) 11(10):e1001696.

Ghalambor CK, Hoke KL, Ruell EW, Fischer EK, Reznick DN, Hughes KA. Non-adaptive plasticity potentiates rapid adaptive evolution of gene expression in nature. Nature (2015) 525 (7569): 372-375

Gianguzza P, Bonaviri C. Arbacia. In: Lawrence, J.M. (Ed.), Sea Urchins: Biology and Ecology, third ed. (2013) Elsevier B.V., London, pp. 275-283.

Gibson AW, Burke RD. The origin of pigment cells in embryos of the sea urchin *Strongylocentrotus purpuratus.* Dev Biol (1985) 107, 414-419.

Gilbert SF. Developmental Biology. Developmental biology, 4th Edition. By Scott F. Gilbert, Sinauer Associates, Inc., Sunderland, Massachusetts, and W.H. Freeman, U.K., 1994, pp. xviii, 894.

Gilbert SF. Ecological Developmental Biology: Developmental Biology Meets the Real World. Dev Biol (2001) 233:1–12.

Gries H. Extracellular MRI contrast agents based on gadolinium, Top. Curr. Chem. (2002), 221, 1–24.

Guss KA, Ettensohn CA. Skeletal morphogenesis in the sea urchin embryo: regulation of primary mesenchyme gene expression and skeletal rod growth by ectoderm-derived cues. Development (1997). 124:1899-1908.

Gustafson T, Wolpert L. Studies on the cellular basis of morphogenesis in the sea urchin embryo. Formation of the coelom, the mouth, and the primary pore-canal. Exp Cell Res (1963) 29:561–582.

Häder DP, Worrest RC, Kumar HD, Smith RC. Effects of increased solar ultraviolet radiation on aquatic ecosystems. Ambio (1995) 24:174-180.

Häder DP, Helbling EW, Williamson CE, Worrest RC. Effects of UV radiation on aquatic ecosystems and interactions with climate change. Photochem Photobiol. Sci (2011) 10: 242-260.

Hamada T, Tanimoto A, Sasaguri Y. Apoptosis induced by cadmium. Apoptosis (1997) 2: 359-367.

Hamdoun A, Epel D. Embryo stability and vulnerability in an always changing world. Proc Natl Acad Sci U S A. (2007) 104(6):1745-50.

Hammond LM, Hofmann GE. Thermal tolerance of *Strongylocentrotus purpuratus* early life history stages: mortality, stress-induced gene expression and biogeographic patterns. Mar. Biol. (2010) 157: 2677-2687.

Hatje V, Bruland KW, Flegal AR. Increases in Anthropogenic Gadolinium Anomalies and Rare Earth Element Concentrations in San Francisco Bay over a 20 Year Record. Environ. Sci. Technol. (2016) 50 (8): 4159–4168

He X, Aker WG, Hwang HM. An in vivo study on the photoenhanced toxicities of S-doped TiO2 nanoparticles to zebrafish embryos (*Danio rerio*) in terms of malformation, mortality, rheotaxis dysfunction, and DNA damage. Nanotoxicology (2014) 8:185–95

Hengartner MO. The biochemistry of apoptosis. Nature (2000) 407(6805): 770–776.

Hereu B, Zabala M, Linares C et al. The effects of predator abundance and habitat structural complexity on serviva juvenile sea urchins. Mar Biol (2005), 146:293-299.

Hibino T, Nishino A, Amemiya S. Phylogenetic correspondence of the body axes in bilaterians is revealed by the right-sided expression of Pitx genes in echinoderm larvae. Dev Growth Differ (2006) 48(9):587-95**.**

Hirano S, Suzuki KT. Exposure, metabolism, and toxicity of rare earths and related compounds. Environ. Health Perspect. (1996) 104(suppl. 1): 85–95.

Hodor PG, Ettensohn CA. The dynamics and regulation of mesenchymal cell fusion in the sea urchin embryo. Dev Biol (1998). 199:111-124.

Hoffmann AA, Sgrò CM. Climate change and evolutionary adaptation. Nature (2011) 470: 479-485.

Huang J, Klionsky DJ. Autophagy and human disease. Cell Cycle (2007) 6:1837–1849

Hwang SPL, Lennarz WJ. Studies on the cellular pathway involved in assembly of the embryonic sea urchin spicule. Exp. Cell Res (1993) 205, 383–387**.**

IAEA-TECDOC-1429. Worldwide marine radioactivity studies WOMARS): radionuclide levels in oceans and seas. Printed by International Atomic Energy Agency, Vienna, Austria, January 2005.

Irie N, Kuratani S. Comparative transcriptome analysis reveals vertebrate phylotypic period during organogenesis. Nat Commun (2011) 2(248): 1–6.

Islam Shahidul M, Tanaka M. Impacts of pollution on coastal and marine ecosystems including coastal and marine fisheries and approach for management: a review and synthesis. Mar Pollut Bull. (2004) 48(7-8):624-49.

Israel JW, Martik ML, Byrne M, Raff EC, Raff RA, McClay DR, Wray GA. Comparative Developmental Transcriptomics Reveals Rewiring of a Highly Conserved Gene Regulatory Network during a Major Life History Switch in the Sea Urchin Genus *Heliocidaris*. PLoS Biol (2016) 14(3): e1002391. doi:10.1371/journal.pbio.1002391

IWW (2014). Pharmaceuticals in the environment: Occurrence, effects, and options for action. Research project funded by the German Federal Environment Agency (UBA) within the Environmental Research Plan No. 371265408. http://www.pharmaceuticals-in-the-environment.org

Kalinka AT, Varga KM, Gerrard DT, Preibisch S, Corcoran DL, Jarrells J, et al. Gene expression divergence recapitulates the developmental hourglass model. Nature (2010) 468(7325):811–16.

Karakostis K, Costa C, Zito F, Brümmer F, Matranga V. Characterization of an Alpha Type Carbonic Anhydrase from *Paracentrotus lividus* Sea Urchin Embryos. Mar Biotechnol (NY). (2016) 18(3):384-95.

Karakostis K, Zanella-Cleon I, Immel F, Guichard N, Dru P, Lepage T, Plasseraud L, Matranga V, Marin F. A minimal molecular toolkit for mineral deposition? Biochemistry and proteomics of the test matrix of adult specimens of the sea urchin *Paracentrotus lividus*. J. Prot. (2016) http://dx.doi.org/10.1016/j.jprot.2016.01.001.

Keesing JK. *Heliocidaris erythrogramma*. In: Lawrence, J.M. (Ed.), Sea Urchins: Biology and Ecology, third ed. (2013) Elsevier B.V., London, pp. 369-379.

Kelly MW, Sanford E, Grosberg RK. Limited potential for adaptation to climate change in a broadly distributed marine crustacean. Proc. R. Soc. B (2011) 279: 349-356.

Killian CE, Wilt FH. Characterization of the proteins comprising the integral matrix of Strongylocentrotus purpuratus embryonic spicules. J. Biol. Chem. (1996) 271: 9150–9159.

Killian CE, Croker L, Wilt FH. SpSM30 gene family expression patterns in embryonic and adult biomineralized tissues of the sea urchin, *Strongylocentrotus purpuratus*. Gene Expr Patterns. (2010) (2-3):135-9.

Kinjo S, Shirayama Y, Wada H. Evolutionary history of larval skeletal morphology in sea urchin Echinometridae (Echinoidea: Echinodermata) as deduced from mitochondrial DNA molecular phylogeny. Evol. Dev. (2008) 10(5), 632-41

Klionsky DJ, Emr SD Autophagy as a regulated pathway of cellular degradation. Science (2000) 290:1717–21.

Klionsky DJ, Meijer AJ, Codogno P. Autophagy and p70S6 kinase. Autophagy (2005);1:59–61

Knappe A, Möller P, Dulski P, Pekdeger A. Positive Gadolinium Anomaly in Surface Water and Ground Water of the Urban Area Berlin, Germany. Chem. der Erde, Geochem. (2005) 65 (2): 167-189.

Knapp RT, Wu CH, Mobilia KC, Joester D. Recombinant sea urchin vascular endothelial growth factor directs single-crystal growth and branching in vitro. J Am Chem Soc (2012) 134(43):17908-11.

Kroh A, Smith AB. The phylogeny and classification of post-Palaeozoic echinoids. J. Syst. Palaeontol. (2010) 8: 147–212.

Kroemer G, Galluzzi L, Vandenabeele P, Abrams J, Alnemri ES, Baehrecke EH, Blagosklonny MV, El-Deiry WS, Golstein P, Green DR, Hengartner M, Knight RA, Kumar S, Lipton SA, Malorni W, Nuñez G, Peter ME, Tschopp J, Yuan J, Piacentini M, Zhivotovsky B, Melino G; Nomenclature Committee on Cell Death 2009. Classification of cell death: recommendations of the Nomenclature Committee on Cell Death 2009. Cell Death Differ. (2009) 16(1):3-11

Kulaksiz S, Bau M. Contrasting behaviour of anthropogenic gadolinium and natural rare earth elements in estuaries and the gadolinium input into the North Sea. Earth Planet. Sci. Lett. (2007) 260 (1-2): 361-371.

Kulaksiz S, Bau M. Anthropogenic gadolinium as a microcontaminant in tap water used as drinking water in urban areas and megacities. Applied Geochem., (2011) 26, 1877– 1885.

Kümmerer K, Helmers E. Hospital Effluents as a Source of Gadolinium in the Aquatic Environment. Environ. Sci. Technol. 34 (2000) 573-577.

Langer G, Nehrke G, Probert I, Ly J, Ziveri P. Strain-specific responses of *Emiliania huxleyi* to changing sea water carbonate chemistry. Biogeosciences (2009) 6: 2637-2646.

Lansman JB. Blockade of current through single calcium channels by trivalent lanthanide cations: effect of ionic radius on the rates of ion entry and exit. J. Gen. Physiol (1990) 95, 679–696.

Larkin K, Wouters N, Caetano AT, McDonough N. (Ed.) EurOcean 2014. Connecting Science, Policy and People. Conference report and Rome Declaration 7-9 October 2014, Rome, Italy. Publications Office of the European Union: Luxemburg.

Lawrence JM. Sea Urchins: Biology and Ecology, third ed. (2013) Elsevier, London.

Leaf DS, Anstrom JA, Chin JE, Harkey MA. Antibodies to a fusion protein identify a cDNA clone encoding msp130, a primary mesenchyme-specific cell surface protein of the sea urchin embryo. Dev Biol (1987) 121:29-40.

Lepage T, Sardet C, Gache C. Spatial expression of the hatching enzyme gene in the sea urchin embryo. Dev Biol. (1992) 150(1):23-32.

Levin M. Left-right asymmetry in embryonic development: a comprehensive review. Mech Devc(2005) 122: 3–25.

Lide DR, Haynes WMM, Baysinger G, Berger LI, Roth DL, Zwillinger D, Frenkel M, Goldberg RN (2009). CRC Handbook of Chemistry and Physics, 2009−2010, 90th edition, volume 131.

Lindberg RH, Östman M, Olofsson U, Grabic R, Fick J. Occurrence and behaviour of 105 active pharmaceutical ingredients in sewage waters of a municipal sewer collection system. Water Res. (2014) 58:221-9.

Lister KN, Lamare MD, Burritt DJ. Pollutant resilience in embryos of the Antarctic sea urchin *Sterechinus neumayeri* reflects maternal antioxidant status. Aquat. Toxicol. (2015) 161: 61-72

Luo D, Broad LM, Bird GSJ, Putney Jr JW. Signaling pathways underlying muscarinic receptor-induced [Ca2+]i oscillations in HEK293 cells. J. Biol. Chem. (2001) 276, 5613–5621.

Lyons BP, Thain JE, Stentiford GD, Hylland K, Davies IM, Vethaak AD. Using biological effects tools to define good environmental status under the European union Marine strategy framework directive. Mar. Poll. Bull. (2010) 60:1647-1651.

Martino C, Bonaventura R, Byrne M, Roccheri M, Matranga V. Effects of exposure to gadolinium on the development of geographically and phylogenetically distant sea urchins species. Mar Environ Res. (2016) pii: S0141-1136(16)30098-8. doi: 10.1016/j.marenvres.2016.06.001.

Massey A, Kiffin R, Cuervo AM. Pathophysiology of chaperone-mediated autophagy. Int J Biochem Cell Biol (2004); 36:2420–2434.

Matranga V, Bonaventura R. Sea urchin coelomocytes, the progenitors of vertebrate immune effectors, as bio-indicators of stress and pollution. In Yokota Y, Matranga

V, Smolenicka Z (eds) (2002) The sea urchin: from basic biology to aquaculture. Swets and Zeitlinger, Lisse, The Netherlands, pp 161-176.

Matranga V, Zito F, Costa C, Bonaventura R, Giarrusso S, Celi F. Embryonic development and skeletogenic gene expression affected by X-rays in the Mediterranean sea urchin *Paracentrotus lividus*. Ecotoxicology (2010) 19:530-7.

Matranga V, Bonaventura R, Costa C, Karakostis K, Pinsino A, Russo R, Zito F. Echinoderms as blueprints for biocalcification: regulation of skeletogenic genes and matrices. Prog Mol Subcell Biol. (2011) 52:225-48.

Matranga V, Pinsino A, Bonaventura R, Costa C, Karakostis K, Martino C, Russo R, Zito F. Cellular and molecular bases of biomineralization in sea urchin embryos. Cah. Biol. Mar. (2013) 54 : 467-478.

Metzger RJ, Krasnow MA. Genetic control of branching morphogenesis. Science (1999) 284: 1635-1639**.**

Min H, Danilenko DM, Scully SA, Bolon B, Ring BD, Tarpley JE, DeRose M, Simonet WS. Fgf-10 is required for both limb and lung development and exhibits striking functional similarity to *Drosophila* branchless. Genes Dev. (1998) 12: 3156-3161

Mitsunaga K, Makihara R, Fujino Y, Yasumasu I. Inhibitory effects of ethacrynic acid, furosemide, and nifedipine on the calcification of spicules in cultures of micromeres isolated from sea-urchin eggs. Differentiation (1986) 30, 197–204

Mizgerd JP, Molina RM, Stearns RC, Brain JD, Warner AE. Gadolinium induces macrophage apoptosis. J Leukoc Biol. (1996) 59(2):189-95.

Moore MN, Depledge MH, Readman JW, Leonard P. An integrated biomarker-based strategy for ecotoxicological evaluation of risk in environmental management. Mutation Res. (2004) 552:247-268.

Moore MN, Allen JI, McVeigh A Environmental prognostics: an integrated model supporting lysosomal stress responses as predictive biomarkers of animal health status. Mar Environ Res (2006) 61:278–304.

Moore MN, Koehler A, Lowe D, Viarengo A Lysosomes and autophagy in aquatic animals. In: Daniel J. Klionsky, Editor(s), Methods in enzymology, Academic Press. (2008) 451:581-620.

Morici G, Agnello M, Spagnolo F, Roccheri MC, Di Liegro CM, Rinaldi AM. Confocal microscopy study of the distribution, content and activity of mitochondria during *Paracentrotus lividus* development. J Microsc (2007) 228:165-73.

Morteani G, Möller P, Fuganti A, Paces T. Input and fate of anthropogenic estrogens and gadolinium in surface water and sewage plants in the hydrological basin of Prague (Czech Republic). Environ. Geochem. Health (2006) 28: 257–264.

Murdoch K. Pharmaceutical pollution in the environment: Issues for Australia, New Zealand and Pacific Island countries, published by the National Toxics Network (NTN) (2015).

Nakano E, Okazaki K, Iwamatsu T. Accumulation of radioactive calcium in the larvae of the sea urchin *Pseudocentrotus depressus*. Biol Bull (1963) 125:125-136.

Nozaki Y, Lerche D, Alibo DS, Tsutsumi M. Dissolved indium and rare earth elements in three Japanese rivers and Tokyo Bay: evidence for anthropogenic Gd and In. Geochim. Et Cosmochim. Acta (2000) 64 (23), 3975–3982.

Ogata T, Terakado Y. Rare earth element abundances in some seawaters and related river waters from the Osaka Bay area, Japan: significance of anthropogenic Gd. Geochem. J. (2006) 40 (5): 463-474.

Okazaki K. Spicule formation by isolated micromeres of the sea urchin embryo. Am Zool (1975) 5:567–581.

Oliveri P, Davidson EH. Gene regulatory network controlling embryonic specification in the sea urchin. Curr Opin Genet Dev (2004) 14:351–360.

Oliveri P, Tu Q, Davidson EH. Global regulatory logic for specification of an embryonic cell lineage. Proc Natl Acad Sci (2008). 105:5955-5962.

Paxton CW, Davy SK, Weis VM. Stress and death of cnidarians host cells play a role in cnidarian bleaching. J Exp Biol (2013) 216:2813–2820

Pinsino A, Roccheri MC, Costa C, Matranga V. Manganese interferes with calcium, perturbs ERK signaling, and produces embryos with no skeleton. Toxicol Sci (2011) 123:217-230.

Rabiet M, Brissaud F, Seidel JL, Pistre S, Elbaz-Poulichet F. Positive gadolinium anomalies in wastewater treatment plant effluents and aquatic environment in the Hérault watershed (South France). Chemosphere (2009) 75(8):1057-64.

Radenac G, Fichet D, Miramand P. Bioaccumulation and toxicity of four dissolved metals in Paracentrotus lividus sea urchin embryo, Mar. Environ. Res. (2001) 51 151–166.

Range R, Lapraz F, Quirin M, Marro S, Besnardeau L, Lepage T. Cis-regulatory analysis of nodal and maternal control of dorsal-ventral axis formation by Univin, a TGF-beta related to Vg1. Development (2007) 134(20):3649-64.

Roccheri MC, Agnello M, Bonaventura R, Matranga V. Cadmium induces the expression of specific stress proteins in sea urchin embryos. Biochem Biophys Res Commun (2004) 321:80-7.

Röttinger E, Saudemont A, Duboc V, Besnardeau L, Mc Clay D, Lepage T. FGF signals guide migration of mesenchymal cells, control scheletal morphogenesis and regulate gastrulation during sea urchin development. Development (2008). 135:354-365.

Runge VM. Gd-DTPA: an i.v. contrast agent for clinical MRI. Int. J. Radiat. Appl. Instrum. B (1988) 15(1): 37–44.

Russo R, Bonaventura R, Zito F, Schroder HC, Muller I, Muller WE, Matranga V. Stress to cadmium monitored by metallothionein gene induction in Paracentrotus lividus embryos, Cell Stress Chaperones 8 (2003) 232–241.

Saitoh M, Kuroda R, Muranaka Y, Uto N, Murai J, Kuroda H. Asymmetric inhibition of spicule formation in sea urchin embryos with low concentrations of gadolinium ion. Dev Growth Differ (2010) 52(9):735-46.

Samali A, Cotter TG. Heat shock proteins increase resistance to apoptosis. Exp. Cell Res (1996) 223: 163-170.

Sgroi A, Colombo P, Duro G, Fried M, Izzo V, Giudice G. cDNA sequence analysis and expression of the expression of the ribosomal protein S24 during oogenesis and embryonic development of the sea urchin *Paracentrotus lividus*. Biochemical and biophysical research communications (1996) 221(2), 361–7.

Sherry AD, Caravan P, Lenkinski RE. Primer on gadolinium chemistry. J. Magn. Reson. Imaging (2009) 30: 1240-1248

Soars N, Byrne M. Contrasting arm elevation angles of multi- and two-armed sea urchin echinoplutei supports Grünbaum and Strathmann's hydromechanical model. Mar. Biol. (2015) 162(3), 607-616. doi: 10.1007/s00227-014-2608-2.

Spencer AJ, Wilson SA, Batchelor J, Reid A, Rees J, Harpur E. Gadolinium chloride toxicity in the rat. Toxicol Pathol. (1997) 25(3):245-55.

Stenzel P, Angerer LM, Smith BJ, Angerer RC, Vale W. The univin gene encodes a member of the transforming growth factor-beta superfamily with restricted expression in the sea urchin embryo. Dev Biol (1994) 166, 149–158.

Stumpp M, Hu MY, Melzner F, Gutowska MA, Dorey N, Himmerkus N, Holtmann WC, Dupont ST., Thorndyke MC, Bleich M. Acidified seawater impacts sea urchin larvae pH regulatory systems relevant for calcification. Proc. Natl. Acad. Sci. U. S. A. (2012) 109 (44): 18192-18197.

Tamboline CR, Burke RD. Secondary mesenchyme of the sea urchin embryo: Ontogeny of blastocoelar cells. J Exp Zool (1992) 262, 51-60.

Tanida I, Ueno T, Kominami E. LC3 and Autophagy. Methods Mol Biol. (2008) 445:77-88.

Tasdemir E, Galluzzi L, Maiuri MC, Criollo A, Vitale I, Hangen E, Modjtahedi N, Kroemer G. Methods for assessing autophagy and autophagic cell death. Methods Mol Biol. (2008) 445:29-76.

Telgmann L, Sperling M, Karst U. Determination of gadolinium-based MRI contrast agents in biological and environmental samples: a review. Anal Chim Acta. (2013) 764:1-16.

Thakral C, Alhariri J, Abraham JL. Long-term retention of gadolinium in tissues from nephrogenic systemic fibrosis patient after multiple gadolinium-enhanced MRI scans: case report and implications. Contrast Media Mol Imaging. (2007) 2(4):199-205.

Time To Get Clean, 08 October 2015. Editorial. Nature 526 (164). http://dx.doi.org/10.1038/526164a.

Traganos F, Darzynkiewicz Z. Lysosomal proton pump activity: supravital cell staining with acridine orange differentiates leukocyte subpopulations. Methods Cell Biol (1994) 41:185-194.

Vandegehuchte MB, Janssen CR. Epigenetics in an ecotoxicological context. Mutat. Res. Genet. Toxicol. Environ. Mutagen (2014) 764-765:36-45.

Weis VM. Cellular mechanisms of cnidarian bleaching: stress causes the collapse of symbiosis. J Exp Biol (2008) 19:3059–66

Whitehead A. Evolutionary genomics of environmental pollution. Adv. Exp. Med. Biol. (2014) 781: 321-337.

Whitman M. Nodal signaling in early vertebrate embryos: themes and variations. Dev Cell. (2001) 1(5):605-17.

Wilde EW, Berry CJ, Goli MB. Toxicity of gadolinium to some aquatic microbes. Bull Environ Contam Toxicol (2002) 68(3):420-7.

Wilson MP, Schwarzman MR (2009). Toward a New U.S. Chemicals Policy: Rebuilding the Foundation to Advance New Science, Green Chemistry, and Environmental Health. Environ Health Perspect (2009) 117:1202-1209.

Wilt FH. Biomineralization of the spicules of sea urchin embryos. Zoolog Sci. (2002) 19(3):253-61.

Wilt FH, Killian CE, Hamilton P, Croker L. The dynamics of secretion during sea urchin embryonic skeleton formation. Cell Res (2008) 314:1744-1752.

Wray GA. Rates of Evolution in Developmental Processes. Am Zool. (1992) 32:123–134

Yang XC, Sachs F. Block of stretch-activated ion channels in Xenopus oocytes by gadolinium and calcium ions. Science (1989) 243, 1068–1071.

Yuan J, Kroemer G. Alternative cell death mechanisms in development and beyond. Genes Dev (2010) 24:2592–602.

Zhu Y, Hoshino M, Yamada H, Itoh A, Haraguchi H. Gadolinium anomaly in the distributions of rare earth elements observed for coastal seawater and river waters around Nagoya City. Bull. Chem. Soc. Jpn. (2004) 77 (10), 1835–1842

Zito F, Tesoro V, McClay DR, Nakano E, Matranga V. Ectoderm cell-ECM interaction is essential for sea urchin embryo skeletogenesis. Dev Biol (1998) 196:184-192.

Zito F, Costa C, Sciarrino S, Poma V, Russo R, Angerer LM, Matranga V. Expression of univin, a TGF-β growth factor, requires ectoderm–ECM interaction and promotes skeletal growth in the sea urchin embryo. Developmental Biology (2003), 264(1), 217–227.

Zito F, Matranga V. Secondary mesenchyme cells as potential stem cells of the sea urchin embryo. Chapter 8 in Stem Cells in Marine Organisms, Rinkevich e Matranga eds (2009), Springer.

Zito F, Koop D, Byrne M, Matranga V. Carbonic anhydrase inhibition blocks skeletogenesis and echinochrome production in Paracentrotus lividus and Heliocidaris tuberculata embryos and larvae. Dev. Growth Differ. (2015) 57(7), 507-14. doi: 10.1111/dgd.12229.